Photodynamic antimicrobial chemotherapy activities of porphyrin- and phthalocyanine-platinum nanoparticle conjugates

A thesis submitted in fulfilment of the requirements for the degree of

MASTER OF SCIENCE

Of

RHODES UNIVERSITY

By

Muthumuni Elizabeth Managa

November 2014

DEDICATION

To

My Mother

Avhurengwi Angelinah Managa

(1954 - 2011)

Vhovha vha zwothe kha nne mme anga

ACKNOWLEDGEMENTS

Psalm 136:1 “Give thanks to Jehovah, for he is good; His loyal love endures forever”. None of this would have been possible without you. You are worthy Jehovah.

First and foremost I humbly acknowledge my supervisor: Distinguished Professor T. Nyokong, Thank you for your patience, guidance and support that you gave me throughout this work. Without you my love for research would not have been increased. Thank you for opening new avenues by sending me to United Kingdom (University of East Anglia).

My gratitude also goes to Dr Edith Antunes and Dr Edith K. Amuhaya for the love, guidance and support. You have been a pillar of strength when it seemed impossible.

To my Father, Mr N.M. Managa, No words can ever express my gratitude. You have always been my pillar of strength and my reason to keep going regardless of obstacles. You have always believed in me and with no doubt I can do anything I put my mind into.

To my siblings Tshinanne, Khumbudzo, Tshifhiwa, Halatedzi and Mikovhe thank you for always walking along side me. Your encouragement and prayers kept me going throughout this work.

To my friends thank you so much for all your encouragements and love through this work. You are all highly appreciated.

It was a privilege and an honor to have worked with the Rhodes University Chemistry Department S22 Nanotechnology Research Group. You guys are indeed a family away from home.

Financial support from Pearson Young foundation is gratefully acknowledged

ABSTRACT

This work reports on the conjugation of differently shaped Pt nanoparticles (PtNPs) with ClGa(III) 5,10,15,20-tetrakis-(4-carboxyphenyl) porphyrin (**1**) as well as chloro - (5,10,15,20-tetrakis (4- (4- carboxy phenycarbonoimidoyl) phenyl) porphyrinato) gallium(III) (**2**) The work also reports on platination of dihydroxosilicon octacarboxyphthalocyanine $(OH)_2SiOCPc$ (**3**) to give dihydroxosilicontris(diaquaplatinum)octacarboxyphthalocyanine $(OH)_2SiOCPc(Pt)_3$ (**4**). The resulting conjugates were used for photodynamic antimicrobial chemotherapy against *S. aureus, E. coli* and *C. albicans.* The degree of photo-inactivation is dependent on concentration of the conjugates, light dose (fluence) and illumination time. The log reduction obtained for **1** when conjugated to cubic PtNPs was 4.64 log (which indicate 99.99% of the bacteria have been killed), which is much higher than 3.94 log unit for **1**-hexagonal PtNPs and 3.31 log units for **1**-unshaped PtNPs. Complex **2** conjugated to hexagonal PtNPs showed 18 nm red shift in the Soret band when compared to **2** alone. Complex **2** and **2**-hexagonal PtNPs as well showed promising photodynamic antimicrobial chemotherapy (PACT) activity against *S. aureus*, *E. coli* and *C. albicans* in solution where the log reduction obtained was 4.92, 3.76, and 3.95 respectively for **2**-hexagonal PtNPs. The singlet oxygen quantum yields obtained were higher at 0.56 for **2**-hexagonl PtNPs in DMF while that of **2** was 0.52 in the same solvent. This resulted in improved PACT activity for **2**-hexagonal PtNPs compared to **2**. Complex **4** showed slight blue shifting of the absorption spectrum when compared to complex **3** The antimicrobial activity of **4** were promising as

the highest log reduction value was observed when compared to the porphyrin conjugates.

TABLE OF CONTENTS

LIST OF ABBREVIATIONS

A/abs	**Absorbance**
Acetone-d_6	**Deuterated acetone**
ADMA	**Tetrasodiuma,a-(anthracene-9,10-diyl)dimethylmalonate**
C. albicans	***Candida albicans***
DBU	**1,8-diazabicyclo[5.4.0]undec-7-ene**
DMSO	**Dimethyl sulfoxide**
DMSO-d_6	**Deuterated dimethylsulfoxide**
E. coli	***Escherichia coli***
EDTA	**Ethylenediaminetetraacetic acid**
EDS	**Energy dispersive spectroscopy**
F	**Fluorescence**
Gram (-)	**Gram negative**
Gram (+)	**Gram positive**
H_2Pc	**Free base phthalocyanine**
^1H NMR	**Proton nuclear magnetic resonance**
HOMO	**Highest Occupied Molecular Orbital**
IC	**Internal conversion**
IR	**Infrared**
ISC	**Intersystem crossing**
LUMO	**Lowest Unoccupied Molecular Orbital**
MPc	**Metallophthalocyanine**
NPs	**Nanoparticles**

ODE	**1-octadecene**
PACT	**Photodynamic antimicrobial chemotherapy**
Pc	**Phthalocyanine**
PDT	**Photodynamic therapy**
PtNPs	**Platinum nanoparticles**
H-PtNPs	**Hexagonal platinum nanoparticles**
C-PtNPs	**Cubic platinum nanoparticles**
U-PtNPs	**Unshaped platinum nanoparticles**
PS	**Polystyrene**
ROS	**Reactive Oxygen Species**
S. aureus	***Staphylococcus aureus***
SEM	**Scanning electron microscope**
TEM	**Transmission electron microscope**
THF	**Tetrahydrofuran**
TAPP	**Tetrakis-5,10,15,20-(4-aminophenyl) porphyrin**
UV/Vis	**Ultraviolet/visible**
XRD	**X-ray diffractometer**

LIST OF SYMBOLS

α	**non-peripheral position**
β	**peripheral position**
ε	**molar extinction coefficient**
λ	**wavelength**
τ	**lifetime**
τ_0	**fluorescence radiative lifetime**
τ_F	**fluorescence lifetime**
Φ	**quantum yield**
Φ_F	**fluorescence quantum yield**
Φ_Δ	**singlet oxygen quantum yield**
$O_2(^1\Delta_g)$	**singlet molecular oxygen**
S_0	**singlet ground state**
S_1	**singlet excited state**
t	**time**
T_1	**triplet excited state**

LIST OF FIGURES

LIST OF SCHEMES

LIST OF TABLES

CHAPTER ONE

Introduction

1.1 Photodynamic antimicrobial chemotherapy (PACT)

The use of antibiotics represents one of the most ground-breaking progresses made in medicine, resulting in the treatment and suppression of many incurable microorganism infections **[1, 2]**. At the beginning of the 21st century, microbe-related infections were reduced to a level where they no longer had a serious impact on human health because of availability of antibiotics. However, microorganisms have developed resistance against many antibiotics which were previously highly effective **[1, 3]**. Methicillin-resistant *Staphylococcus aureus* (*S. aureus*) and Vancomycin-resistant *Enterococcus faecium* are species that are causing much concern at present **[4]** and there is an urgent need for the development of novel, convenient, non-resistant and low-cost measures to fight microbial infections **[1, 5, 6]**.

Photodynamic antimicrobial chemotherapy (PACT) represents a potential, alternative for the inactivation of microbial cells and has already shown to be effective in *vitro* against bacteria **[5-8]**, fungi **[9]**, viruses **[10]** and protozoa **[11]**.

1.1.1 Background and working principle

The phenomenon of PACT was first described by Raab in 1890 **[12]**. Raab made an observation that the toxicity of acridine orange against *Paramecia caudatum* was dependent on the amount of light introduced to the cells **[12-14]**. Later on Raab's teacher Van Tappeiner reported that the toxic effects in the presence of light were not due to heat **[15]**. In 1904 Tappeiner introduced the term "Photodynamic reaction" **[15]**.

The understanding of the scientific basis of PACT is still in its infancy, but it follows a similar principle to that of photodynamic therapy (PDT) **[5]**. PACT is based on the concept that a non-toxic photosensitiser, localized preferably in the microorganism can be activated by low doses of visible light of appropriate wavelength as Fig. 1.1 **[16]**. This is followed by transfer of

energy or electrons to molecular oxygen to generate reactive oxygen specie (such as singlet oxygen) that are cytotoxic to target cells **[13, 14, 17]**, leading to cell death through necrosis or apoptosis. There are various photosensitisers which have been developed for PACT **[18]**, which includes porphyrins and phthalocyanines which are synthesised in this work.

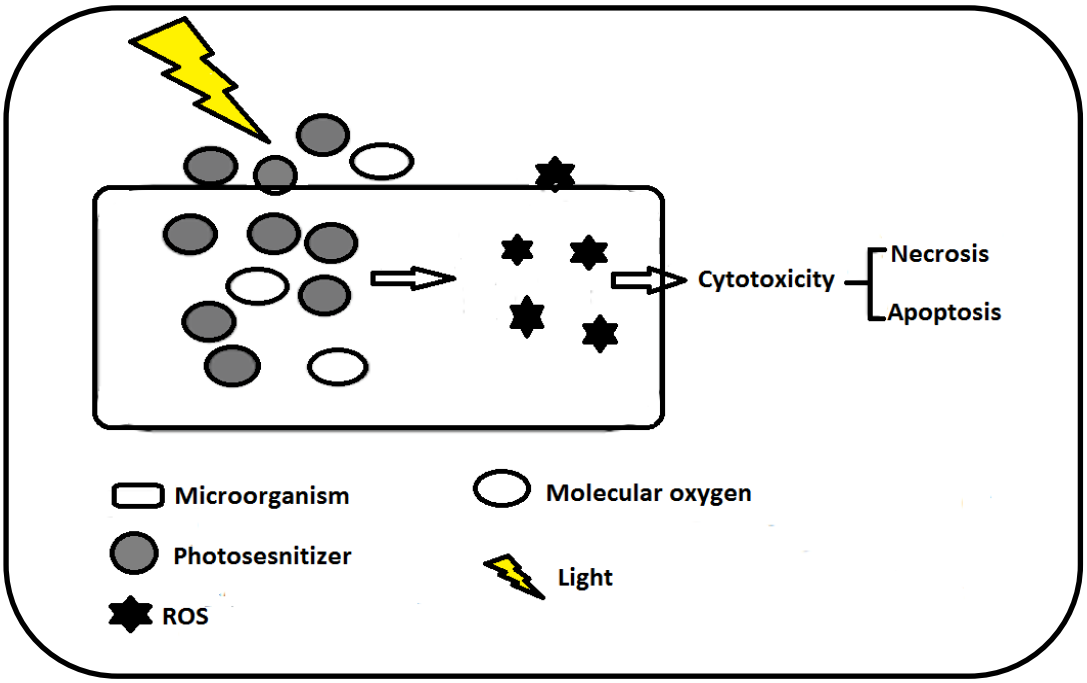

Figure 1.1: Schematic diagram showing principle of PACT [16].

1.1.2 Microorganisms that have been treated with PACT

PACT has been used effectively in the treatment of infections such as gingivitis and periodontitis **[19]**, cutaneous leishmaniasis **[20]** as well as root canal biofilm infection **[21]**. PACT appears to offer various advantages over antibiotics with minimal possibility of developing resistance.

The target microorganisms for photoinactivation are mainly bacteria **[19]** but fungal inactivation has also gained much interest in the last few years. Bacteria fall into two main classes depending on their ability to retain the Gram stain which reflects difference in their morphology as illustrated in Fig 1.2 **[1].** Gram (-) and Gram (+) bacteria differ in the composition of their

outer surface and respond differently to antimicrobial agents **[22-24]**. Gram (-) bacteria such as *Escherichia coli* (*E. coli*), have an additional layer called the outer membrane, which is absent in Gram (+) bacteria such as *S. aureus* **[22].**

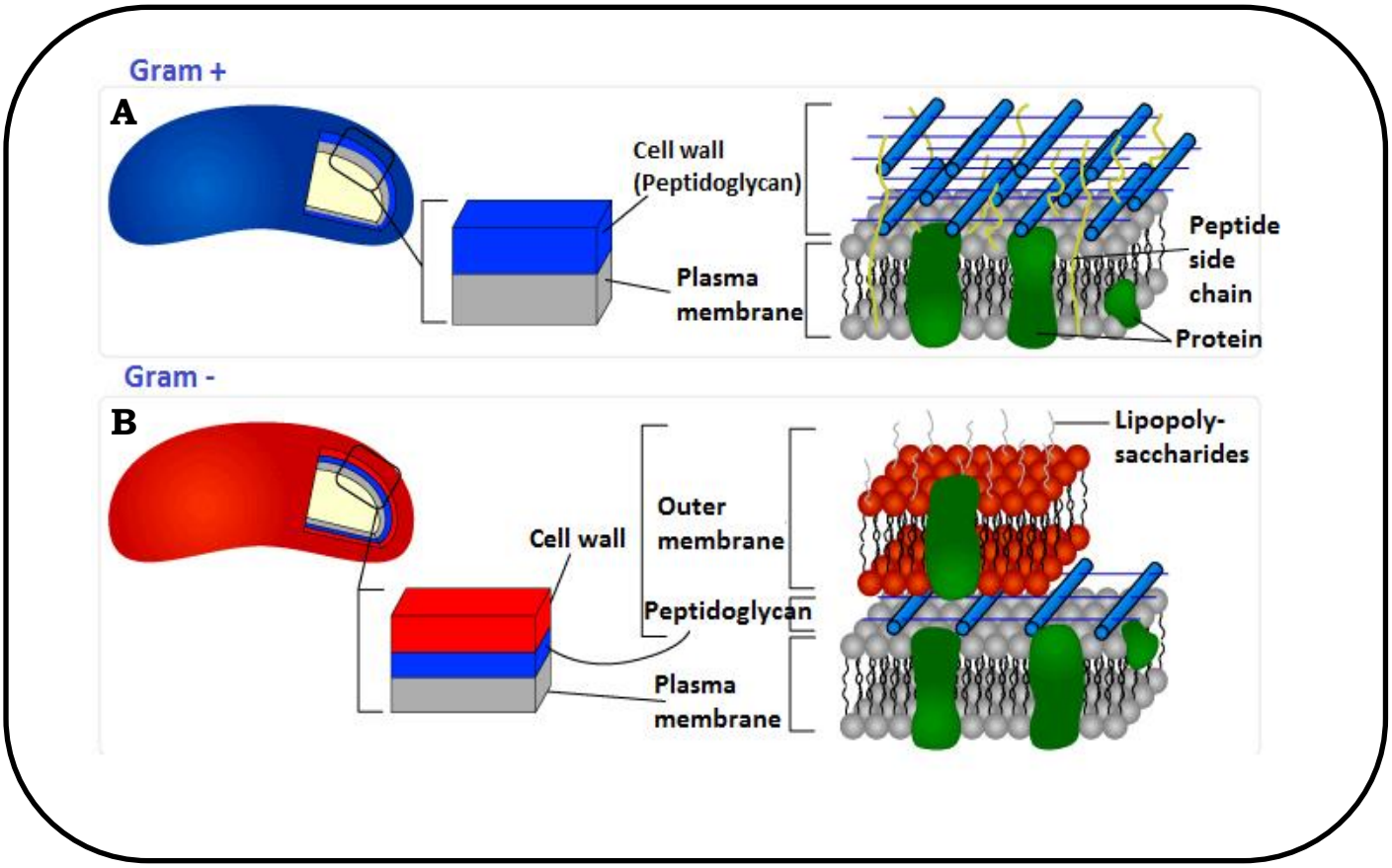

Figure 1.2: Schematic representations of the arrangement of the cell walls of Gram (+) (A) and Gram (-) (B) bacteria [23, 24].

Gram (+) bacteria cell wall has a 15–80 nm thick cell wall composed of up to 100 interconnecting layers of peptidoglycan Fig.1.2 (**A**). Teichoic acids are interwoven in the peptidoglycan layers. Some have a lipid attached (lipoteichoic acid) **[25]**. Also proteins are ingrained in the peptidoglycan layers. Gram (−) bacteria cell wall consists of a thin, inner wall composed of 2–3 layers of peptidoglycan (2–3 nm thick), a periplasmic space and an outer lipid bilayer (7 nm). The outer membrane contains phospholipids,

lipoproteins, lipopolysaccharides (LPS) and proteins like porins Fig. 1.2 (**B**) **[26]**.

Gram (+) bacteria can easily take up photosensitisers and can therefore readily undergo photoinactivation. This is not the case for Gram (-) due to their highly negatively charged surface. Neutral or anionic photosensitisers cannot easily penetrate the cell wall of Gram (-) **[1]** but cationic ones can. It has been shown that many neutral or anionic photosensitisers can become effective against Gram (-) bacteria when the bacterial cells are pre-treated with cationic (outer membrane disrupting) agents such as polymixin, $CaCl_2$ or ethylenediaminetetraacetic acid (EDTA) **[1, 26-28]**.

Fungal inactivation has also gained much interest. Some fungi are Gram (+) (example *Candida albicans (C. albicans)*) and can easily be photoinactivated by either anionic or neutral photosensitisers.

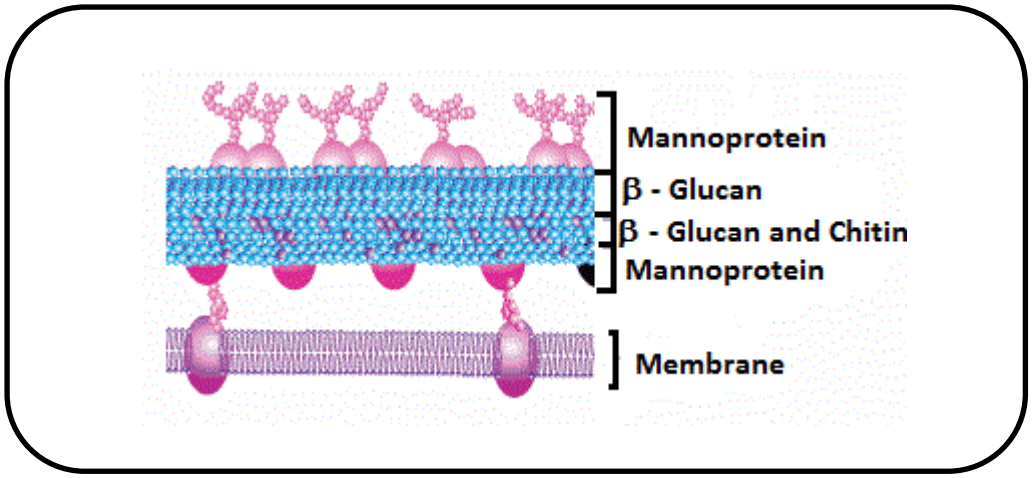

Figure 1.3: Schematic representation of the arrangement of fungal cell wall [10].

The fungal cell wall is composed of multiple layers, with mannoproteins being predominantly expressed at the external surface (Fig. 1.3). An underlayer of β-glucan creates a supporting matrix for the mannoproteins and therefore provides structural rigidity to the cell wall. The glucan structure is strengthened by frequent β(1→3) and additional β(1→6) linkages and by chitin interspersed with the β-glucan. Mannoproteins and

glucan make up more than 80% of the cell wall composition, while chitin represents less than 2%. It has been reported that photosensitisers are not taken up by yeast cells (fungi) and the phototoxic activity is largely due to the unbound photosensitiser molecules in the bulk aqueous medium **[10]**. In this work fungi (*C. albicans*) and bacteria (*E.coli* and *S. aureus*) are treated using PACT and porphyrins and phthalocyanines are used as the photosensitizers.

1.2. Porphyrins

Porphyrins are an important class of compounds of natural or synthetic origin. Those that are naturally occurring are important in biological systems and are central to the roles of photosynthesis, biological oxidation and reductions and the transport of oxygen **[17, 19, 29]**. Synthetic porphyrins have been used in different fields from medicinal to industrial fields.

1.2.1. Structure and naming of porphyrins

Porphyrins are aromatic tetrapyrrolic macrocycles (Fig. 1.4) which follow Hückel's rule of 4n+2n, electrons, where n = 4, 5 or 6.

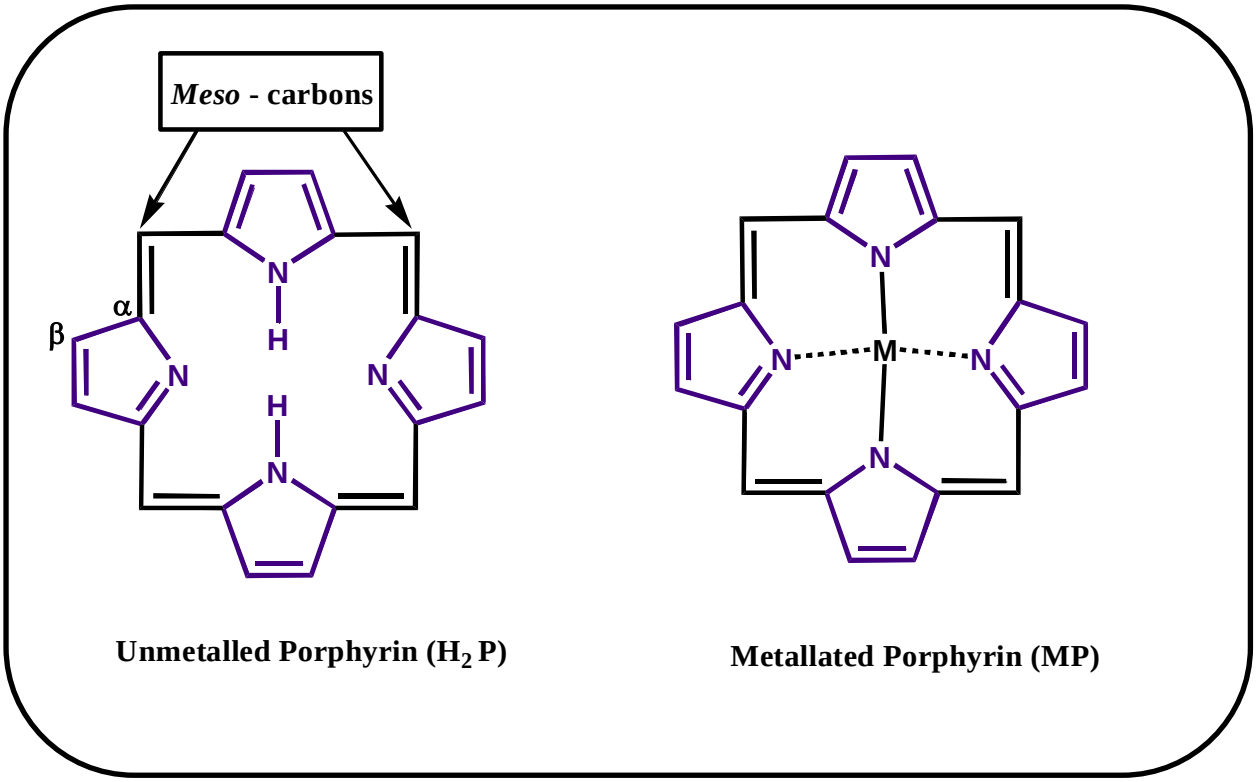

Figure 1.4: The structure of free base (unmetallated) porphyrin and metalloporphyrin.

The structure of porphyrin was first proposed by Küster **[30]** in 1912, but nobody believed him because such a large ring was thought to be unstable. Years later, Fischer and Zeile proposed the same structure when he succeeded in synthesizing heme from pyrrolic starting materials **[31]**.

The unsubstituted porphyrin macrocycle consists of four pyrrole type residues, linked together by four methine bridging groups. Carbons on the pyrrole fragments are the α-positions or the β-positions, and the carbon atoms bridging the pyrroles are the *meso*-positions **[31]**. Substitution occurs on β and *meso* carbons.

1.2.2. Synthesis of *meso*-tetra porphyrins

The synthetic world of porphyrins is extremely rich and its history began in the middle of 1930s. In principle, there are many chemical strategies to synthesize porphyrins, involving different building blocks, like pyrroles, aldehydes, dipyrromethanes, dipyrromethenes, tripyrranes and linear tetrapyrroles. Tetraphenyl phorphyrins are employed in this work, hence they are discussed below.

The first synthesis of tetraphenylporphyrin was achieved by Rothemund in 1936 **[32]**. He reacted benzaldehyde and pyrrole in the presence of pyridine in a sealed tube at 220 ^{o}C for 48 hours; resulting in a tetraphenylporphyrin (9% yield) that was isolated as deep-purple sparkling crystals (Scheme 1.1 A) **[32]**. In addition to the low and irreproducible yields, the most severe limitation of the Rothemund synthesis was the harsh reaction conditions, which resulted in failure with all but a small selection of rather inert aldehydes **[32]**. This resulted in finding better synthetic routes for porphyrins which was carried out by Alder *et al* **[33]**.

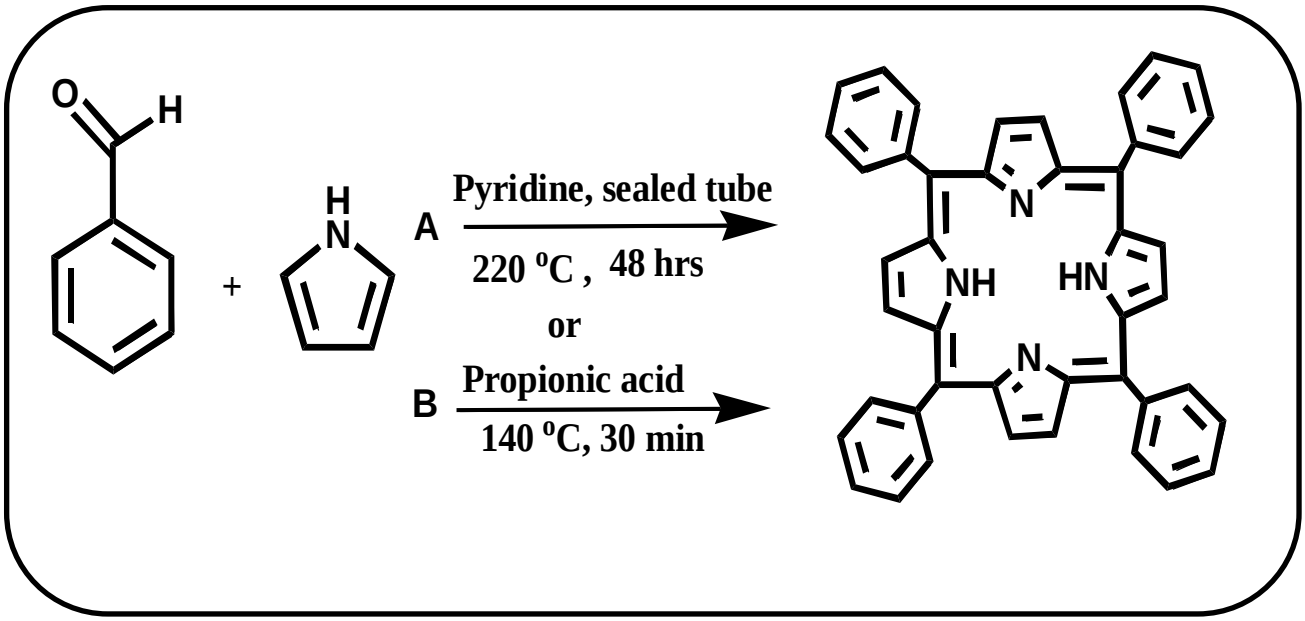

Scheme 1.1: Rothemund (A) and Alder *et al* (B) Synthetic routes.

Adler *et al* altered Rothemund's synthesis by reacting benzaldehyde with pyrrole in propionic acid for 30 mins at reflux temperature, in a system that was open to air, Scheme 1.1B. The milder conditions of the Adler *et al* reaction meant that substituted benzaldehydes can be converted to their corresponding porphyrins in high yields **[33]**.

Unsymmetric porphyrins can also be made in this way by using two or three different benzaldehydes; however extensive column chromatography is needed in order to separate the products. If acid sensitive functional groups on the benzaldehyde are present, porphyrins can not be made in this way and this problem was addressed by Lindsey *et al* in 1987 **[34]**.

The Lindsey method relies on the formation of porphyrinogen as an intermediate in porphyrin synthesis **[34]**, Scheme 1.2. A chemical oxidant, for example 2,3,dichloro-5-6-dicyanobenzoquinone (DDQ), which is hydrogenated to 2,3,dichloro-5-6-dihydroxyphthalonotrile is added to convert the porphyrinogen to the corresponding porphyrin. The advantages of this method are that it allows functional groups that are acid sensitive to be introduced, as well as allowing more facile purification and higher yields.

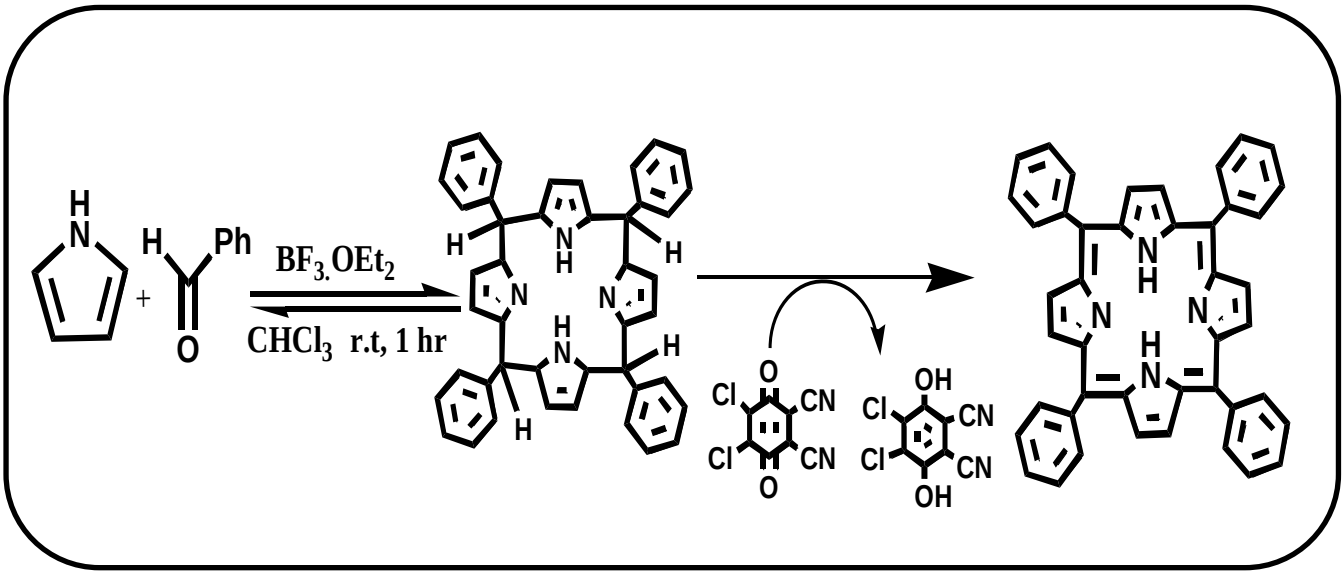

Scheme 1.2: Lindsey synthetic route.

1.2.3. Examples of *meso*-tetra porphyrins used for PACT.

Applications of porphyrins are extensive mainly as molecules of life **[35, 36]**. In this work we will concentrate on those molecules being used for PACT. Table 1.1 shows porphyrins which have been used for PACT **[3, 37-41]**. As this table shows porphyrins have been used mainly for bacteria such as *E. coli* but not fungi. Antibiotic resistance bacteria such as *S. aureus* have not been studied hence in this work, PACT on *E. coli* is compared to *S. aureus* and *C. albicans*. In addition porphyrins studied contained central metals such as Mn, Pd which do not efficiently produce excited triplet state. Metal free porphyrins were also employed. This work uses Ga as a central metal, which produces triplet excited state in good yield hence more reactive oxygen species (ROS). Table 1.1 also shows the porphyrin used in this work, the COOH enhances water solubility therefore making studies in biological media easy. Complex **1** and **2** contain terminal carboxy phenoxy groups, but **2** has a spacer between the porphyrin ring and the phenoxy group. The effect of the spacer on PACT will be discussed.

Table 1.1: Examples of known *meso*-tetra porphyrins that have been used for PACT.

Compound	Microorganism	Reference
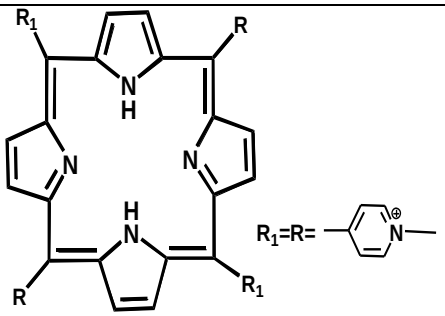 meso-tetra (4-N-methyl-pyridyl)porphine tetraiodide, T_4(4-N-MePy)P	*E. coli* *Acinetobacter baumannii* *Enterococcus seriolicid.* and *Vibrio anguillarum*	**[37,38]**
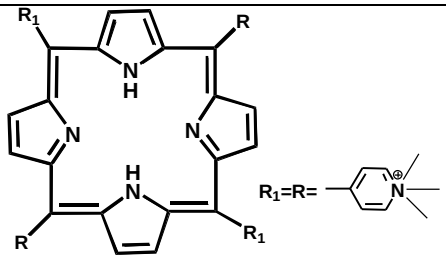 5, 10, 15, 20-tetra (4-N, N, Af-trimethyl-anilinium) porphyrin (T_4MAP) 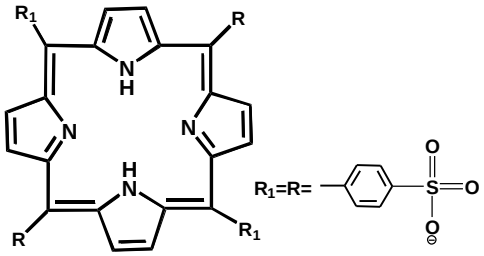 5, 10, 15, 20-tetra (4-sulphonatophenyl) porphyrin ($TPPS_4$)	*Dinococcus radiodurans* *E. coli* *Enterococcus seriolicida* and *Vibrio anguillarum*	**[3, 38]**
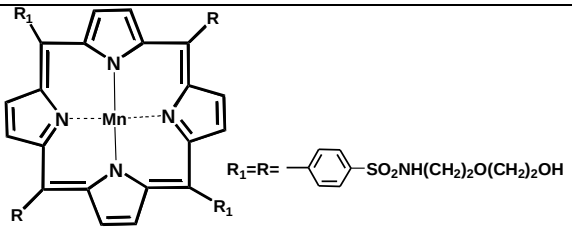 Mn-5,10,15,20-Tetra(4-N-ethoxyethanolsolfonamidophenyl)-porphyrin (MnTEtOHSPP)	*E.coli, Pseudomonas aeruginosa* and *S. aureus*	**[39]**

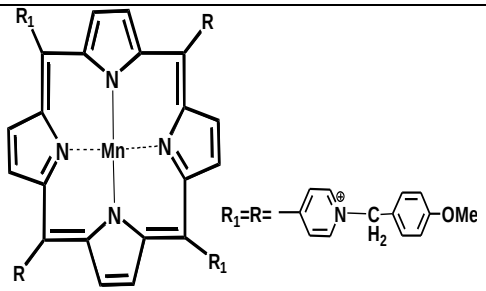 Mn-5,10,15,20-Tetra(N-(4-methoxybenzyl)-4-pyridyl) porphyrin etrachloride (MnTMBPyP)		
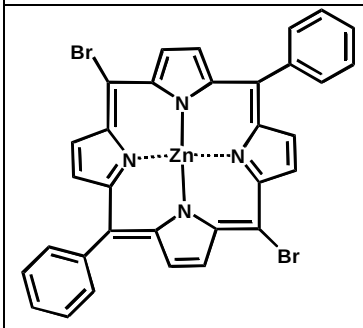 Zinc-5,15-dibromo-10,20-diphenylporphyrin ($ZnDPPBr_2$)	*S. aureus, E. coli, Enterococcus faecalis, Bacillus anthracis* and *Saccharomyces cerevisiae.*	**[40]**
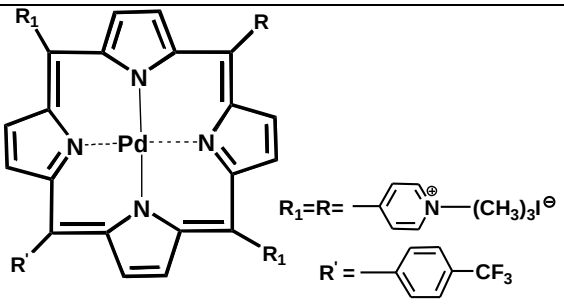 Palladium 5-(4-trifluorome- thylphenyl)-l0,15,20-tris(4-trimethylammoniumphenyl)porphyrin odide (PdTFPP)	*E. coli*	**[41]**
Conjugated to Platinum nanoparticles		
1 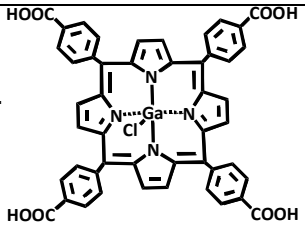 ClGa(III) 5,10,15,20-tetrakis-(4-carboxyphenyl) porphyrin (ClGaTCPP)	*S. aureus*	Synthesised in this work

2 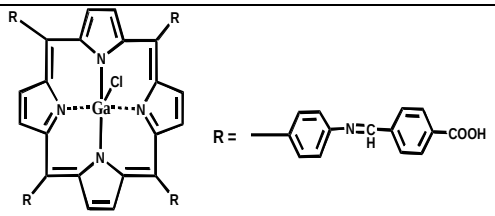 Chloro - (5,10,15,20-tetrakis (4- (4- carboxyphenycarbonoimidoyl) phenyl) porphyrinato) gallium(III) (ClTCPIPPGa)	*E. coli, S. aureus* and *C. albicans*	Synthesised in this work

1.3. Phthalocyanines (Pcs)

Phthalocyanines (Pcs) are a class of synthetic tetrapyrrolic compounds, similar in structure to porphyrins **[42]**. The structural differences between a Pc and porphyrin macrocycles are the four extended benzo subunits and four nitrogen atoms at the meso position on the macrocycle of Pcs (Fig 1.4 and Fig 1.5). Pcs are often referred to as tetra-benzotetraazaporphyrins and are a unique set of organic pigments that provide stable and strongly blue and green colours **[43]**.

1.3.1. History and discovery

Phthalocyanines (Pcs) were first discovered accidentally by Braun and Tcherniac as by-products during the synthesis of *o*-cyanobenzamide from phthalamide **[36, 44]**. These complexes were observed as unknown insoluble bluish compounds which were later identified as metal-free Pcs **[45, 46]**. The first copper phthalocyanine was synthesized by de Diesbach and coworkers in 1927 when they tried to convert o-dibromobenzene into phthalonitrile but its structure was not correctly formulated **[35]**. Later Linstead clarified the structure **[45]**. In 1928 an iron Pc was also accidentally discovered, when a blue product was found in a reaction flask where only a white product was expected at the Scottish Dyes Ltd **[46, 47]**. At a later stage this structure was confirmed by X-ray crystallography in 1935 by Robertson, showing that the phthalocyanine molecule is a rather

planar molecule with chemical formula $C_{32}H_{18}N_8$ for the metal-free Pc **[48, 49]**.

1.3.2. Structure and applications of phthalocyanines

Phthalocyanines are conjugated, aromatic molecules that have 32 carbons, 8 nitrogens, 16 hydrogens at the periphery, and 2 hydrogens in the center of the ring for metal free. The hydrogens can be substituted upon addition of a central metal ion (Fig. 1.5) **[50]**. This structure was described as having inner aromatic ring which is responsible for the intense blue-green colour (as stated previously) of the macrocyclic. The presence of four benzene rings causes solubility and aggregation problems, adding functional groups on these benzene rings can overcome these problems **[50-52]**.

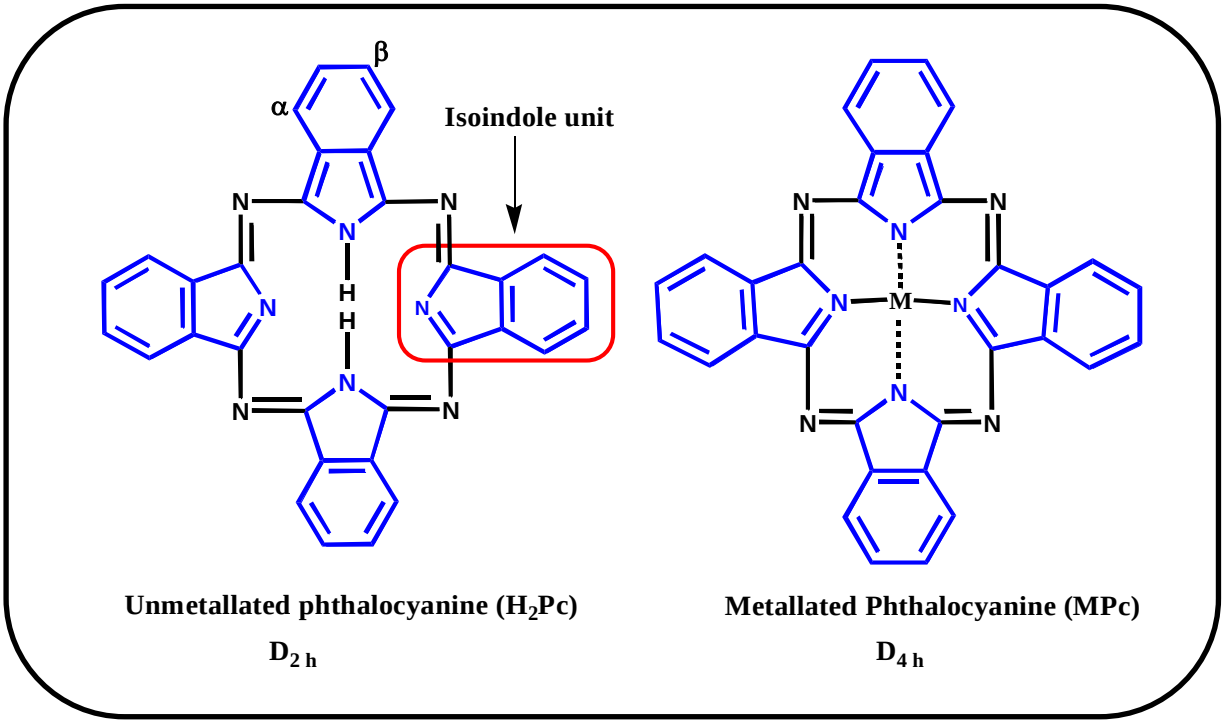

Figure 1.5 Structure of metallophthalocyanine

Pcs derivatives have gained importance in different fields including their use as photosensitizers **[53]**. The effectiveness of these derivatives as PDT agents

is due to their high absorption in the phototherapeutic window (600-800 nm) coupled with a long triplet lifetime to generate cytotoxic singlet oxygen ($^1O_2$). A large number of photosensitizers have been tested *in vivo* and *in vitro* in PDT experiments but very few have proven to be ideal for PDT **[53]**.

1.3.3. Examples of phthalocyanine used for PACT.

A section of phthalocyanines which have been used for PACT are shown in Table 1.2 **[54-68].**

Table 1.2: Examples of known phthalocyanine that have been used for PACT

Compound	Microorganism	Reference
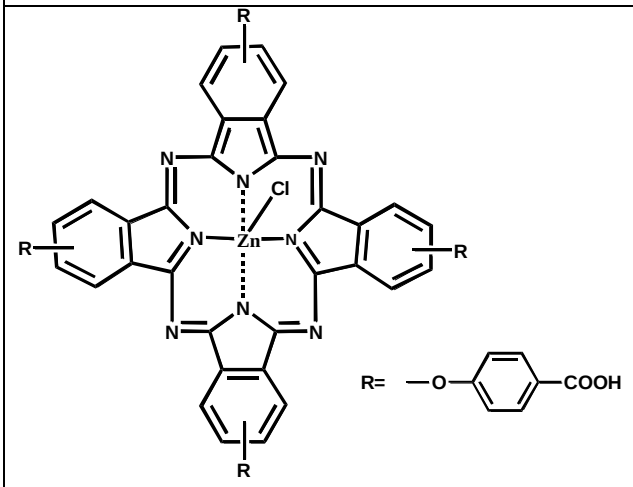 Zinc tetraphenoxy carboxy phthalocyanine (ZnTPCPc)	*S. aureus*	**[54]**

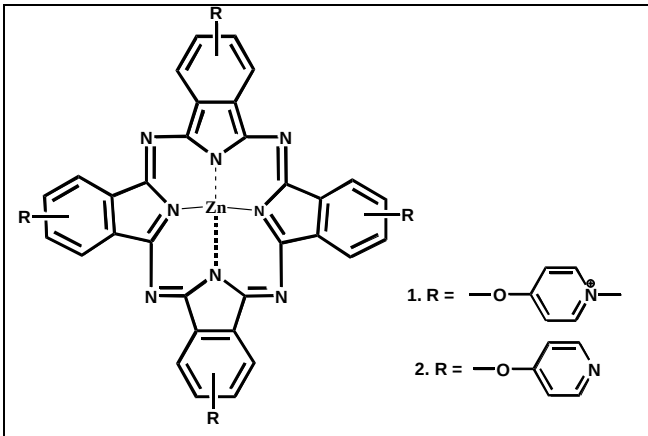 **1. Zn(II) N-methylpyridyloxyphthalocyanine (ZnTmPyPc)** **2. Zn(II) pyridyloxyphthalocyanine (ZnTPyPc)**	*E. coli*	**[55]**
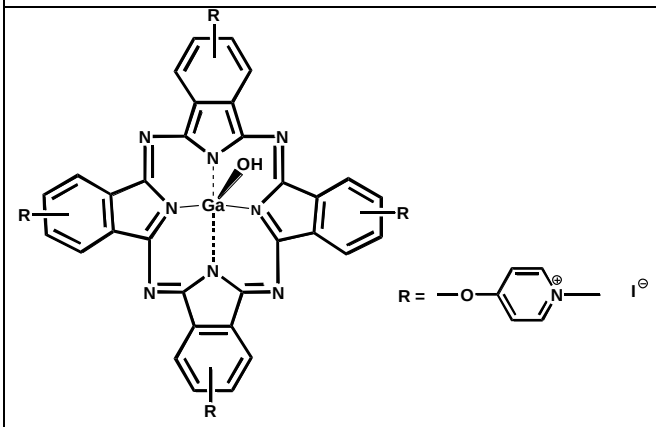 **Hydroxygallium(III) 2,9,16,23-tetrakis[3-(N-methyl)pyridyloxyl]-phthalocyanine tetraiodide (GaTMPyPc)**	*S. aureus,* *C. albicans* *Pseudomonas aeruginosa* and *Enterococcus faecalis*	**[56]**
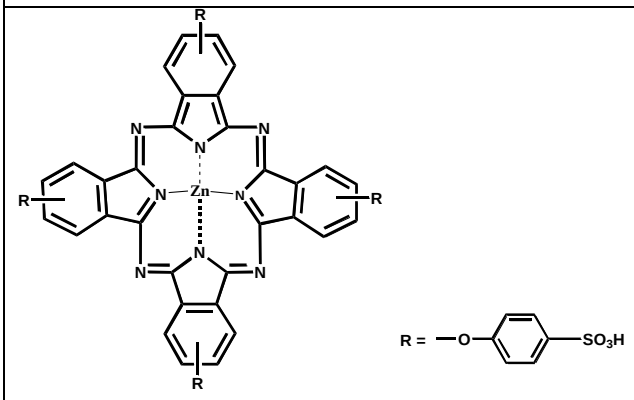 **Tetrakis-(4-sulfophenoxy)-phthalocyanine zinc(II) (ZnTSPPc)**	*S. aureus* *Pseudomonas aeruginosa* *C. albicans*	**[57]**

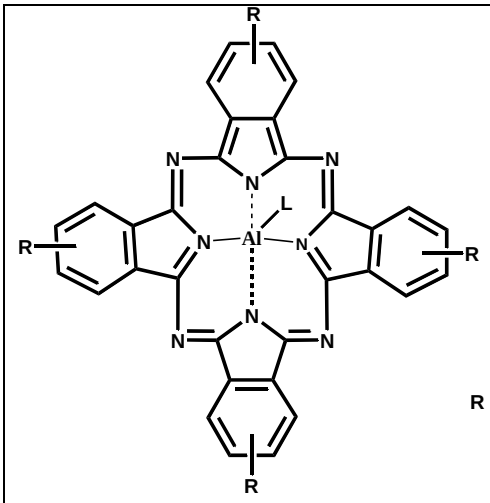 **Tetrasulphonated aluminium phthalocyanine (AlTSPc)**	*S. aureus* *Streptococcus sanguis* *Magnaporthe grisea*	**[5, 58]**
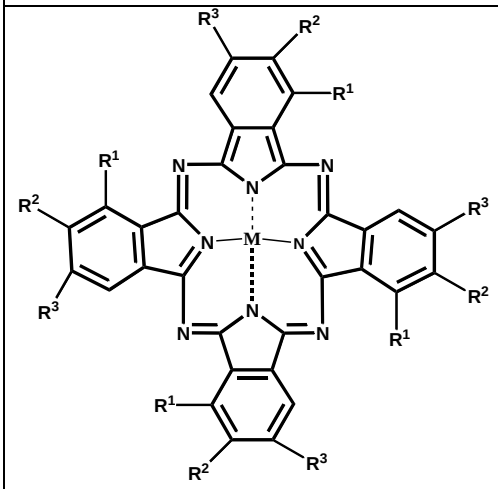 **Phthalocyanine metal complexes (PcMC)**	*Peronosclerospora sorghi* *Magnaporthe grisea*	**[58]**
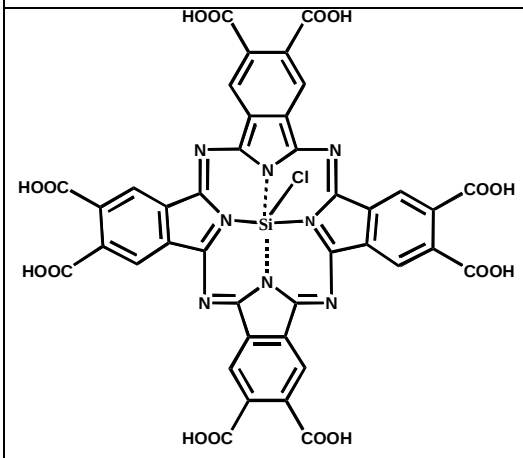 **3** **Octacarboxy siliconphthalocyanine (SiOCPc)**	*C. albicans* and *E. coli*	Synthesised in this work
Conjugated to Platinum complex		

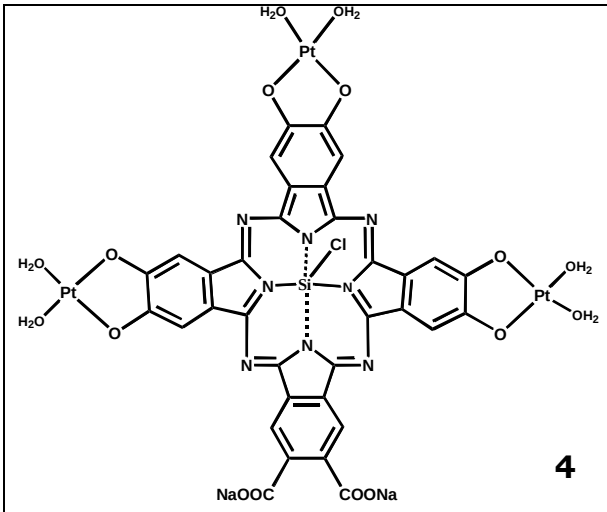 **4** dihydroxosilicon tris(diaquaplatinum)octacarboxyphthalocyanine $(OH)_2SiOCPc(Pt)_3$)	*C. albicans* and *E. coli*	Synthesised in this work

As Table 1.2 shows central metals used are Zn, Al, Co, Cu, Fe and Ga. Co, Cu and Fe are not appropriate for PACT due to their paramagnetic nature which shortens their triplet state, hence they produce low ROS. Al is too small hence encourages fluorescence rather than intersystem crossing (ISC) to triplet state. Zn and Ga Pcs used have been positively charged but as stated above negatively charged Pcs are useful for Gram (+) and fungi such as *C. albicans*. Hence in this work SiPc containing carboxyl substituent which is negatively charged is employed for Gram (+), Gram (-) bacteria and fungi. Table 1.2 also shows the Pcs used in this work, complexes **3** and **4**. The Pcs are used alone or in the presence of external Pt nanoparticles for heavy atom effect. In addition platinated Pc (**4**) is employed.

1.3.4. Synthesis of octacarboxy phthalocyanines

The synthesis of octacarboxy Pcs can be achieved by cyclotetramerisation of phthalonitrile (**5**) precursors in the presence of a metal salt (for metallated phthalocyanine (MPc)) and a catalyst (1, 8-diazabicyclo [5.4.0]undec-7-ene (DBU)). MPc can also be obtained by the use of phthalimides, phthalic acids and other precursors such as pyromellitic dianhydride (**6**) using urea as a solvent and nitrogen source **[59]** Scheme 1.3. Water solubility of

phthalocyanines can be achieved by introduction of substituents such as carboxylic **[59]**, sulfonic and phosphonic acids groups on the periphery of the Pc ring, either for octasubstitution or tetrasubstitution **[60-62]**.

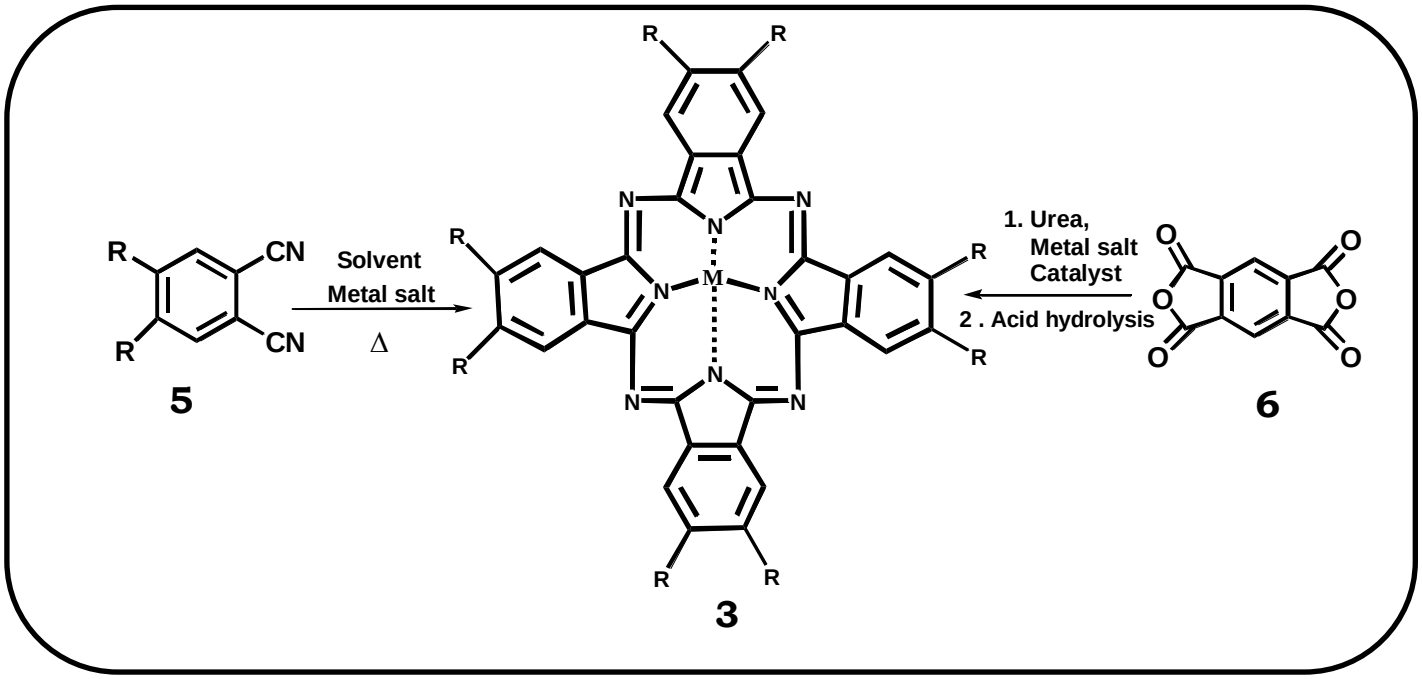

Scheme 1.3: Synthesis of octacarboxy phthalocyanines [56].

Octacarboxy Pcs have been linked to Pt complexes for different applications. Platinated cobalt Pc **[63]**, zinc Pc **[64]** and aluminium Pc **[65]** have been synthesised for PDT application. Platinated iron Pc **[66]** has been of high interest in the electrocatalysis, energy storage and conversion systems field. In this work octacarboxy Pcs was linked to Pt complex for PACT applications.

1.4. Electronic absorption spectra of porphyrins and phthalocyanines

The absorption spectrum of porphyrins and phthalocyanines has long been understood in terms of the Gouterman's four-orbital model **[67-71]**. In this model the two highest occupied molecular orbitals (HOMO) and lowest unoccupied molecular orbitals (LUMO) model are taken into account **[71]**.

Generally, porphyrins are characterized by an intense band called the Soret or B band at about 400 nm. The Q bands are observed between 500-600 nm **[72-74]**, and four are observed for metal free (Fig.1.6 Black). In the presence of a central metal, the Q bands are reduced (Fig. 1.6 Red) **[74, 75]**

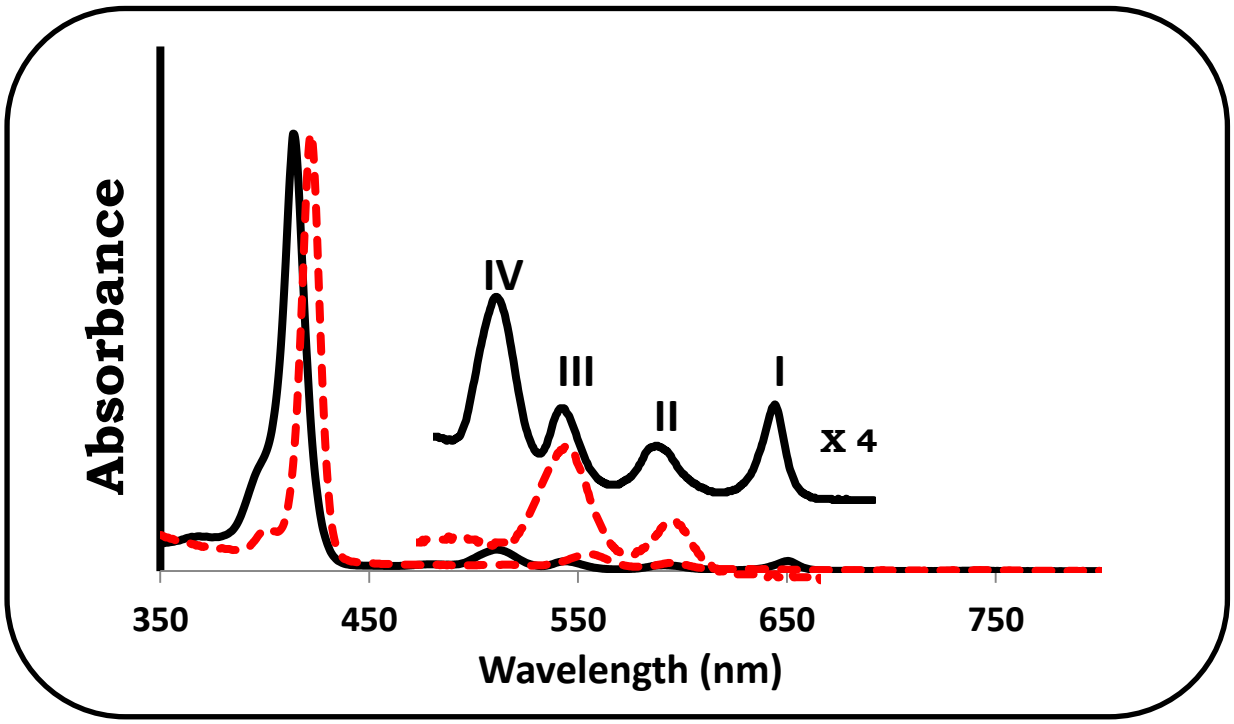

Figure 1.6: Ground state electronic absorption spectra of metallated (red) and unmetallated (black) porphyrin.

Phthalocyanines are characterized by an intense and isolated absorption band in the red region of the electromagnetic spectrum **[76]** which is called the Q-band, Fig. 1.7. The B-band appears in the region between 300 - 400 nm and is a less intense band when compared to the Q-Band. The B-band is broad due to the overlapping of the B_1 and B_2 bands (Fig. 1.8). Other absorption bands such as N, L, and C are also present at high energy in transparent solvents for example chloroform **[77, 78]**.

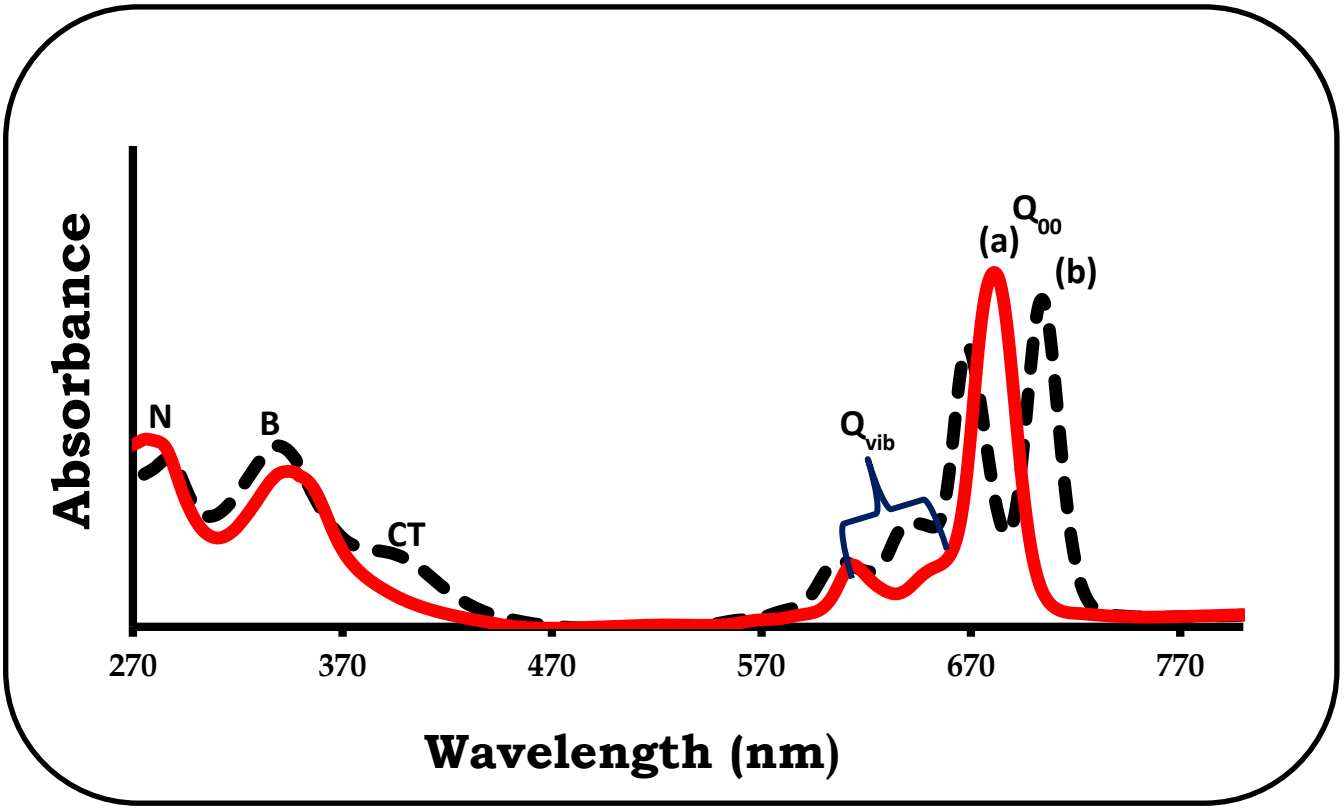

Figure 1.7: Ground state electronic absorption spectra of metallated (red) and unmetallated (black) phthalocyanines.

The absorption bands in porphyrin systems arise from transitions between two HOMOs and a LUMO Fig. 1.8. The HOMOs are a_{1u} and an a_{2u} orbital, while the LUMO is degenerate set of e_g orbitals **[73]**.

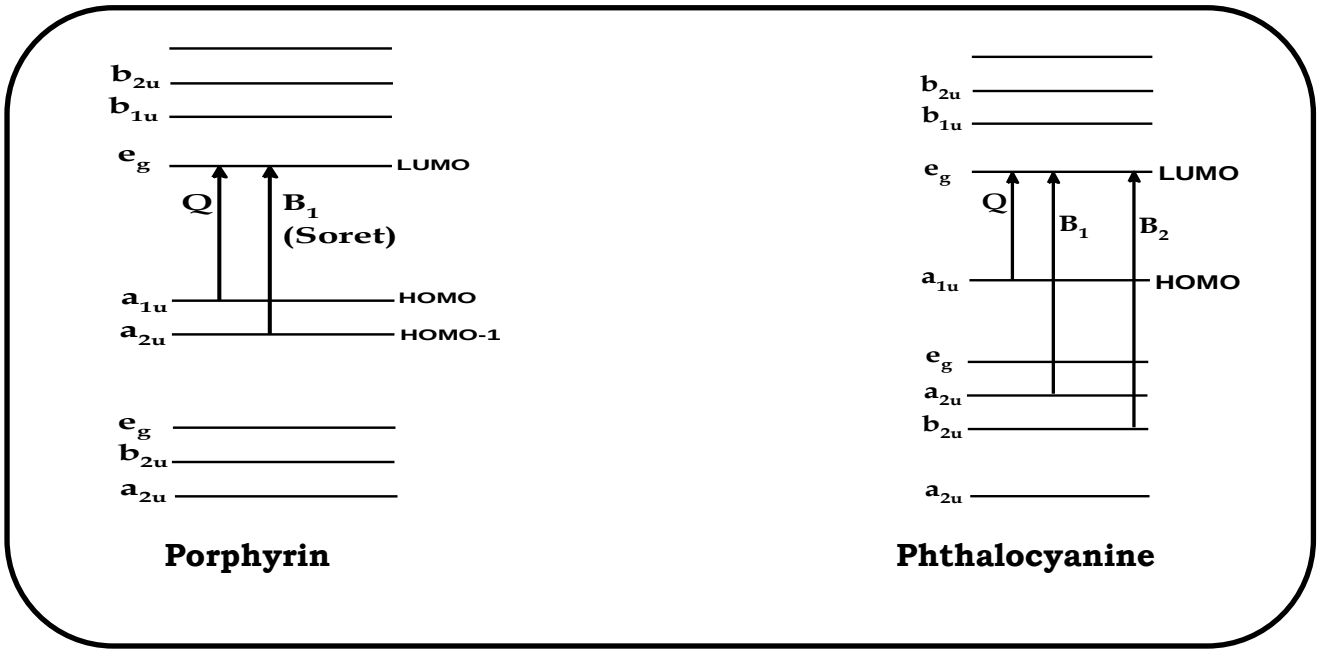

Figure 1.8: Electronic transitions in porphyrins and MPcs showing the origin of Q and B (Soret) absorption bands.

The Q-band absorption in Pcs is due to a transition from the a_{1u} of the HOMO to a doubly degenerate transition e_g of the LUMO, while a transitions that are from a_{2u} or b_{2u} to the e_g of the LUMO result in the B-band absorptions **[71]** Fig. 1.8. For H_2Pc, the Q band splits into a two (Fig. 1.7). This splitting of the Q band is due to the low symmetry (D_{2h}) of H_2Pc in comparison with metallophthalocyanine (D_{4h}). The LUMO orbital loses degeneracy due to the presence of the two core protons giving rise to a split Q- band **[67-70]** in H_2Pc, Fig 1.7.

1.5. Metal Nanoparticles (MNPs)

"Nano" is a Greek word synonymous to dwarf meaning extremely small **[79]**. Nanoparticles (NPs) are small clusters of atoms that are made from inorganic or organic materials and have sizes in the range of 1-100 nm **[80, 81]**. Metallic NPs have unique optical, electronic, chemical and magnetic properties that are very different from those of the individual atoms and their bulk counterparts **[82, 83]**. In the last few decades metal nanoparticles have been of great interest due to the novel properties that are associated with their reduced dimensions **[84, 85]** and have found wide range of applications for example in catalysis **[86, 87]**, electronics **[88, 89]**, photonics **[90]**, optoelectronics **[91]**, information technology **[92]**, sensing **[93]** as well as medicine **[94]**.

1.5.1. Properties and application of platinum nanoparticles

Platinum nanoparticles (PtNPs) have been intensively investigated because of their promising technological applications in catalysts, sensors, nanoscale devices **[95]** and medicine **[96]**. Platinum is one of the rarest and most expensive metals. It has high corrosion resistance and numerous catalytic applications including automotive catalytic converters and petrochemical cracking catalysts **[97]**. PtNPs are usually used in the form of colloid or suspension in a fluid. PtNPs are an important catalyst for fuel-cell reactions where they catalyse hydrogen oxidation at the anode and oxygen reduction at the cathode **[97]**. They have been the subject of extensive research due to their antioxidant and medicinal properties (such as bactericidal) **[96, 98]**. PtNPs are known to inactivate microbes by interacting with their enzymes, proteins or DNA. PtNPs restrain cell proliferation or cell division. PtNPs also has the ability to bind to negatively-charged bacterial cells changing the functionality of the cell membrane therefore preventing bacterial generation **[96]**.

1.5.2. Synthesis of platinum nanoparticles

Generally PtNPs are synthesised by the reduction of platinum salts by hydrogen, photochemical, pulsed-radiolytical, or thermal methods **[99]**. The method used in this work involves the reduction of platinum salt in the presence of 1, 2-hexadacanediol as well as oleylamine and oleic acid Scheme 1.4. Oleylamine is not only used as a stabilizer but also as a capping agent **[95]**. It has been generally accepted that a capping agent could selectively stick to certain nanoparticles, therefore ensuring slow growth as well as preventing particle agglomeration and providing stability to the resulting nanoparticle **[100]**. It has also been accepted that the surfactants which act as structure directing agents **[100]**.

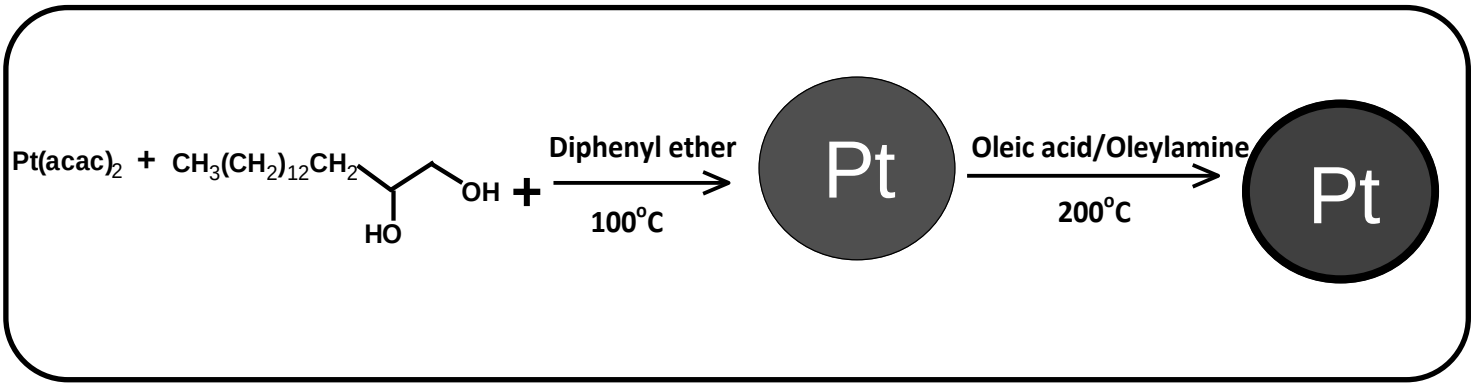

Scheme 1.4: Synthetic route of PtNPs

NPs can be characterized by several methods including x-ray diffractometry (XRD) and transmission electron microscopy (TEM) which are used in this work, hence discussed. The crystal structure and the size of PtNPs can be determined using XRD, Fig. 1.9. The PtNPs are characterized by their face centered cubic (FCC) lattice crystal structure with hkl Miller indices at (111), (200), (220), (311) and (222) corresponding to their 2θ values at 39.86°, 46.44°, 67.69°, 81.56° and 86.09° respectively **[97, 101]**.

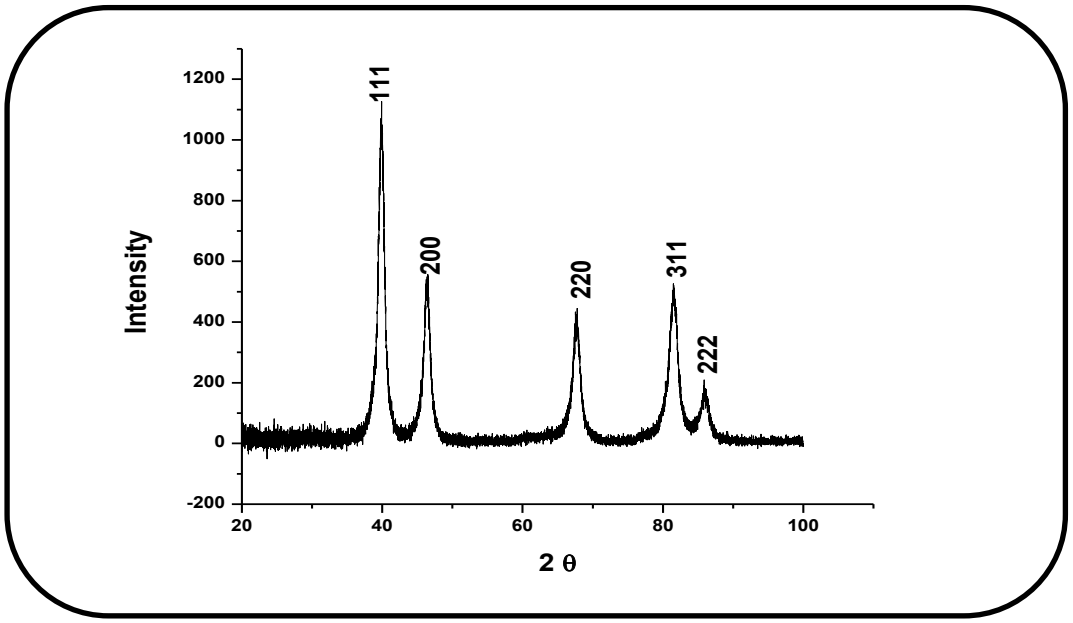

Figure 1.9: X-Ray diffractograms of PtNPs [101]

The crystal size is calculated from XRD pattern (Fig. 1.9) using the Debye Scherrer equation 1.1 **[102]**:

$$L = \frac{0.9\lambda}{BCos\theta} \qquad (1.1)$$

where λ is the X-ray wavelength in nanometer (nm), β is the peak width of the diffraction peak profile at half maximum height in radians.

Further confirmation of the nanoparticles size can be done using TEM **[103]**. This technique is used to help visualize the shape of the nanoparticles, size distribution and their dispersion **[103]**, as shown in Fig.1.10.

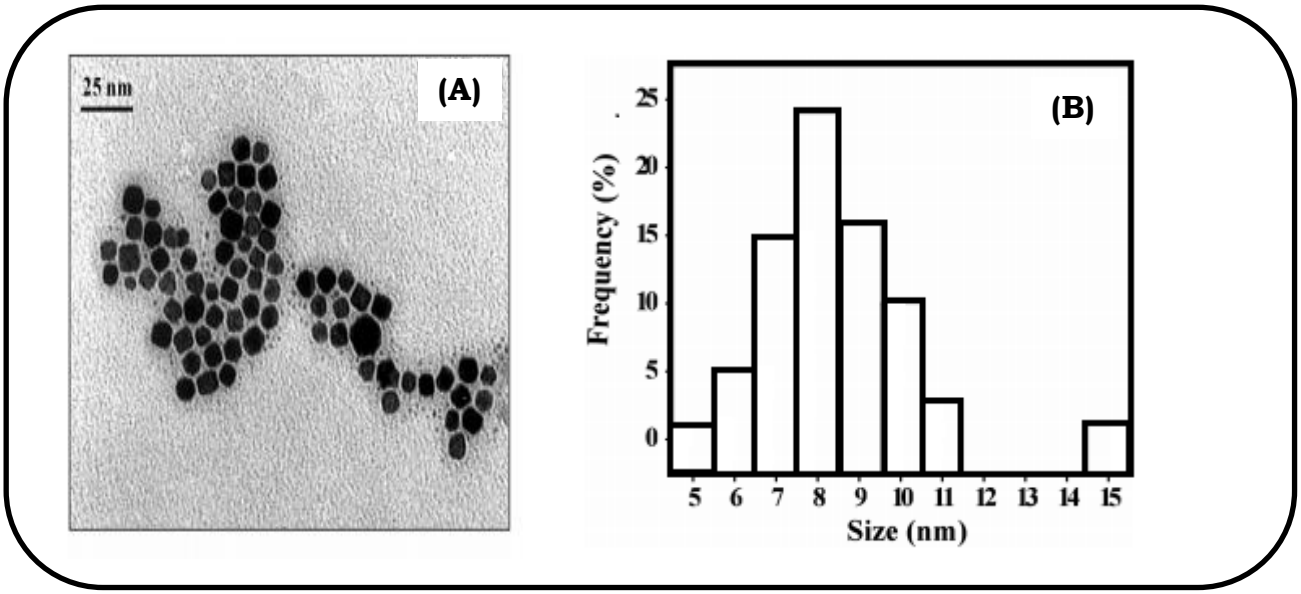

Figure 1.10: TEM image of PtNPs (A) and size distribution histogram (B) [103].

Porphyrins have been conjugated to platinum complexes for antitumor activity **[104]** but not to PtNPs. This work also involves the conjugation of PtNPs to porphyrins for antimicrobial activity. Gallium tetra – (4-carboxyphenyl) porphyrin **1** and chloro - (5,10,15,20-tetrakis (4- (4-carboxyphenycarbonoimidoyl) phenyl) porphyrinato) gallium(III) **2** were conjugated to PtNPs for the first time. The porphyrins alone or in the presence of PtNPs are then electrospun into fibers; while Pcs (**3** and **4**) Table 1.2 were employed only in solution for PACT.

1.6. Electrospinning

The concept of electrospinning was first proposed around the 20th century. In 1914 Zeleny described the principles of electrospinning **[105]** and then in 1969 Taylor brought the fundamental concepts of the Taylor cone, and the voltage values at which Taylor cones are formed **[106]**. Electrospinning is currently the most widely used method for the production of polymeric nanofibers because of its simplicity, cost-effective and suitability to yield very long fibers from various polymers and composite materials **[107]**.

1.6.1 Basics of electrospinning

Electrospinning is a technique that generates fibers with diameters in micro- and nanometer scale through an electrically charged jet of the polymer solution **[108, 109]** and the general electrospinning set-up is shown in Fig. 1.11. The electrospinning process is highly flexible since various parameters such as solution concentration and molecular weight of the polymer **[110]** can be varied as to obtain fibers of different diameters to meet the requirements for various applications **[111].** These applications include filtration **[112]**, composites **[113]**, scaffolds **[114]** and medical applications **[115]**. The main advantages of electrospun fibers, besides their small fiber diameter, are their high porosity **[116]**, small pore sizes and high specific surface areas **[117]**.

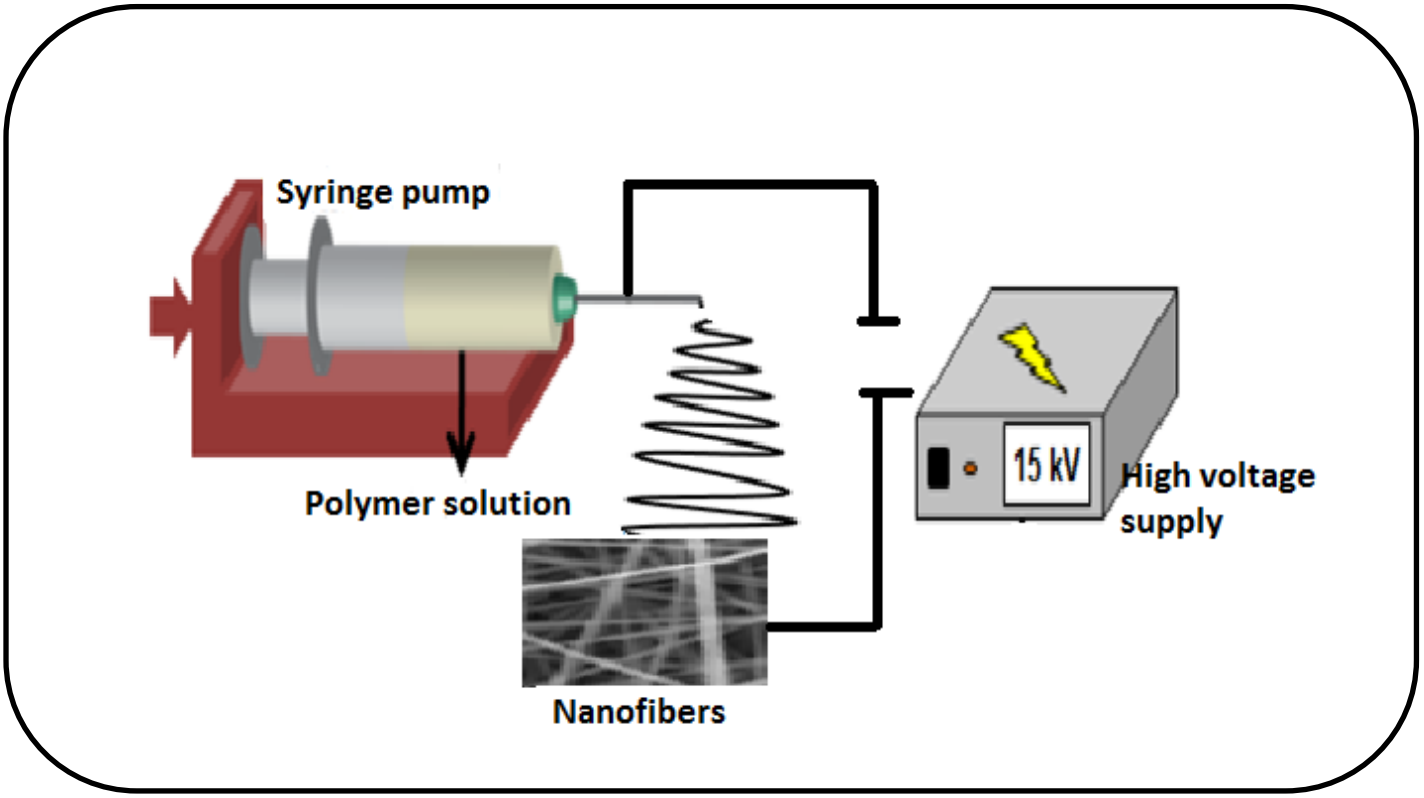

Figure 1.11: Schematic diagram of an electrospinning set-up [118].

In an ordinary electrospinning process a polymer solution is pumped through a thin nozzle where the nozzle simultaneously serves as an electrode where high electric field is applied **[118, 119]**. The current that flows during the process ranges from hundred nanoamperes to microamperes. The substrate on which the electron fibers are collected is typically brought into contact with the counter electrode. The applied voltage causes a cone-shaped deformation of the drop of the polymer solution in the direction of the counter electrode as the solvent evaporates, and the solid fibres are precipitated on the counter electrode **[118]**.

The shape and dimensions of the fibres that are formed are mostly dependent on parameters; for example the properties of the polymer itself (in this, work polystyrene was chosen) and properties of the polymer solution (viscosity, concentration, surface tension). The vapour pressure of the solvent and the relative humidity of the surroundings can also have significant impact **[118]**.

Various characterization techniques have been introduced to understand the basic properties of electrospun fibers including the morphology (fiber diameter, porosity), molecular structure and mechanical properties.
Scanning electron microscopy (SEM) (Fig. 1.12) and transmission electron microscopy (TEM) are valuable techniques in understanding fiber morphology and both techniques yield two-dimensional representations of electrospun fibers and pores **[120,121]**.

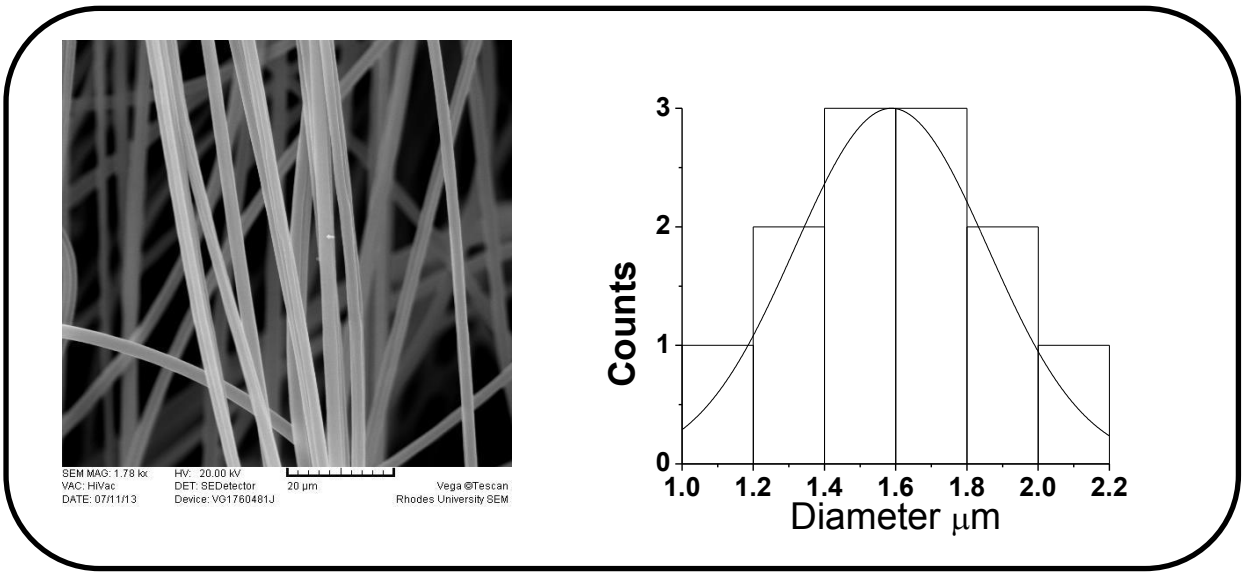

Figure 1.12: Scanning electron microscopic (SEM) images of polystyrene electrospun fiber with the size distribution histogram [120].

1.6.2. Polymer used.

Polystyrene (PS) is a thermoplastic amorphous, stiff polymer with limited flexibility**.** It is considered to be one of the most versatile, easily fabricated, and cost-effective plastics **[107]**. It is used in many different applications including packaging for food, disposable cutlery, plastic models, packing materials, insulation, and disposable beverage cups **[107]**.

Polystyrene (PS) was chosen in this work because of its aromatic system (Fig.1.13) which allows for π-π electronic interactions between the aromatic systems of the porphyrin or Pc and the polymer, hence preventing the leaching of the porphyrin or Pc from the polymer **[122]**.

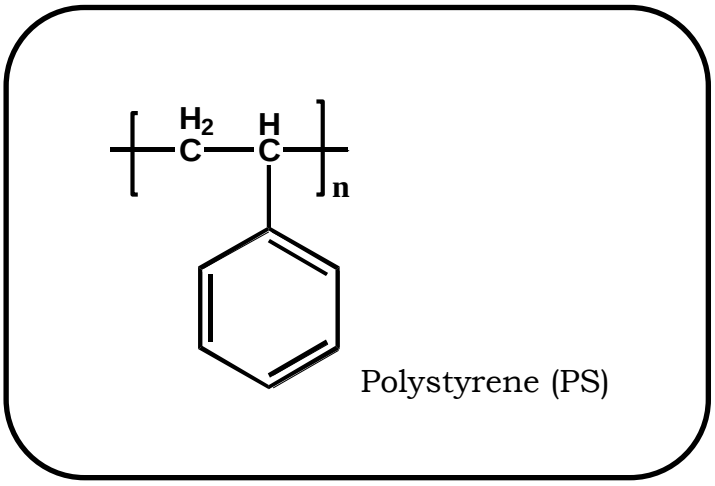

Figure 1.13: Structure of polymer used in this work.

For fiber applications to be more successful, electrospun polymer fibers must be functionalized because they are chemically inert and do not have specific functions. Therefore photosensitizers may be immobilized on polymer fiber supports allowing their reuse and recycling.

Incorporation of porphyrin and Pc into electrospun polymer fibers has been reported with the properties of both molecules still maintained within the fiber matrix **[122-124]**, Table 1.3. This work reports for the first time the incorporation of porphyrin conjugated to PtNPs and electrospun into polymer fibers.

Table 1.3: Examples of known polystyrene electrospun nanofibers functionalized with porphyrin/ Porphyrin-PtNPs conjugate and phthalocyanine for PACT

Compound	Microorganism	Reference
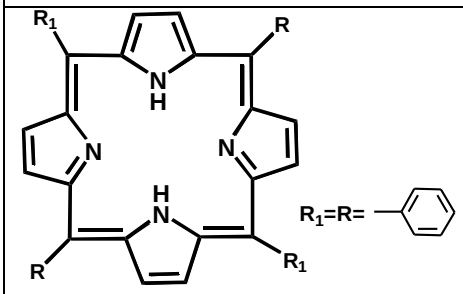 5,10,15,20-tetraphenylporphyrin (TPP)	*E.coli*	**[122]**
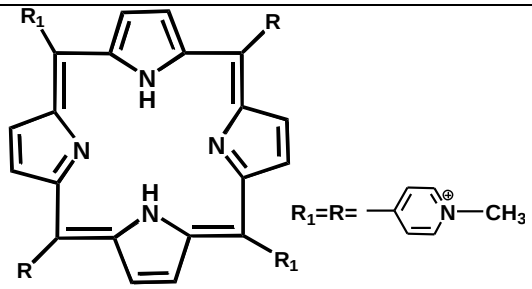 5,10,15,20-tetrakis(1-methylpyridnium-4-yl)porphyrin (TMPyP)	*E. coli*	**[123]**
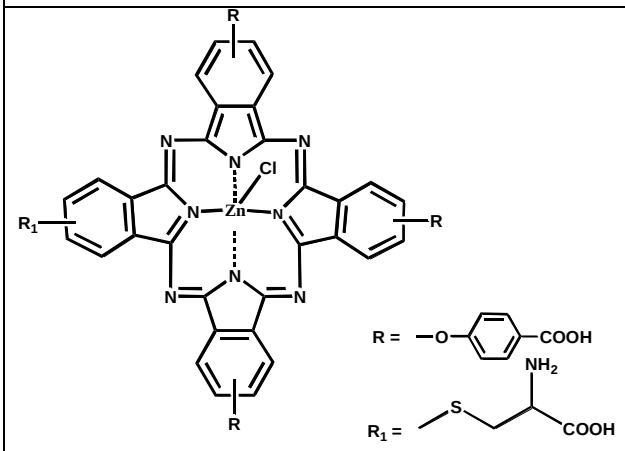 Tris{9 (10), 16 (17), 23 (24)-(4-phenoxy)-2-(4-cysteinyl) phthalocyanine} Zn (ZnMCsPc)	*S.aureus*	**[54]**

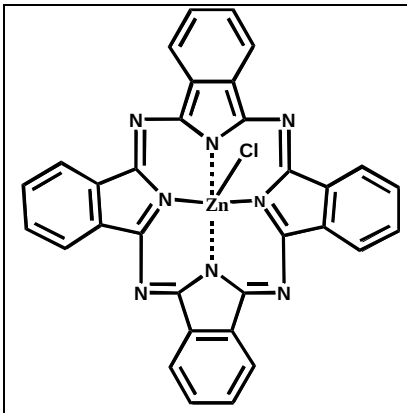 Zinc phthalocyanine (ZnPc)	*E. coli*	**[124]**
Nanofibers functionalized with Porphyrin-PtNPs conjugate		
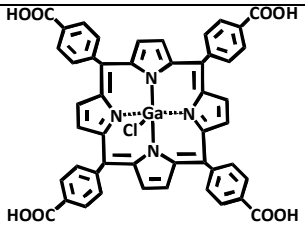 ClGa(III) 5,10,15,20-tetrakis-(4-carboxyphenyl) porphyrin (ClGaTCPP)	*S.aureus*	Synthesised in this work
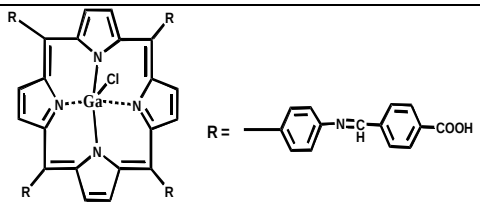 Chloro - (5,10,15,20-tetrakis (4- (4- carboxyphenycarbonoimidoyl) phenyl) porphyrinato) gallium(III) (ClTCPIPPGa)	*C. albicans, E. coli* and *S. aureus*	Synthesised in this work

1.7. Summary of Aims for this thesis.

The aim of this work is the fabrication of multi-functional nanocomposites which are based on porphyrins, phthalocyanines and platinum nanoparticles. Therefore the combination of these different types of functional nanostructured materials enables the development of multi-functional nanomaterials to be used as antimicrobial agents for photodynamic antimicrobial chemotherapy.

Aims in point form.

- Syntheses of tetra-*meso* substituted porphyrin, silicon octacarboxy phthalocyanine (SiOCPc) and platinum nanoparticles (PtNPs)
- Conjugation of PtNPs to porphyrin
- Conjugation of platinum complex to SiOCPc.
- Characterization of the porphyrin-PtNPs and SiOCPc-platinum conjugates using ultraviolet-visible spectroscopy (UV/Vis), Fourier transform infrared spectroscopy (FTIR), X-ray diffractometer (XRD), transmission electron microscopy (TEM)
- Study the fluorescence and photochemical properties of the conjugates.
- Optimization of elecrospinning parameters of polystyrene.
- The development of electrospun fibers containing of porphyrin and porphyrin-nanoparticles conjugate.
- Characterization of the electrospun fibers using scanning electron microscopic (SEM).
- Investigation of the antimicrobial activity of these complexes.

CHAPTER TWO

Experimental

2. Experimental

This chapter reports on all the experiments procedures that were carried out in this work. This includes all the synthetic procedures and methods of characterization for all complexes used in this work.

2.1. Materials

2.1.1 General reagents and Solvents

Dimethylformamide (DMF), isopropanol, diphenyl ether, pyrrole, DMSO-d_6, acetone-d_6 and anthracene-9,10-bis-methylmalonate (ADMA) were purchased from Sigma. Tetrahydrofuran (THF), was purchased from MERCK. Methanol (MeOH), ethanol, ethylacetate, hexane and propionic acid were purchased from Saarchem. Ultra-pure water was obtained from a Milli-Q Water System (Millipore Corp., Bedford, MA, USA).

2.1.2 Reagents for the synthesis of porphyrin and their conjugates to PtNPs

The metal free 5,10,15,20-tetrakis-(4-carboxyphenyl) porphyrin (H_2TCPP) was synthesized according to literature **[125]**. 4–Formyl benzoic acid, gallium (II) chloride and N,N-dicyclohexalcarbodiimide (DCC) were purchased from Sigma. Tetrakis-5,10,15,20-(4-aminophenyl) porphyrin (H_2TAPP) was synthesized according literature methods **[126]**.

2.1.3 Reagents for the synthesis of phthalocyanines

Zinc phthalocyanine (ZnPc) and potassium hexachloroplatinate were purchased from Aldrich. Dihydroxy silicon octacarboxy phthalocyanine (OH_2SiOCPc) was synthesized according to literature methods **[127]**. $AlPcS_{Mix}$ (containing a mixture of sulfonated derivatives), was used as a standard for the determination of singlet oxygen quantum yields in water

and it was synthesized according to literature methods **[128]**. Potassium tetrachloroplatinate was synthesized from potassium hexachloroplatinate according to modified literature methods **[63].**

2.1.4 Reagents for the synthesis of platinum nanoparticles

Sulphonamide, $Fe(CO)_5$, and 1-octadecene (ODE), were purchased from Sigma Aldrich. Oleic acid and platinum acetylacetonoate ($Pt(acac)_2$) were purchased from Fluka. Oleylamine and 1,2-hexadecanediol were purchased from Aldrich. Bio-Beads S-X1 were from Bio-Rad.

2.1.5 Reagents for bacterial work

Ethylenediaminetetraacetic acid (EDTA was purchased from Sigma Aldrich. Polystyrene (PS, Mw = 192,000 g/mol), Agar bacteriological BBL Mueller Hinton broth (HG000C24.500) and nutrient agar (HG0000C1.500) were purchased from MERCK Chemical Ltd. *S. aureus* (ATCC 6538), *E. coli* (ATCC 25922) and *C. albicans* (ATCC 24433) were purchased from Microbiologics.

2.2. Instrumentation

a). Ground state electronic absorption spectra were performed on a Shimadzu UV-2550 spectrophotometer. Quartz cells with 1 cm path-length were used.

b). Fluorescence emission spectra were recorded on a Varian Eclipse fluorescence spectrofluorometer.

c). Elemental analyses for CHNS were done using a Vario-Elementar Microcube ELIII Series.

d). Mass spectral data were collected with a Bruker AutoFLEX III Smartbeam TOF/TOF Mass spectrometer. The instrument was operated in

positive ion mode using a m/z range of 400 – 3000 amu. The voltage of the ion sources was set at 19 and 16.7 kV for ion sources 1 and 2 respectively, while the lens was set at 8.50 kV. The reflector 1 and 2 voltages were set at 21 and 9.7 kV respectively. The spectra were acquired using α-cyano-4-hydroxycinnamic acid as the MALDI matrix and a 354 nm nitrogen laser as the ionizing source.

e). ^{1}H-nuclear magnetic resonance spectra (^{1}H-NMR) were recorded in deuterated solvents (DMSO-d_6 or acetone-d_6) using Bruker AMX600 MHz spectrometer.

f). Infrared (IR) spectra were recorded using the Perkin-Elmer Universal Attenuated Total Reflectance (ATR) Sampling accessory spectrum 100 FT-IR Spectrometer.

g). The $^1O_2$ generation was directly quantified, in the absence and presence of sodium azide (NaN_3), a physical quencher of singlet oxygen, using an ultrasensitive Germanium detector (Edinburgh Instruments, EI-P) combined with a 1000 nm long pass filter (Omega, 3RD 1000 CP) and a 1270 nm band pass filter (Omega, C1275, BP50) to detect the intensity of the phosphorescence band at 1270 nm. The detection direction was perpendicular to that of a 421 nm excitation beam from the optical parametric oscillator (OPO) unit of an Ekspla NT 342B-20-AW laser (0.5 mJ/7 ns, 10 Hz), which ran through a 1 cm quartz fluorescence cell holding the sample solution. The signal was averaged over 128 measurement pulses with a digital oscilloscope (Tektronix TDS 3032C) to obtain the dynamic decay curve for $^1O_2$ formation. The lifetime of the $^1O_2$ was calculated by decay curve fitting using the approach described by Woehrle and co-workers **[129]**, and the quantum yield for $^1O_2$ formation (Φ_Δ) was determined. The data obtained was analysed using ORIGIN Pro 8 software.

h). Determination of singlet oxygen quantum yields was done using General Electric Quartz lamp (300 W) as irradiation source. A 600 nm glass (Schott) and water filters were used to filter off ultra-violet and far infrared radiations respectively. The intensity of the light reaching the reaction vessel, was measured with a power meter (POWER MAX 5100, Molectron Detector Inc), Fig. 2.1.

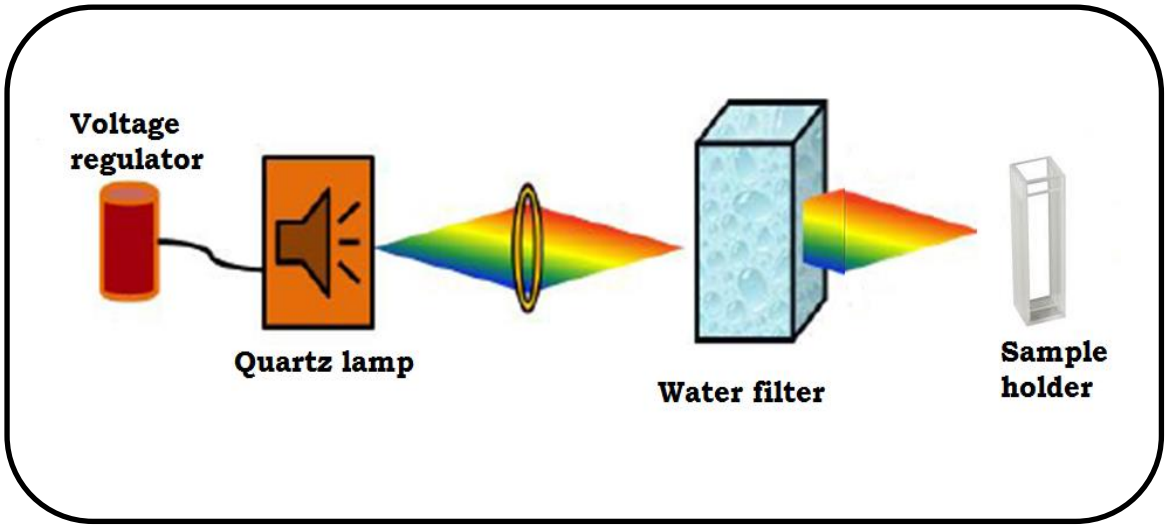

Figure 2.1: Schematic diagram of a photochemical setup.

i). X-ray analysis was performed on a Bruker D8 Discover diffractometer, equipped with a Lynx Eye detector, under Cu-Kα radiation (λ= 1.541 Å). Data were collected in the range from 2θ = 5° to 100°, scanning at 1° min^{-1} with a filter time-constant of 2.5 s per step and a slit width of 6.0 mm The samples were placed on a zero background silicon wafer slide. The x-ray diffraction data were processed using the Eva (evaluation curve fitting) software. Baseline correction was performed on each diffraction pattern by subtracting a spline fitted to the curved background.

j). Transmission electron microscopy (TEM) images were obtained using a ZEISS LIBRA® 120 transmission electron microscope. Samples were

prepared by evaporation of a very dilute solution of the nanoparticles (or the Porphyrin-PtNPs) on a standard carbon-coated copper TEM grid.

k). Scanning electron microscope (SEM) images of electrospun polymer fibers were obtained using a JOEL JSM 840 scanning electron microscope and the average diameters obtained using Cell^D software from Olympus.

l). Electrospun fibers were obtained from a set-up consisting of a syringe pump, a KD Scientific Syringe Pump Series 100, used to feed the polymer solution through a 20 ml plastic syringe fitted with a 15.24 cm needle with an inner diameter of 1.024 mm at varying flow rates depending on the polymer solution. The voltage was adjusted using a Glassman High Voltage Series EL source. Polymer solution viscosity and conductivity were measured with a Brookfield Viscometer LVDV-II and a CDM210 conductivity meter (Radiometer Analytical) respectively. The morphology of the electrospun nanofibers was examined using a scanning electron microscope at an accelerating voltage of 20 kV. Before SEM analysis, the sample was coated with gold using a sputter coater (Balzers Union SKD 030). The diameter of a nanofiber sample was calculated by taking an average of 50 measurements.

m). Photo-irradiations for PACT studies were done using a General electric Quartz line lamp (300 W, light intensity = 8.27×10^{20} photons s^{-1} cm^{-2}). A water filter was used to filter off infrared radiation, Fig. 2.2.

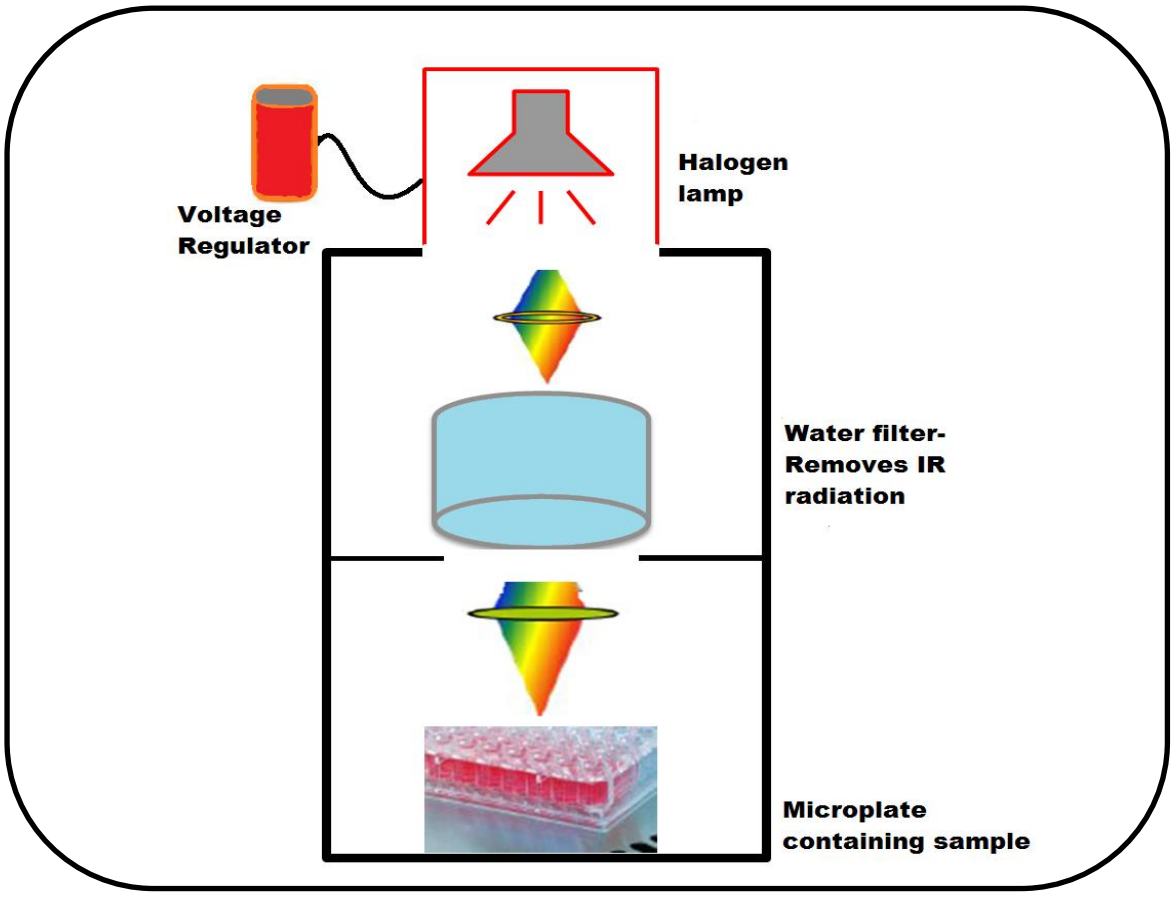

Figure 2.2: Schematic diagram of a photochemical setup in a box for microbial photo-irradiation.

n). Energy dispersive spectroscopy (EDS) was done on an INCA PENTA FET coupled to the VAGA TESCAM using 20 kV accelerating voltage.

o). All plate readings (Optical density) for the antimicrobial studies were obtained using the LEDETECT 96 for in vitro diagnostic from LABXIM PRODUCTS

2.3. Syntheses

2.3.1. Synthesis of ClGa(III)TCPP (1), Scheme 3.1.

The metal free 5,10,15,20-tetrakis-(4-carboxyphenyl) porphyrin (H_2TCPP) was synthesized according to literature **[126]**. The synthesis of ClGa(III)TCPP was as follows (Scheme 3.1): DMF was brought to reflux temperature in a two necked flask while stirring and then H_2TCPP (4 g, 5.1 mmol) was added and temperature brought to 100 ^oC. Gallium chloride (1 g, 5.6 mmol) was then added and reaction was allowed to stir at this temperature for 15 min. The completion of the reaction was checked using UV/ Vis spectrophotometer. The four bands in the Q band region of the metal free H_2TCPP collapsed into two on metalation. The reaction vessel was then allowed to cool in an ice water bath. Ice cold water (500 mL) was then added to the resulting partially crystalline precipitate, which was then filtered and washed with water then air dried.

Yield: (31%). IR (KBr, cm^{-1}): 35,443 (O-H), 2938 (C–H), 1732 (C=O), 1443 (C=C), 1365 (CH2), 1037 (C–O). ^{1}H NMR (DMSO-d6): δ, ppm 8.50 (2H, b, Ar–H), 8.31 (1H, s, Ar–H), 8.27–8.12 (5H, b, Ar–H), 7.95–7.79 (8H, m, Ar–H), 7.51 (2H, m, Ar–H), 7.35–7.25 (4H, b, Ar–H), 7.11 (2H, m, Ar–H). UV–Vis (DMF) λ_{max} nm (log ε): 421 (4.50), 587 (3.70), 550 (3.43). Calc. for $C_{48}H_{28}N_4O_8GaCl$: C 64.49; H, 3.16; N, 6.26. Found: C, 64.22; H, 3.09; N, 6.12%. MALDI-TOF-MS *m/z* calc: 893.914; Found $(M-H)^-$ 892.99.

2.3.2 Synthesis of ClTCPIPPGa (2), Scheme 3.2.

Tetraamino phenyl porphyrin (TAPP) (0.5 g, 0.74 mmol) was dissolved in dry ethanol (15 ml) and 4–formyl benzoic acid (0.1g, 0.66 mmol) was added to the solution. The reation mixture was allowed to reflux for 12 h (Scheme 3.2). The mixture was then allowed to cool to room temperature, after which the product was centrifuged at 2500 rpm. The resulting precipitate was air

dried overnight then purified by column chromatography, using ethyl acetate and hexane 8:1 as eluting solvents.

Yield: (22%). IR (KBr, cm-1): 2159 (O-H), 1785(C=O), 1658(C=N), 1430(C=C), 1362(CH2), 1250 (O-H), 1060(C-O) 870(C-H). ^{1}H-NMR (Acetone-d6): δ, ppm 9.17-9.23 (4H, m, Ar-H), 8.84-8.90 (4H, m, Ar-H), 8.74(3H, b, Ar-H), 8.55 (3H, m, Ar-H), 8.26(6H, b, Ar-H), 8.00 (8H, b, Ar-H), 7.82-7.86 (8H, m, Ar-H), 7.57-7.59 (4H, m, Ar-H), 3.84(4H, 2, -CH). UV/Vis (DMF) λ_{max} nm (log ε): 425, (4.85), 597, (3.27), 557(3.78). Calc. for $C_{76}H_{48}N_8O_8GaCl$: C 69.88, H 3.70, N 8.58; Found: C 69.05, H 3.19, N 8.41. MALDI-TOF-MS m/z calc: 1306.06; Found $(M-4H)^-$ 1302.12

2.3.3. Synthesis of Hexagonal Platinum nanoparticles

The hexagonal PtNPs were synthesized using literature methods **[97, 130]** with modifications as follows:

$Pt(acac)_2$ (0.21 g, 0.54 mmol), 1,2-hexadecanediol (0.54 g, 2.08 mmol) and diphenyl ether (25 mL) were added into a three neck flask. Under a nitrogen atmosphere, the mixture was heated under reflux for 10 min. Oleic acid (167 µL) and oleylamine (170 µL) were added as stabilizers and the mixture was refluxed for 20 min. The reaction was then allowed to cool to room temperature. Ethanol (60 mL) was added to the solution and immediately, a black precipitate formed. The liquid was removed from the product by centrifugation. The precipitate was washed with ethanol and then further dispersed in hexane (60 mL) solution containing stabilizers oleic acid (167 µL) and oleylammine (170 µL). The black solution was then cooled to 37 ^{o}C and then sulphonamide (0.4 g, 2.32 mmol) was added as a capping agent. The product was dried overnight under vacuum.

2.3.4. Cubic Platinum nanoparticles

The Pt nanocubes were synthesized according to literature **[97]** with slight modification as follows:

Pt $(acac)_2$ (0.2 g, 0.50 mmol) was mixed with 10 mL 1-octadecene (ODE), oleic acid (1ml) and oleylamine (1 ml) in a three neck flask under nitrogen flow. The solution was heated to 120 ^oC for 30 min. This was followed by addition of 2-3 drops of $Fe(CO)_5$ solution (prepared by mixing 0.1 ml of $Fe(CO)_5$, 0.76 mol/L with 1 mL of ODE). $Fe(CO)_5$ is employed as a shape directing agent. The temperature was increased to 210 ^oC and the reaction mixture allowed to stir at this temperature for an additional 30 min. The solution was cooled down to room temperature overnight. Isopropanol (40 mL) was added to the solution and the product was separated by centrifugation (4000 rpm for 10 min). The product was then dispersed in hexane.

2.3.5. Unshaped platinum nanoparticles

Unshaped Pt NPs were synthesized using the same procedure as for cubic PtNPs except, the shape directing $Fe(CO)_5$ was not added in this case. Following the addition of isopropanol described above for the cubic PtNPs, the solution was left overnight. Then oleic acid (167 µL) and oleylammine (170 µL) were added and the product was separated by centrifugation (4000 rpm for 10 min). The product was then dispersed in hexane.

2.3.6. Spherical PtNPs for comparison with $(OH)_2SiOCPc(Pt)_3$

$Pt(acac)_2$ (0.2mg, 0.5 mmol), 1,2-hexadecanediol (0.535 g) were added to diphenyl ether (20 ml) and the mixture was heated at 110 °C. Oleylamine (1.67 ml, 5 mmol) was then added to the reaction followed by oleic acid (1.7 ml, 5 mmol) under Ar and stirred for 20 min at 120 °C. The reaction was

then heated to 260 °C for 40 min. The heat source was then removed and the reaction was allowed to cool to room temperature overnight under Ar atmosphere. The black product was precipitated out with ethanol and then dried at 60 °C.

2.3.7. Conjugation of ClGa(III)TCPP (1) and ClTCPIPPGa (2) to PtNPs

The porphyrins (0.01 g, 0.01 mmol) were firstly dissolved in DMF (10 mL), then 0.03 g, 0.145 mmol of DCC was added to convert the carboxylic group (–COOH) of the porphyrin into an active carbodiimide ester group. This mixture was stirred at room temperature for 24 h. After this time 0.02 g of either hexagonal, cubic or unshaped PtNPs were added and the mixture was allowed to stir for further 24 h. The porphyrin –PtNPs conjugates were separated from the un-conjugated nanoparticles using Bio-Beads S-X1

2.3.8. Synthesis of hydroxosilicon tris (diaquaplatinum) octacarboxy phthalocyanine $(OH)_2SiOCPc(Pt)_3$. (4)

The silicon-phthalocyanine was synthesised, purified and characterized according to literature methods **[127]**. Aqueous solution of the sodium salt of $(OH)_2SiOCPc$ (**3**, 0.061 g, 0.055 mmol) and potassium tetrachloroplatinate(II) (0.076 g, 0.19 mmol) were mixed together and then stirred for 4 hours at 50 °C, following literature methods **[63]**. A precipitate was formed over two days. This was filtered and washed successively with water, ethanol, acetone and ether.

Yield 0.082 g (79%) IR (KBr, cm^{-1}): 3368 (OH), 2914 (C-H), 1717 (C=O), 1697 (COO-Pt), 1411, 1349 (Al-N), 1105 (C-O), 817 (Na-O), UV-Vis (1% NaOH DMSO): λ_{max} (log ε): 342 (4.74), 687 (5.15) nm). (MALDI-TOF) m/z: calculated: 1657 found: 1072 $[M-3Pt]^+$.

2.4. Electrospinning method

Electrospun fibers were prepared by mixing solutions containing 1.5 × 10^{-5} mol of polystyrene (PS) and 1.0 × 10^{-6} mol of **1**, **1**-hexagonal PtNPs, **1**-cubic PtNPs, **1**-unshaped PtNPs, **2** and **2**-hexagonal PtNPs in 10 mL DMF/THF (1:1). The resulting solutions were then stirred for 24 hrs to produce a homogeneous solution. The solutions were then placed in a cylindrical plastic tube which was fitted with a capillary needle. A potential difference between anode and cathode of 15 kV was applied to provide the charge for the spinning process. The distance between the cathode (static fiber collection point) and anode (tip of capillary needle) was 17 cm. The pump rate was maintained at 0.25 mL/h. The resulting modified fibers are represented as **1**/PS, **1**-hexagonal PtNPs/PS, **1**-cubic PtNPs/PS, **1**-unshaped PtNPs/PS, **2/**PS and **2**-hexagonal PtNPs/PS.

2.5. Photophysical methods

2.5.1. Fluorescence quantum yields (Φ_F).

Fluorescence quantum yields (Φ_F) of the **1**, **1**-hexagonal PtNPs, **1**-cubic PtNPs, **1**-unshaped PtNPs, **2** and **2**-hexagonal PtNPs were determined using a comparative method (Eq. 2.1) using Zn tetraphenyl porphyrin (ZnTPP) as a standard in DMF; Φ_{Fstd} = 0.11 **[131]**, while for **3** and **4**, ZnPc in DMSO was used as a standard, Φ_F = 0.20 **[132]**. Both samples and the standard were excited at the same wavelength. The absorbances of the solutions at the excitation wavelength were about 0.05 to avoid any inner filter effects.

$$\Phi_F = \Phi_{F(std)} \frac{F.A_{std}n^2}{F_{std}.An^2_{std}} \quad (2.1)$$

where F and F_{Std} are the areas under the fluorescence curves of the complex and the standard, respectively. A and A_{Std} are the absorbances of the

complex and standard at the excitation wavelength, and n and n_{Std} are the refractive indices of solvents used for the complex and standard.

2.5.2. Singlet oxygen (Φ_Δ)

The determination of Φ_Δ was achieved by employing an optical and chemical method. The optical method involves the observation time resolved phosphorescence decay curve of the singlet oxygen generated at 1270 nm in air. For **1, 1**-hexagonal PtNPs, **1**-cubic PtNPs, **1**-unshaped PtNPs, **2** and **2**-hexagonal PtNPs in DMF, sodium azide (NaN_3) was used as singlet oxygen quencher, using equation used (2.2) **[133]**

$$I(t) = B\frac{\tau_D}{\tau_T - \tau_D}[e^{-t/\tau_T} - e^{-t/\tau_D}] \qquad (2.2)$$

where, I(t) is the phosphorescence intensity of $^1O_2$ at time t, τ_D is the lifetime of $^1O_2$ phosphorescence decay, τ_T is the triplet state lifetime of the standard or sample and B is a coefficient involved in sensitizer concentration and $^1O_2$ quantum yield. The singlet oxygen quantum yield, of the complex was then determined in aqueous media, using Equation (2.3):

$$\Phi_\Delta = \Phi_\Delta^{Std} \cdot \frac{B.A^{Std}}{B^{Std}.A} \qquad (2.3)$$

where Φ_Δ^{Std} is the singlet oxygen quantum yield for the standard ZnTPP = 0.53 in DMF **[129]** for **1**, **1**-hexagonal PtNPs, **1**-Cubic PtNPs, **1**-unshaped PtNPs, **2** and **2**-hexagonal PtNPs and the standard was $AlPcS_{mix}$ Φ_Δ^{Std} = 0.42 **[134]** in water for **3** and **4**, B and B^{Std} refer to coefficient involved in sensitizer concentration and $^1O_2$ quantum yield for the sample and standard, respectively; while A and A^{Std} refer to the absorbances of the sample and standard, respectively at the excitation wavelength.

Absolute method was used to determine singlet oxygen quantum yield (Φ_Δ) values using ADMA as a quencher. The fibers were suspending the modified fibers in aqueous solution and irradiated using the photolysis system described Fig. 2.1 and equation 2.4 derived before was used **[135]**:

$$\frac{1}{\Phi_{\mathrm{ADMA}}} = \frac{1}{\Phi_\Delta} + \frac{1}{\Phi_\Delta}\frac{k_d}{k_a}\frac{1}{[ADMA]} \qquad (2.4)$$

where k_d is the decay constant of singlet oxygen, k_a is the rate constant of the reaction of ADMA with O_2 ($^1\Delta_g$) and Φ_{ADMA} is the quantum yield for degradation of ADMA. The intercept obtained from the plot of $1/\Phi_{ADMA}$ versus 1/[ADMA] gives the Φ_Δ values. The light intensity measured refers to the light reaching the spectrophotometer cells, and it is expected that some of the light may be scattered, hence the Φ_Δ values of the **1**, **1**-hexagonal PtNPs, **1**-cubic PtNPs, **1**-unshaped PtNPs, **2** and **2**-hexagonal PtNPs in the fiber were calculated.

2.6. Antimicrobial experiments

2.6.1. Antimicrobial activities in solution

The antimicrobial activity of the **1**, **1**-hexagonal PtNPs, **1**-cubic PtNPs, **1**-unshaped PtNPs, **2**, **2**-hexagonal PtNPs, **3** and **4** were studied. *S. aureus*, *E. coli* or *C. albicans* were grown on a nutrient agar plate prepared according to the manufacturer's specifications. A colony of *S. aureus*, *E. coli* and *C. albicans* were then inoculated into Luria nutrient broth separately and then *S. aureus* and *E. coli* plates were incubated overnight at 37 °C while *C.*

albicans plates were incubated at 30°C on a rotary shaker (~200 rpm), to produce a bacteria culture. The optical density at 600 nm of the microbial culture was adjusted to approximately 0.8 and 0.6 for *C. albicans* in nutrient broth. *E. coli* cells were pre-treated with EDTA before being inactivated. The *E. coli* cells were harvested by centrifugation at room temperature. The washed cells were then suspended in Luria broth and were placed in a shaker at 37 ^{o}C and EDTA (0.45 M) was added **[136]**.

The inactivation of *S. aureus*, *E. coli* and *C. albicans* were carried out by placing aliquots of 200 µL of the bacteria culture in a 96-well plate containing 50 µL **1**, **1**-hexagonal PtNPs, **1**-cubic PtNPs, **1**-unshaped PtNPs, **2**, **2**-hexagonal PtNPs, **3** and **4** (concentrations: 0.025, 0.05, 0.1 and 0.25 mg/mL in DMF). The plates were then illuminated with the setup described Fig. 2.2 using different times (0, 30, 60 and 90 min).

Fluences ranged from 0 to 0.8 J cm^{-2} at an irradiance of 0.05 Wcm^{-2}. Following irradiation of the plates aliquots (50 µL) were taken to determine the colony forming unit (CFU), survival fraction and % survival of the bacteria and then compared with the control which contained no photosensitizer. The content of the wells were mixed before sampling, the aliquots were serially diluted 10-fold in Luria broth to give dilutions of 10^{-1}–10^{-8} times. The dilution which was used for survival fraction was 10^{-8} as the colonies were not too numerous to count (TNTC). Complex **1**, **1**-hexagonal PtNPs, **1**-cubic PtNPs, **1**-unshaped PtNPs, **2**, **2**-hexagonal PtNPs and PtNPs alone were dissolved in DMF while complex **3** and **4** were dissolved in NaOH. DMF was employed since the solubility of the conjugate in water was low. When DMF or NaOH alone was used without the photosensitiser, there was no bacterial inactivation.

Colony-forming unit (CFU) is an estimate of viable bacterial number. CFU values may be calculated using Eq. (2.5) **[137,138].**

$$\text{CFU/ml} = \frac{Total\ colonies \times dilution\ factor}{volume\ plated} \quad (2.5)$$

when bacterial colonies are too numerous to count they are called a lawn where they are recorded as Too Numerous To Count (TNTC) **[139]**

2.6.2. Statistical analysis

All experiments were done in triplicate. Statistical significance (p value) was determined using Anova (analysis of varience) and a Student's t-Test (analysis between two components) using error limits from at least three determinations. A p-Values < 0.05 was considered significant.

2.6.3 Antimicrobial behaviour in fiber matrices

Antimicrobial experiments were also tested for **1**, **1**-hexagonal PtNPs, **1**-cubic PtNPs, **1**-unshaped PtNPs, **2** and **2**-hexagonal PtNPs supported in a fiber matrix (**1**/PS, **1**-hexagonal PtNPs/PS, **1**-cubic PtNPs/PS, **1**-unshaped PtNPs/PS, **2/**PS and **2**-PtNPs/PS). Nanofiber samples modified with these complexes were placed on the Baird Parker agar base plates which were pre-inoculated with 100 ml of liquid broth containing a suspension of *S. aureus* or *E. coli* or *C. albicans* (~10^{-7} to10^{-9} CFU/mL). One pair of agar plates was kept in the dark and the other pair was kept under illumination with visible light for 60 min. All the samples were incubated for 16 h at 37 °C for bacteria and 30 °C for *C. albicans* and evaluated. Electrospun nanofibers without the porphyrin were placed on bacterial agar plates as controls, both in the dark and under illumination. The experiments were done in triplicates.

PUBLICATIONS

The results discussed in the following chapters have been presented in the articles below that have been published or submitted for publication to peer-reviewed journals. These articles have not been referenced in this thesis

1. **M. Managa**, E. Antunes, T. Nyokong, Conjugates of platinum nanoparticles with gallium tetra – (4-Carboxyphenyl) porphyrin and their use in photodynamic antimicrobial chemotherapy when in solution or embedded in electrospun fiber. Polyhedron 76 (2014) 94-101.

2**. M. Managa**, M.A. Idowu E. Antunes, T. Nyokong, Photophysicochemical behavior and antimicrobial activity of dihydroxosilicon tris (diaquaplatinum) octacarboxyphthalocyanine. Spectrochimica Acta Part A: Molecular and Biomolecular Spectroscopy 125 (2014) 147–153.

3. **M. Managa**, T. Nyokong, Photodynamic antimicrobial chemotherapy activity of gallium tetra - (4-carboxyphenyl) porphyrin when conjugated to differently shaped platinum nanoparticles. Submitted to Journal of Molecular Structure

4. **M. Managa**, E. K. Amuhaya, T. Nyokong, Photodynamic antimicrobial chemotherapy activity of a new chloro-(5,10,15,20-tetrakis(4-(4-carboxyphenycarbonoimidoyl)phenyl) porphyrinato) gallium(III). Submitted to Spectrochimica Acta A: Molecular and Biomolecular Spectroscopy

CHAPTER THREE

Characterization of porphyrin conjugates

3. Synthesis

This chapter reports on the syntheses and characterization of porphyrins and porphyrin-Pt nanoparticle conjugates employed in this work.

3.1. Porphyrins

ClGaTCPP **(1)** was synthesised by metalation of H_2TCPP **[125]** in DMF, Scheme 3.1. 4–Formyl benzoic acid was chosen as to allow linking to amino functionalized PtNPs as to form an amide bond.

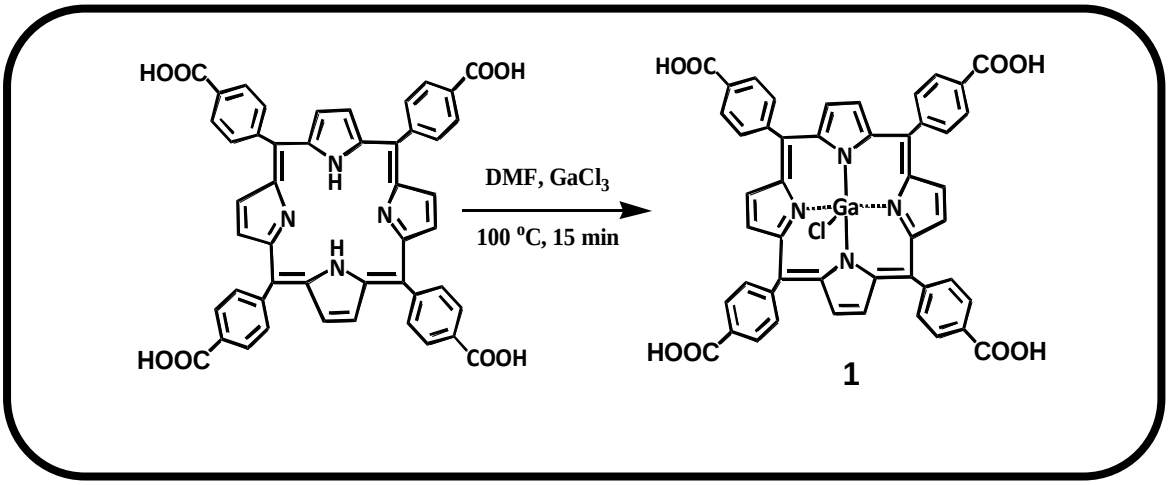

Scheme 3.1. Synthesis of gallium 5,10,15,20-tetrakis-(4-carboxyphenyl) porphyrin (ClGaTCPP).

Another porphyrin **(2)**, Scheme 3.2 was synthesised in this work. The difference between **1** and **2** is the extended conjugation of the substituent. Enhanced π conjugation has been reported to enhance ISC **[140]**, hence complex **2** is expected to show improved PACT activity compared to **1**. The synthesis of **2** was based on the fact the electrophilic carbon atoms of aldehydes (4–formyl benzoic acid) can be a target of nucleophilic attack by amines. The end result of this reaction is a compound in which the C=O double bond is replaced by a C=N double bond, Scheme 3.2. Tetrakis-

5,10,15,20-(4-aminophenyl) porphyrin (H_2TAPP) was synthesized according literature methods **[126]**.

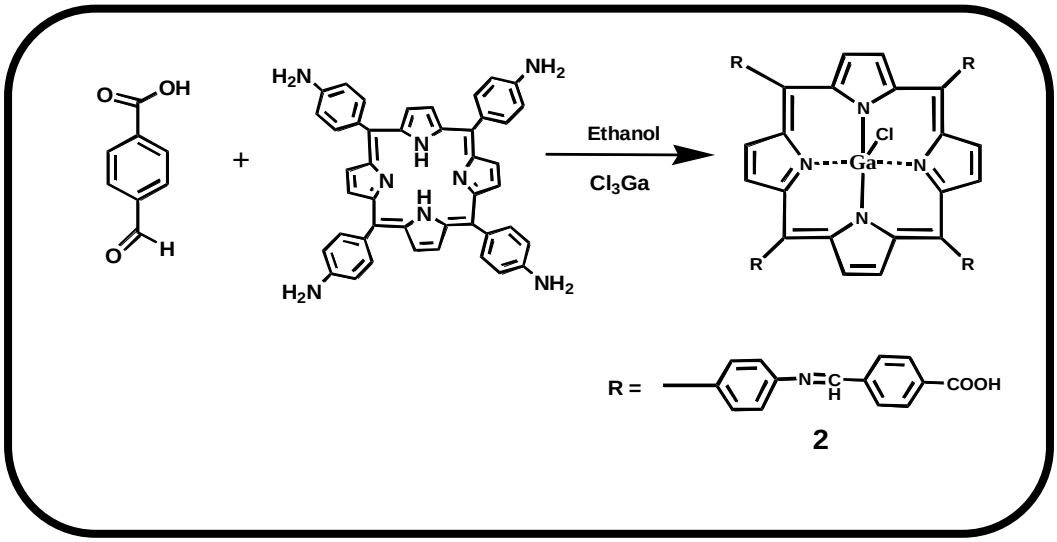

Scheme 3.2. Synthesis of chloro - (5,10,15,20-tetrakis (4- (4- carboxy phenycarbonoimidoyl)phenyl)porphyrinato) gallium(III)

3.2 Porphyrin-Pt nanoparticle conjugates

3.2.1 Synthesis of PtNPs

PtNPs of different shapes and sizes were synthesised. Monodispersed hexagonal platinum NPs of varying sizes were synthesised by reducing platinum acetylacetonate $Pt(acac)_2$ in the presence of oleic acid and aleylamine **[100,130]**. It has been generally accepted that capping agent could selectively stick to certain nanoparticles, ensuring slow growth, prevent particle agglomeration and provide stability to the resulting nanoparticle as stated in the introduction **[100]**.

The presence of $Fe(CO)_5$ during the synthesis of cubic NPs facilitates fast platinum nucleation and therefore the growth of PtNPs with controlled shape can be obtained **[97]**. Without $Fe(CO)_5$ PtNPs with no particular shaped were obtained and are designated as unshaped PtNPs. It was reported that the

formation of platinum nuclei was seen by a colour change of the solution to black immediately after the addition of $Fe(CO)_5$ **[97]**, as it was also observed in this work.

3.2.2. Synthesis of porphyrin-Pt nanoparticle conjugates

The porphyrin (**1** or **2**) was firstly dissolved in DMF and then DCC was added to convert the carboxylic group (-COOH) of the porphyrin into an active carbodiimide ester group. The formation of the amide bond between the COOH group of **1** (used as an example as the process is the same for **2**) and the amino group of the oleylamine used the PtNPs was facilitated by DCC as a coupling agent, Scheme 3.3.

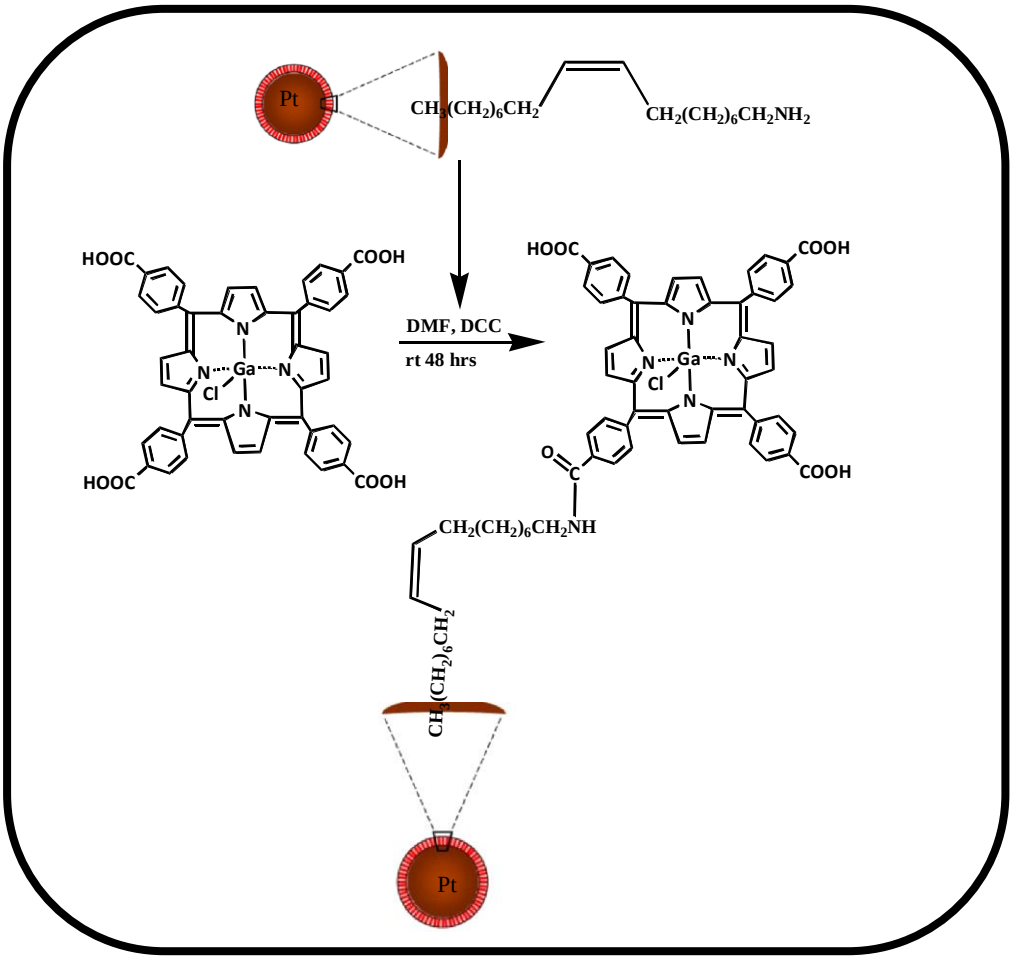

Scheme 3.3: Covalent attachment to PtNPs

3.3. Characterization

3.3.1. Characterization of porphyrin and porphyrin-Pt nanoparticle conjugates

The structural analyses of all the newly synthesized complexes (**1** and **2**) were satisfactory and consistent with the predicted structures as shown in the experimental section. Complexes (**1** and **2**) were successfully characterized using a variety of spectroscopic techniques such as the UV-Vis, IR, NMR and Mass spectra.

In both compounds **1** and **2** comparing the H NMR with the elemental it can be seen that the hydrogens of the carboxylic are not observed in the NMR and this is as a results that the signal could be replaces by the H_2O peak.

3.3.1.1. Fourier transform infrared spectroscopy (FTIR)

The conjugation of the PtNPs with **1** and **2** was confirmed using FTIR, Fig. 3.1. The amide bond for **1**-hexagonal PtNPs (as an example) was observed at 1626 cm^{-1} due to C=O stretch as a result of the bond between the carboxylic group of the porphyrin and the amine group on the oleyamine. This peak is not visible on the FTIR spectra of **1**. The peak at 3323 cm^{-1} is due to N-H stretch, the N-H stretch will also be present in oleyamine alone.

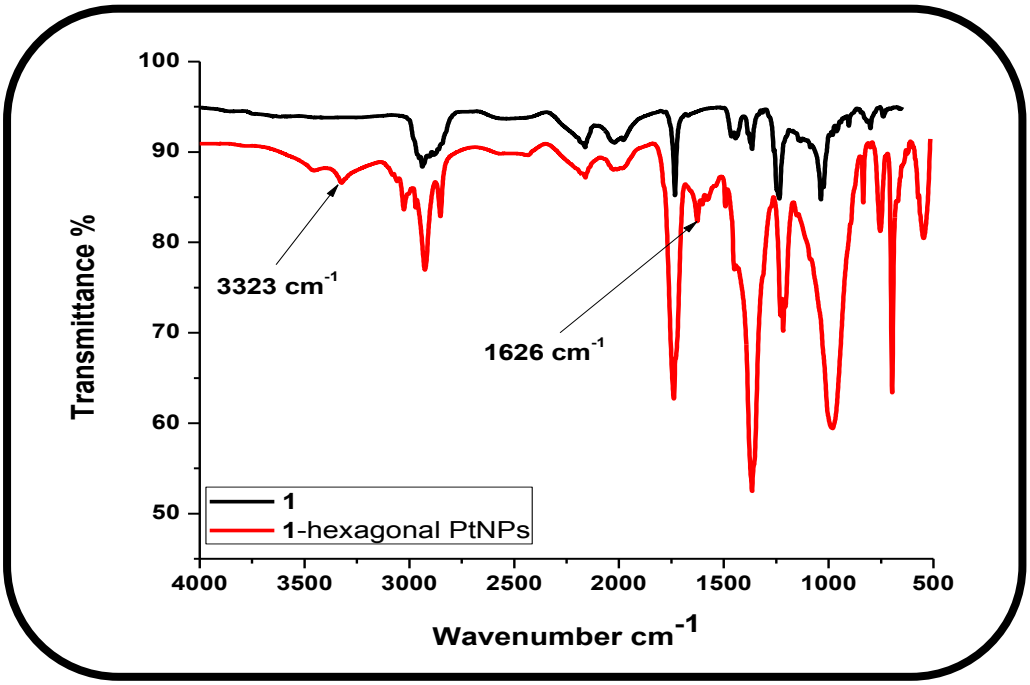

Figure 3.1: Fourier transform infrared spectroscopy (FTIR) of 1 and 1–hexagonal PtNPs conjugate.

The amide bonds for **2**-hexagonal PtNPs were visible at 3323 cm^{-1} due to N-H stretch and at 1711 cm^{-1} due to C=O stretch (Fig. 3.2). These peaks were not visible on the spectra of complex **2** but were visible for **2**-hexagonal PtNPs. Imines have a characteristic peak between 1649-1664 cm^{-1} **[141]**. The imine peak was observed at 1652 cm^{-1} for both **2** and **2**-hexagonal PtNPs, but not for H_2TAPP, confirming the formation of **2**.

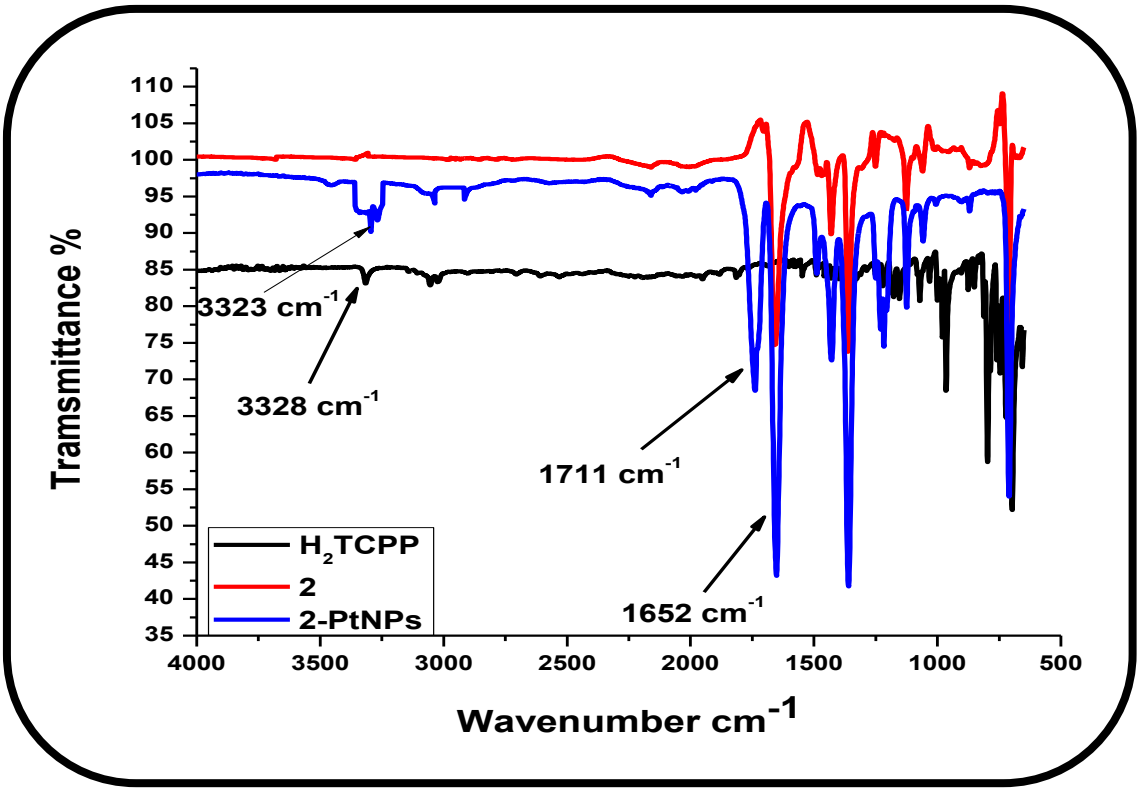

Figure 3.2: FTIR spectra of meso-tetraamine porphyrin (black), 2 (red) and 2-PtNPs (blue).

3.3.2.2. X-ray powder diffraction (XRD)

X-ray diffraction (XRD) pattern for the **1**-cubic, **1**-unshaped and **1**-hexagonal PtNPs, is shown in Fig. 3.3A. Comparison with the International Centre for Diffraction Data (ICDD) revealed the platinum NPs pattern fits the platinum data. The peaks were at 2θ of 39.86°, 46.44, 67.69, 81.56 and 86.09 for the **1**-cubic and **1**-hexagonal PtNPs. The peak at 2θ of 86.09 for the unshaped PtNPs was weak. This could be attributed to the variety of unshaped particles. XRD was employed for crystalline size determination, using Eq 1.1.

Table 3.1: The sizes of PtNPs

PtNPs or conjugate	**Size by TEM (nm)**	**Size by XRD (nm)**
PtNPs-cubes	**22-34**	**28**
1-cubic PtNPs	**28-40**	**32**
PtNPs-Hexagonal	**40-70**	**51**
1-hexagonal PtNPs	**a**	**56**
PtNPs-Unshaped	**a**	**58**
1-unshaped PtNPs	**a**	**62**
2-hexagonal PtNPs	**a**	**54**

a – Undermined due to aggregation or due to unshaped nature

The average size of the cubic PtNPs was determined to be 28 nm while **1**-cubic PtNPs was 32 nm, Table 3.1. The size of the unshaped PtNPs was determined to be 58 nm and **1**-unshaped PtNPs was 62 nm while the hexagonal PtNPs were 51 nm and the conjugate was 56 nm, Table 3.1. The average size of the **2**-hexagonal PtNPs was determined to be 54 nm.

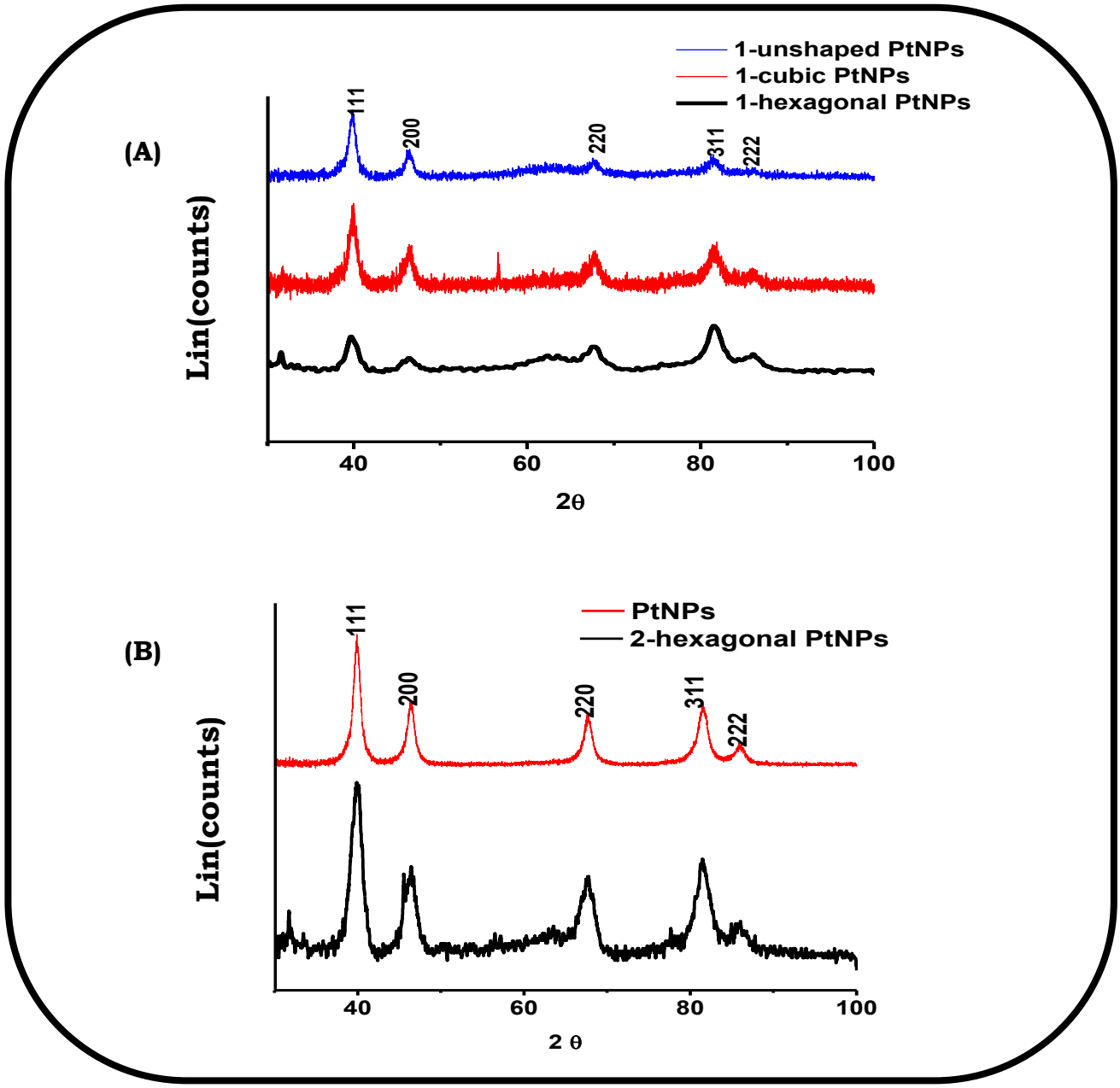

Figure 3.3: X-ray powder diffraction (XRD) of 1-unshaped PtNPs (Blue), 1-cubic PtNPs (Red), and 1-hexagonal PtNPs (Black) (A). X-ray powder diffraction (XRD) of PtNPs (red) and 2-hexagonal PtNPs conjugate (black) (B).

(A)

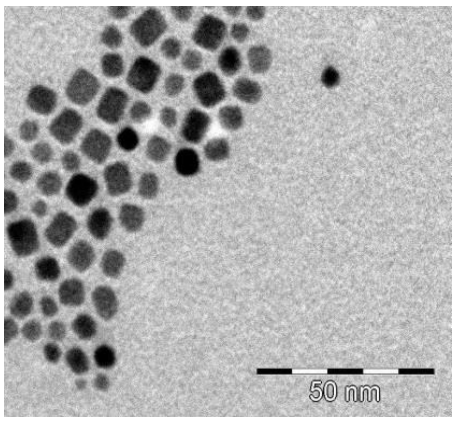
50 nm

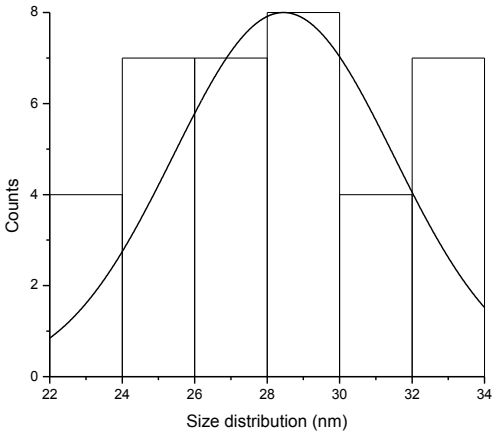
Counts
Size distribution (nm)
0
2
4
6
8
22
24
26
28
30
32
34

(B)

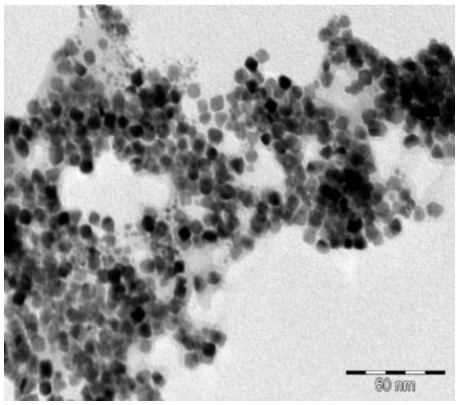
50 nm

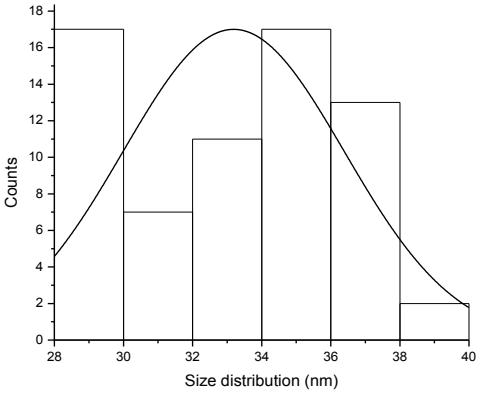
Counts
Size distribution (nm)
0
2
4
6
8
10
12
14
16
18
28
30
32
34
36
38
40

(C)

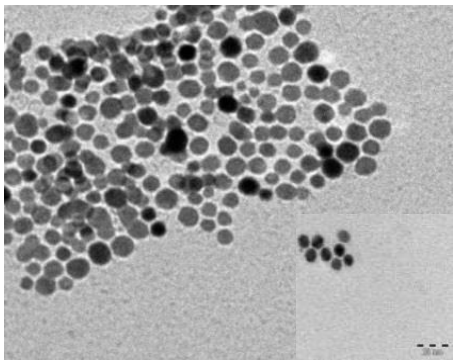

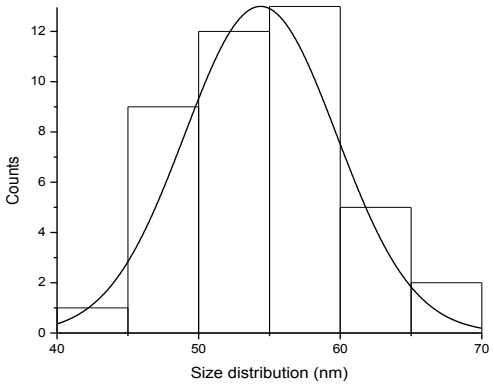
Counts
Size distribution (nm)
0
2
4
6
8
10
12
40
50
60
70

(D)

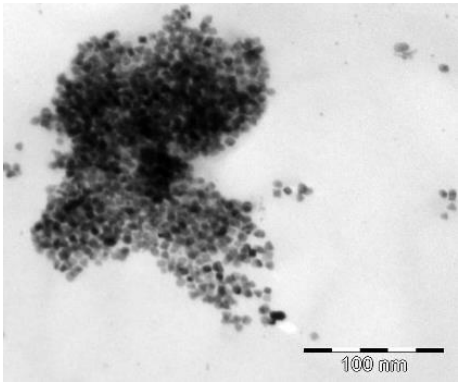
100 nm

(E)

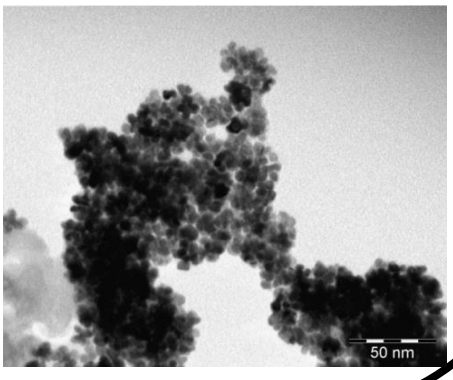
50 nm

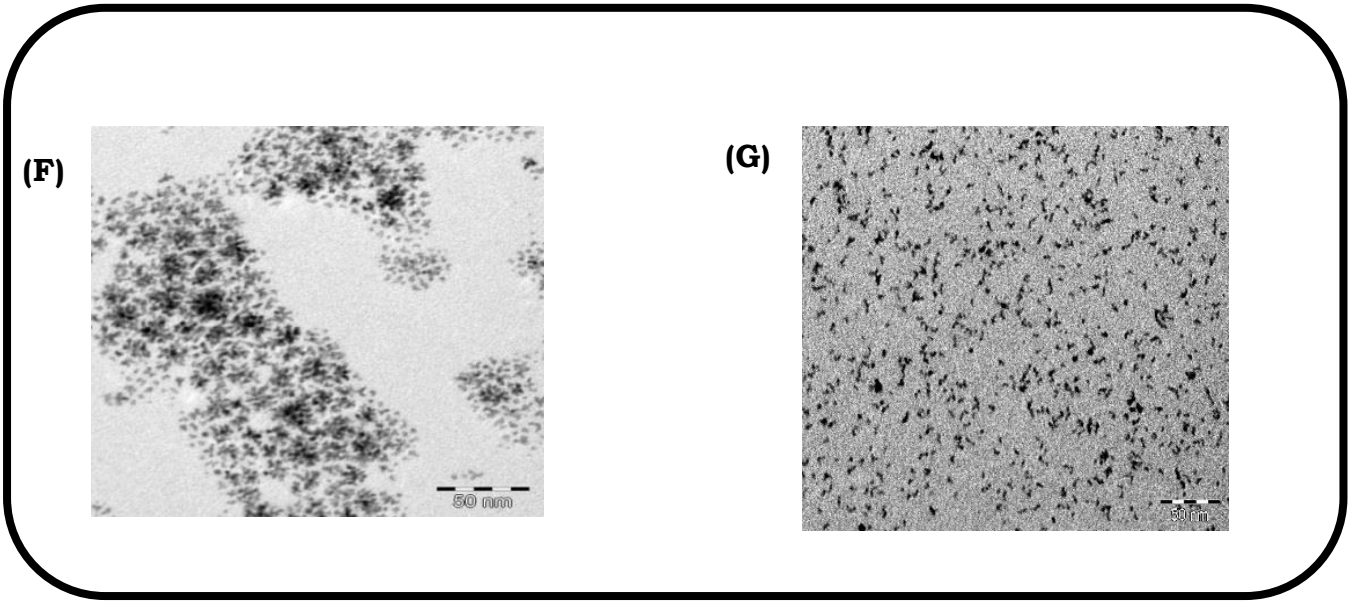

Figure 3.4: TEM images of cubic (A), hexagonal (C) and unshaped (F) PtNPs alone. (B), (D) and (G) are the corresponding conjugates of 1. (E) = 2-hexagonal PtNPs.

3.3.2.3. Transmission electron microscopy (TEM) images

Transmission electron microscopy studies (TEM) image of the cubic PtNPs, Fig. 3.4A, shows that they are well dispersed, with the size distribution of 22 to 34 nm, Table 3.1, (see the accompanying histogram). The TEM image of the **1**-cubic PtNPs conjugate is shown in Fig. 3.4B with an increased size distribution of 28 to 40 nm, Table 3.1. The increase in size may be due to aggregation. The TEM image of the hexagonal PtNPs, Fig. 3.4C shows that they are dispersed, with the sizes distributed from 40 to 70 nm, Table 3.1. Fig. 3.4C (insert) shows individual hexagonal PtNPs more clearly. The TEM images of **1**-hexagonal PtNPs as well as **2**-hexagonal PtNPs (Fig. 3.4D and E) showed extensive aggregation. The size distribution of **1**-hexagonal PtNPs and **2**-hexagonal PtNPs could not be determined due to high aggregation but

XRD showed that the size was 54 nm for **2**-hexagonal and 56 for **1**-hexagonal PtNPs. Fig. 3.4F shows the TEM image of unshaped platinum NPs and Fig. 3.4G show that of **1**-unshaped PtNPs. The size distribution of the unshaped NPs alone could not be determined as there was no defined shape.

3.2.3.4. UV/Vis and fluorescence spectra and data

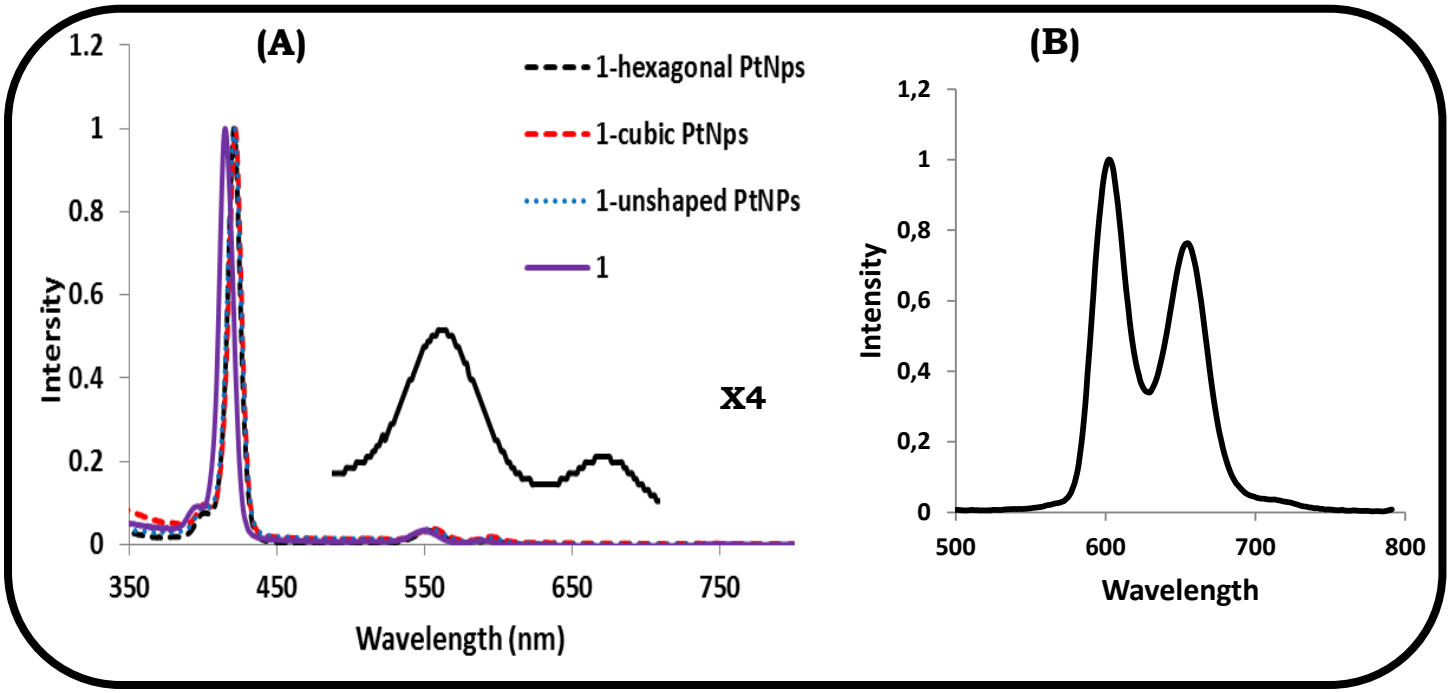

Figure 3.5: Absorption spectrum of 1-cubic conjugate (Dotted red line), 1-hexagonal conjugate Dotted black line), 1-unshaped conjugate (Dotted blue line) and 1 (Purple solid line), Insert = expansion of the Q band area and (B) fluorescence emission spectrum of 1. Solvent = DMF

Porphyrins are characterized by an intense band called the Soret or B band at about 400 nm and the Q bands are observed between 500-600 nm. Fig. 3.5 shows the spectra of **1** and its conjugates with the differently shaped

PtNPs. The UV/Vis spectrum of **1**-hexagonal PtNPs, **1**-cubic PtNPs and **1**-unshaped PtNPs showed a Soret band at 422 nm (Fig. 3.5) which is slightly red shift compared to **1** alone at 414 nm, Table 3.2. Generally red shifts in porphyrins are a result of the formation of side-by-side J-aggregates **[142].** Fig. 3.5B shows the emission spectrum of **1**, which is similar to **2** below.

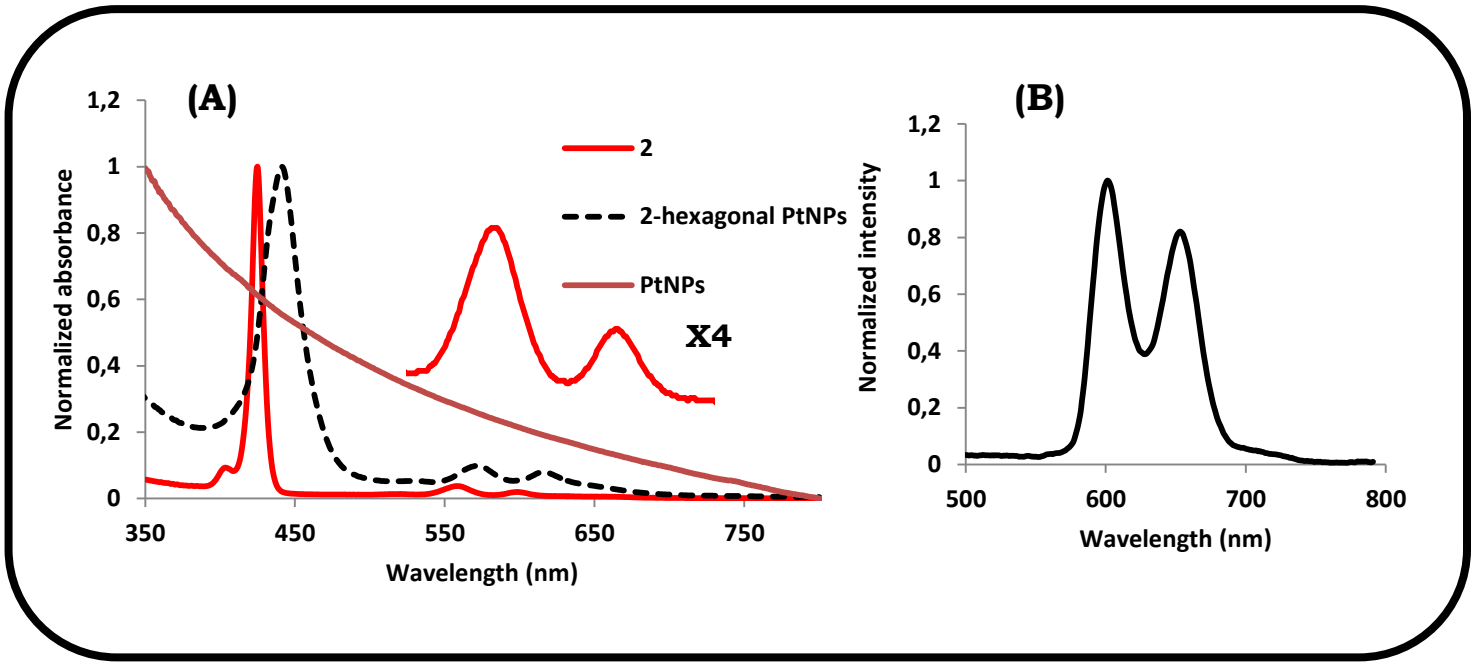

Figure 3.6: Typical absorption (A) of complex 2 (Red line) and 2-PtNPs (Dotted black line) and PtNPs (Gray line) and (B) fluorescence emission spectrum of 2. The solvent used was DMF. Insert = expansion of the Q band area.

Fig. 3.6A shows the spectrum of complex **2** with Soret band at 425 nm, and two Q bands at 600 nm and 560 nm. The Soret band of **2**-hexagonal PtNPs was observed at 443 nm, Table 3.2. Fig. 3.6B showed the emission spectrum of complex **2**, which is typical of a metallated porphyrin with two bands differing in intensity at 598 nm and 650 nm **[143]**.

Fluorescence quantum yield (Φ_F) values for **2** or **2**-hexagonal PtNPs were determined by comparative methods as explained in the experimental section using Zn tetraphenyl porphyrin (ZnTPP) as a standard in DMF; Φ_{Fstd}

= 0.11 in DMF **[131]**. The Φ_F of **2** was calculated to be 0.025 while that of **2**-PtNPs was 0.019 (Table 3.2). The lower value for the latter is due to the effect of the heavy atom effect of PtNPs. The values are also low for both **2** and **2**-hexagonal PtNPs due to the heavy atom effect of the central Ga atom. The Φ_F of **1** was calculated to be 0.094 while that of **1**-hexagonal PtNPs was 0.078, **1**-cubic PtNPs was 0.061 and **1**-unshaped PtNPs was 0.085. The Φ_F values for **2** and **2**-hexagonal PtNPs were lower compared to that of **1** and **1**-PtNPs conjugates and this could be due to the additional phenyl ring (spacer) on **2** therefore decreasing fluorescence and increasing intersystem crossing

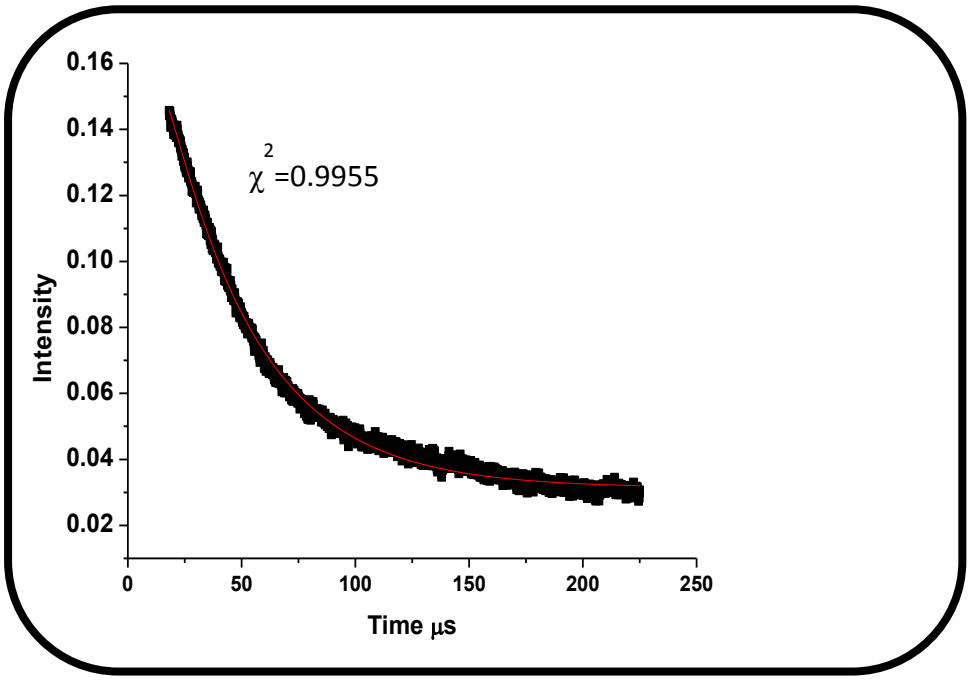

Figure 3.7: Typical singlet oxygen phosphorescence decay curve. Solvent = DMF

3.2.3.5. Singlet oxygen quantum yield (Φ_Δ)

Time resolved phosphorescence decay curve of singlet oxygen (Fig. 3.7) was used to determine singlet oxygen quantum yield as explained in the experimental for all complexes in DMF. The singlet oxygen quantum yields

for **1** and **2** when embedded on fibers will be discussed later. The Φ_Δ values were calculated to be 0.48, 0.38 and 0.34 for **1**-cubic PtNPs, **1**-hexagonal PtNPs and **1**-unshaped PtNPs, Table 3.1. The values for the conjugates in DMF are improved compared to **1** alone with a Φ_Δ 0f 0.32 due to the heavy atom effect of the Pt which encourages intersystem crossing to the triplet state hence allowing for increased singlet oxygen quantum yields. The largest singlet oxygen quantum yield for **1** conjugates was obtained for the **1**-cubic PtNPs at Φ_Δ = 0.48. This could be related to the smaller average size (determined by XRD) of the cubic PtNPs at 32 nm compared to 56 nm and 62 nm (Table 3.1) for **1**-hexagonal PtNPs and **1**-unshaped PtNPs, respectively.

It is possible that that as size of the PtNPs decreases there is large number of atoms on the surface, which may enhance intersystem crossing of the **1**. Then the $^1O_2$ quantum yield was calculated to be 0.52 for complex **2** and 0.56 for **2**-hexagonal PtNPs, as shown in Table 3.2. The values for the conjugates are improved compared to porphyrin alone due to the heavy atom effect of the Pt which encourages intersystem crossing to the triplet state hence allowing for increased singlet oxygen quantum yields as stated above. The Φ_Δ values are higher for **2** or **2**-hexagonal PtNPs due to the extra phenyl ring which encourage intersystem crossing, decreasing Φ_F but increasing Φ_Δ.

Table 3.2: Single oxygen and fluorescence quantum yields in DMF

Complex	**λ_{max} B band**	**(Φ_{Δ})**	**(Φ_F)**
1	414	0.32	0.094
1-hexagonal PtNPs	422	0.38	0.078
1-cubic PtNPs	422	0.48	0.061
1-unshaped PtNPs	422	0.34	0.085
2	425	0.52	0.025
2-hexagonal PtNPs	443	0.56	0.019

CHAPTER FOUR

Characterization of phthalocyanine conjugates

4. Synthesis

4.1. Synthesis of OHSiOCPc-(Pt(H_2O)$_2$)$_3$

The synthesis of SiOCPc has been previously reported **[59, 127]** and the results obtained from the characterization correspond with that of literature. Synthetic route for hydroxosilicon trikis (diaquaplatinum) octacoarboxyphthalocyanine OHSiOCPc-(Pt (H_2O)$_2$)$_3$ is shown in Scheme 4.1. The complex was obtained in good yield (79%) with satisfactory spectroscopic analyses. The complex was found to be water soluble due to the two remaining COONa substituents on the periphery of the Pc. It was also soluble in polar organic solvents such as DMF and DMSO. Mole ratio of Pt:Pc (3:1) was used in order to ensure 3 Pt were coordinated to Pc.

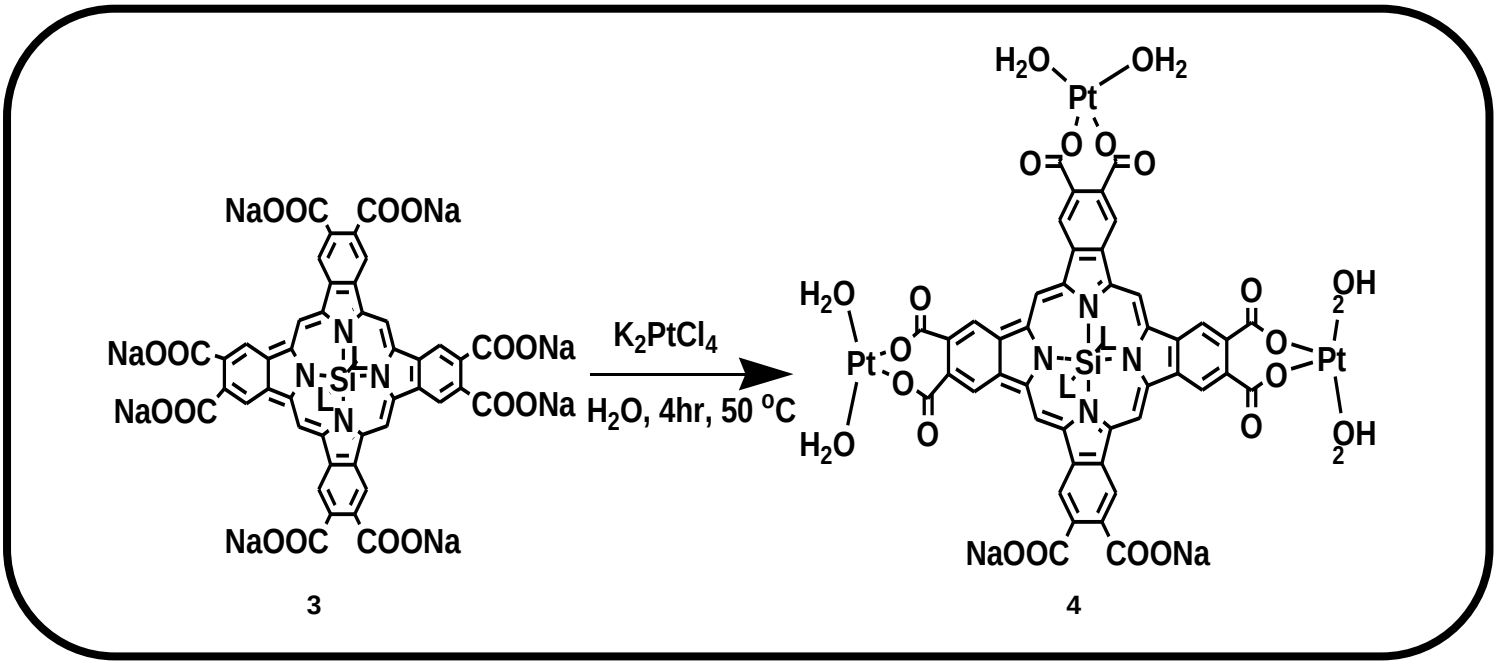

Scheme 4.1: Synthesis of OH$_2$SiOCPc-(Pt(H2O)$_2$))$_3$.

4.2. Characterization of SiOCPc and $OH_2SiOCPc\text{-}(Pt(H2O)_2))_3$.

4.2.1. UV/Vis and fluorescence spectra

Fig. 4.1 shows the comparative ground state electronic absorption spectra of **3** and **4** in 0.1% NaOH solution. No drastic UV–visible spectral change of the Q-band in complex **4** was observed. The Q-bands of the two complexes occur almost at the same wavelength (689 nm) (see Table 4.1), with a slight shift to the blue region (~2 nm) for complex **4**. This shift change is characteristic of the introduction of the Pt at the periphery of the phthalocyanine ring **[65]**. The spectrum of **4** showed monomeric behavior evidenced by a single Q band, typical of octacarboxyl substituted phthalocyanine complexes, **[144]** while the B-band is observed as broad envelope due to the superimposition of the B_1 and B_2 bands **[78]**. This is similar to what is observed in **3**.

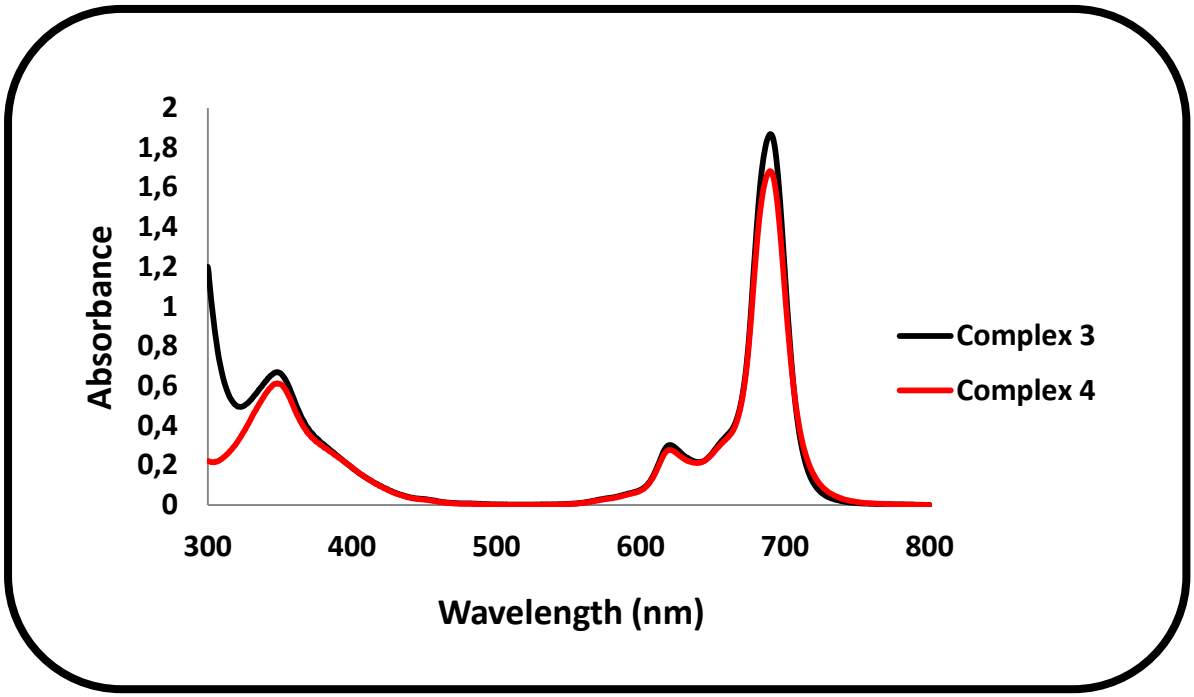

Figure 4.1: Ground state spectra of SiOCPc and $OH_2SiOCPc\text{-}(Pt(H2O)_2))_3$.

The fluorescence excitation and emission spectra, Fig. 4.2, are typical of phthalocyanine complexes, with Stokes' shifts (λ_{ems}–λ_{exc}) of 16 nm for **3** and 12 nm for **4**, Table 4.1. These large Stokes' shift may be an advantage to enable fluorescent signals from the complex to be easily separated from scattered excited light, when applied in photosensitized reactions. The excitation spectra are similar to the absorption spectra and are mirror images to the fluorescence emission spectra for the two complexes confirming no change in symmetry on excitation and lack of aggregation in solution even on introduction of Pt at the periphery of the phthalocyanine ring, Fig. 4.2. The Φ_F for **3** was high as compared to **4** which were 0.14 and 0.08 respectively; the lower Φ_F for **4** is was due to the heavy atom effect of Pt in **4**.

Table 4.1: Spectra parameters and photophysicochemical data of 3 and 4 in 0.1% NaOH.

complex	λ_{abs} (nm)	λ_{exi}	λ_{em}	Φ_F	Φ_Δ
3	689	689	705	0.14	0.26
4	687	689	701	0.08	0.58

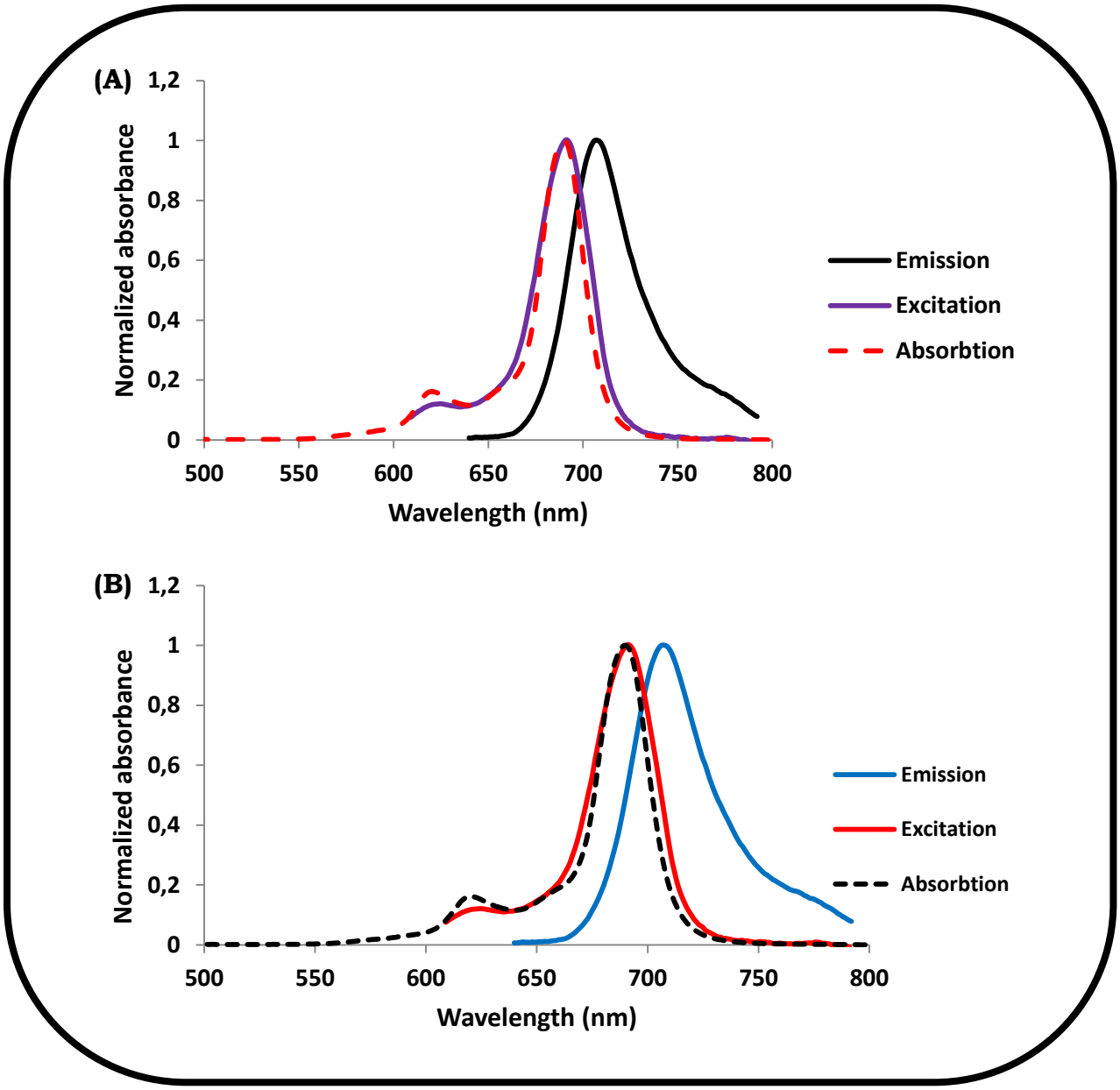

Figure 4.2: Ground state absorption, fluorescence excitation and emission spectra of 3(A) and 4(B) in 0.1% NaOH, λ_{exc} = 620 nm.

4.2.2 X-ray powder diffraction (XRD)

Fig. 4.3 presents XRD patterns of **4** and spherical PtNPs (for comparison). The XRD pattern for complex **3** was typical of Pcs (Figure not shown) **[145]**. The XRD spectrum of the PtNPs in Fig. 4.3A shows a pattern that fits Pt peak positions when compared with the International Centre for Diffraction Data (ICDD) database. Likewise complex **4** revealed patterns that fit Pt peak positions (Fig. 4.3B). Peaks were observed at 2θ = 40°, 46°, 67°, 81° and 86° (Fig. 4.3A and B) in conformity with literature values. The results show complex **4** as a nanoparticle as reported in literature **[65, 66]**.

The peaks around 2θ = 40° and 46° belong to platinum with a 99.9% match and the peaks at 2θ = 67°, 81° and 86° for **4** are broader than those of the PtNPs. This can suggest coupling of the phthalocyanine and the Pt since the MPc could have resulted in the broadening of the peaks. Similar XRD pattern has been observed for the Pt Pc conjugates **[65]**

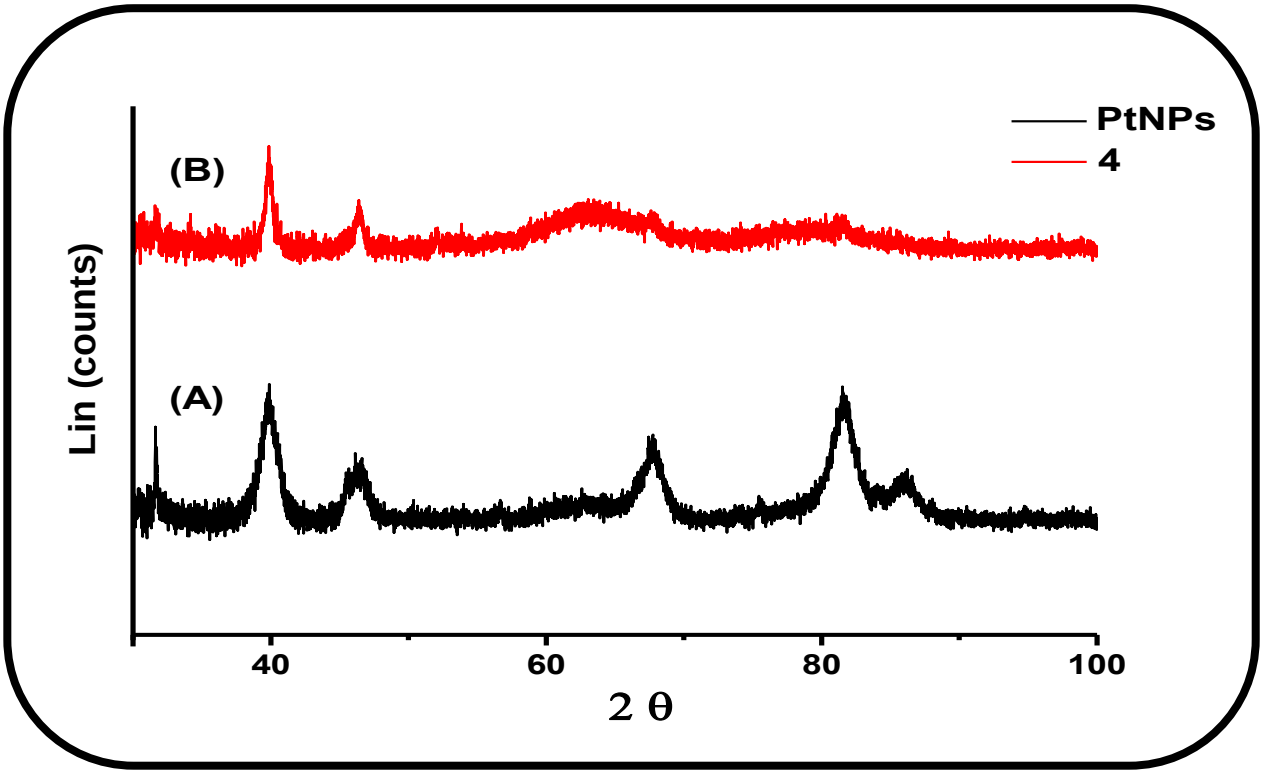

Figure 4.3: XRD patterns of, PtNPs (A) and 4 (B).

4.2.3. Transmission electron microscopy (TEM) images

There was indication of agglomeration from the TEM images though the particles were shown to be in spherical form (Fig. 4.4) large particles with a size distribution from 10 to 24 nm for PtNPs. Aggregates were observed for phthalocyanine-PtNPs conjugate **(4)**. Phthalocyanines are known to readily form aggregates **[146]**, though aggregation may also be a result of the method used in preparing samples for TEM. Size of the conjugate was not determined due to aggregation.

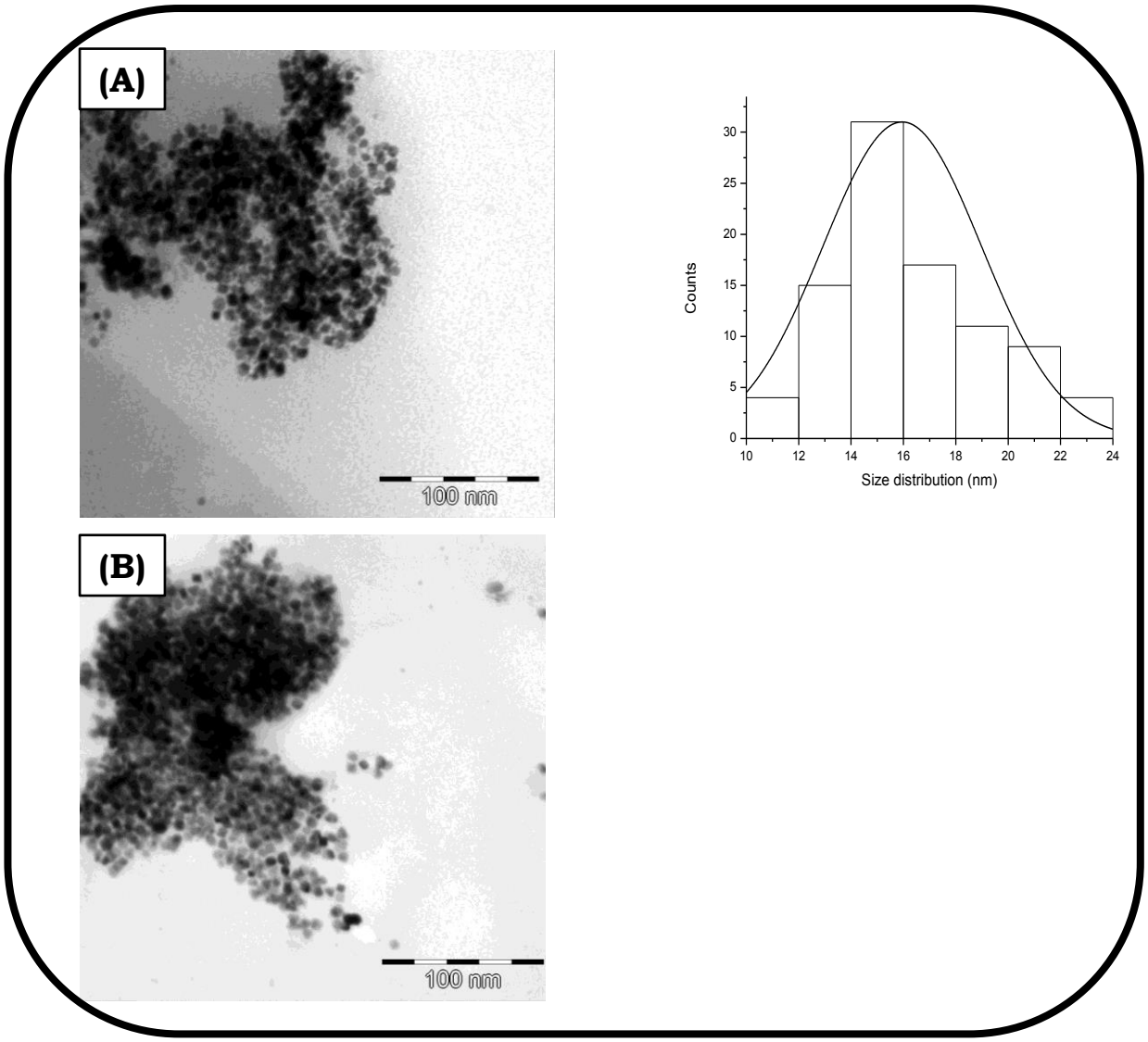

Figure 4.4: TEM images of (A) PtNPs with an accompanying histogram and (B) 4.

The EDS profile of results, Fig. 4.5, showed the presence of Pt in the conjugate.

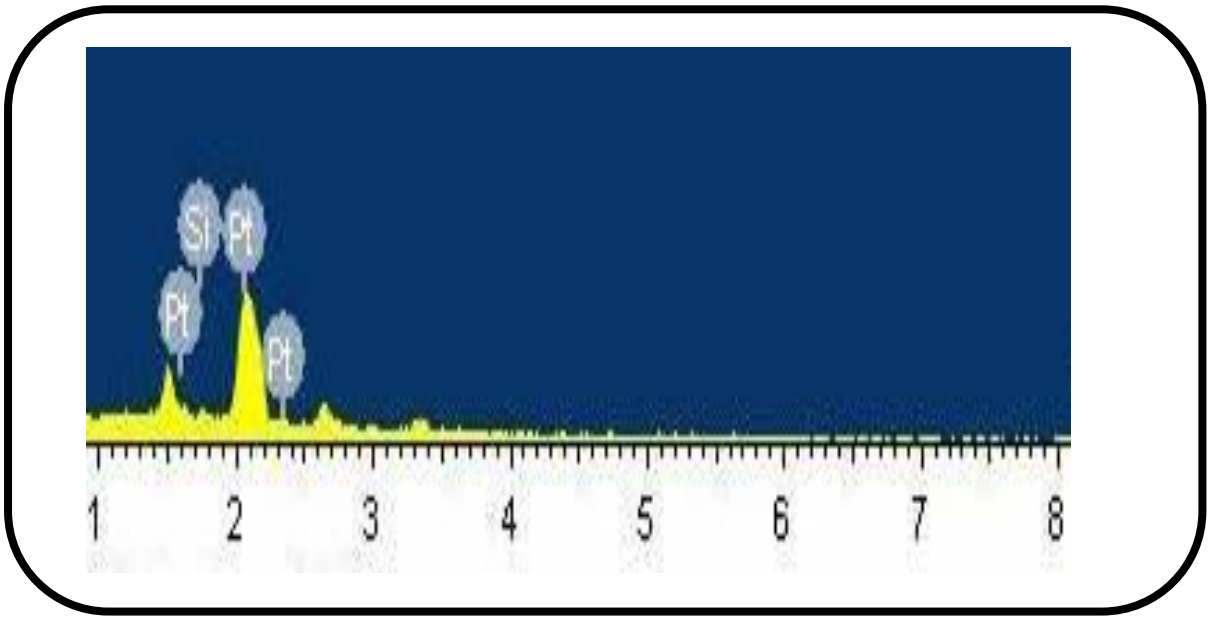

Figure 4.5: Energy dispersive spectrum (EDS) of 4

4.2.4. Φ_Δ values

Singlet oxygen ($^1O_2$), which is considered to be the major cytotoxic species in PDT or PACT, is produced through the interaction between the excited photosensitizer and molecular oxygen present inside the tissues as mentioned in the introduction. The efficiency of $^1O_2$ generation should depend on the population of the triplet state and efficient energy transfer from the excited triplet state to ground state oxygen. The $^1O_2$ quantum yield (Φ_Δ) of **3** (0.26) and **4** (0.58) were measured. A significant improvement in the singlet oxygen quantum yield was observed for **4** compared to **3**, Table 4.1. The improvement in the singlet oxygen quantum yield of the conjugate is due to the heavy atom effect of platinum within the conjugate which enhances intersystem crossing to triplet state, hence resulting in increased singlet oxygen quantum yield as discussed previously.

CHAPTER FIVE

Characterization of the fibers

5. Characterization of the electrospun fibers

This work reports on the investigation of the effect of solution parameters on fiber morphology and size of electrospun fibers. Polystyrene (PS) was chosen for the incorporation of porphyrin and porphyrin-PtNPs conjugate Fig. 5.1 shows a diagrammatic representation of the electrospinning of polystyrene polymer alone and functionalized polymer fibers.

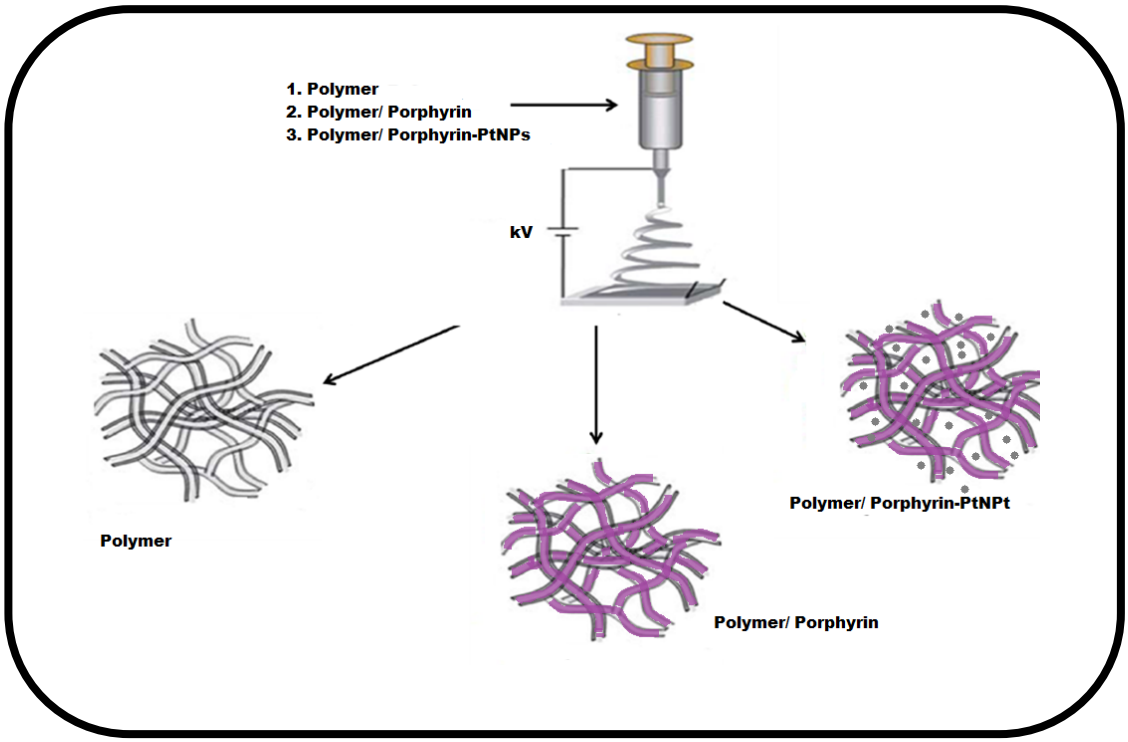

Figure 5.1: Diagrammatic representation of the electrospinning of non-functionalized and functionalized polymers

Electrospun polymer fibers are of industrial and scientific interest due to their long lengths, small diameters, porosity and high surface area per unit volume. Although electrospinning is a relatively simple process, many variables affect fiber quality, thus adding complexity to the method and making process optimization tedious. The size and morphology of the electrospun fiber depends on viscosity, concentration, surface tension. The humidity of the electrospinning environment may have an influence on the

polymer solution during electrospinning as it determines the rate of evaporation of the solvent in the polymer solution.

5.1 Scanning electron microscopic (SEM) images

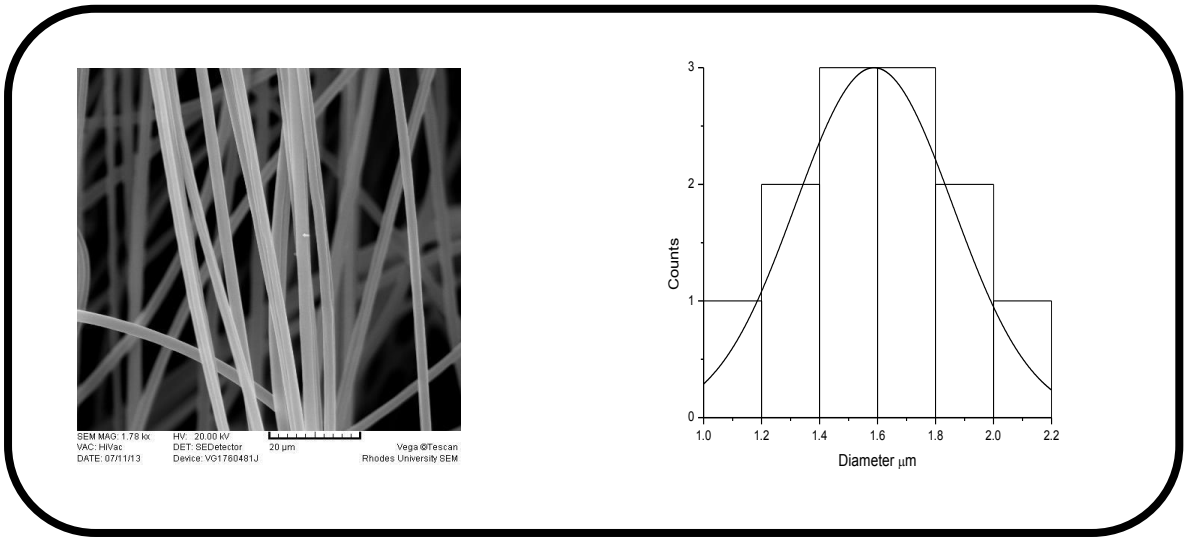

Figure 5.2: Scanning electron microscopic (SEM) images of polystyrene alone

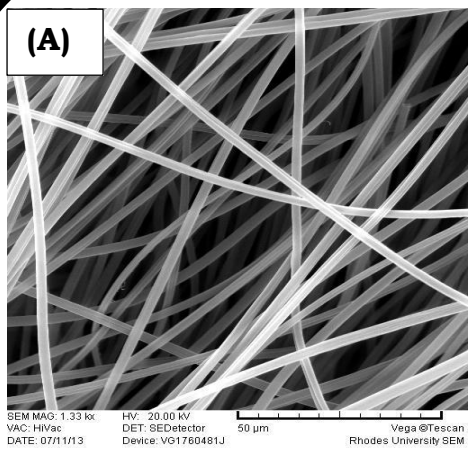
(A)
SEM MAG: 1.33 kx
HV: 20.00 kV
VAC: HiVac
DET: SEDetector
50 µm
Vega ©Tescan
DATE: 07/11/13
Device: VG1760481J
Rhodes University SEM

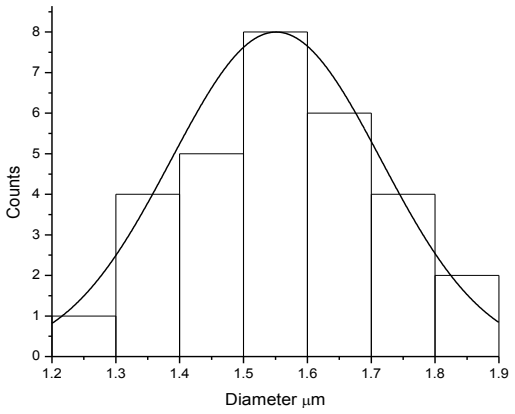
Counts
Diameter µm

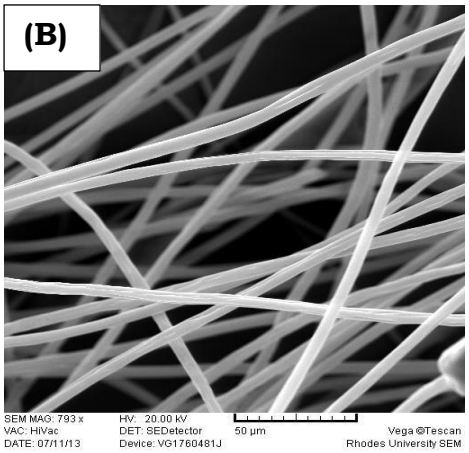
(B)
SEM MAG: 793 x
HV: 20.00 kV
VAC: HiVac
DET: SEDetector
50 µm
Vega ©Tescan
DATE: 07/11/13
Device: VG1760481J
Rhodes University SEM

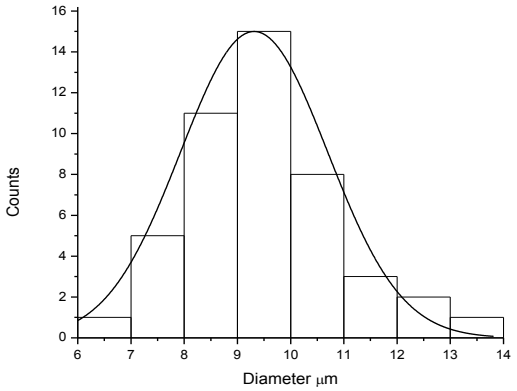
Counts
Diameter µm

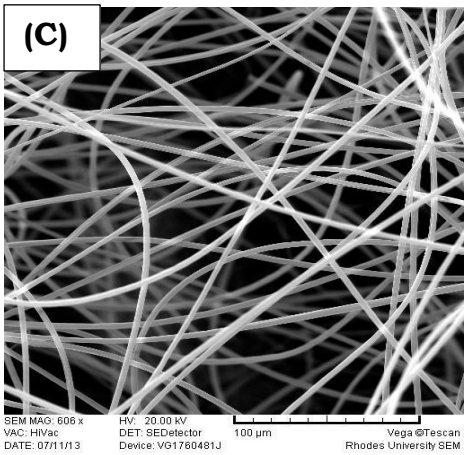
(C)
SEM MAG: 606 x
HV: 20.00 kV
VAC: HiVac
DET: SEDetector
100 µm
Vega ©Tescan
DATE: 07/11/13
Device: VG1760481J
Rhodes University SEM

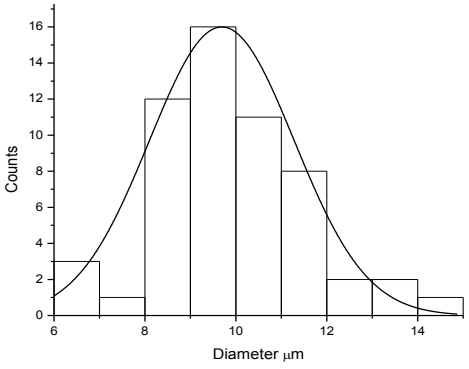
Counts
Diameter µm

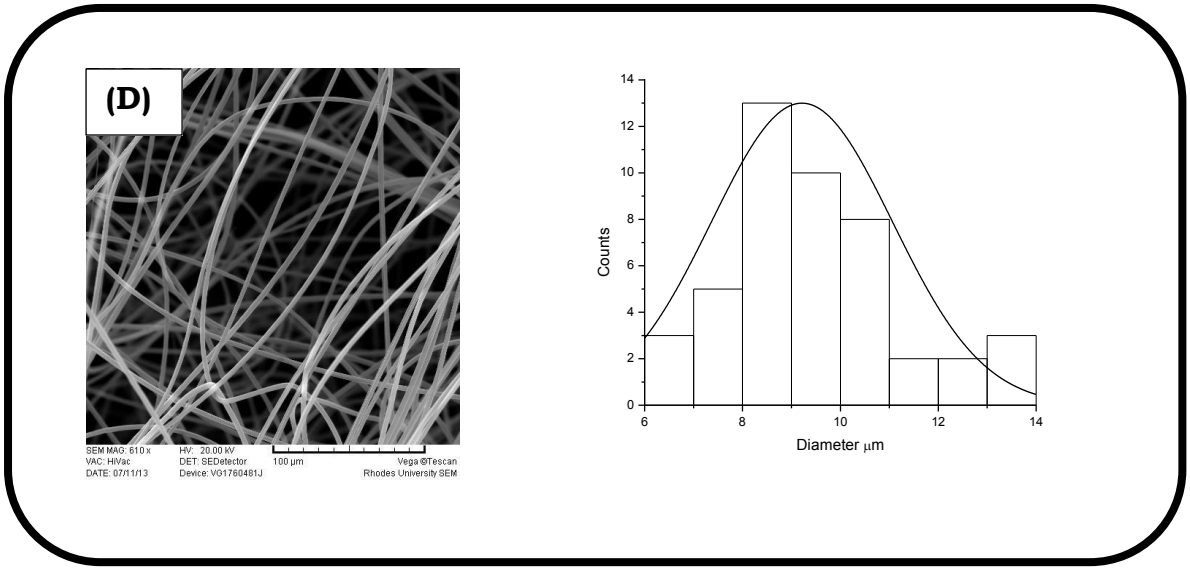

Figure 5.3: Scanning electron microscopic (SEM) images of 1/PS (A) electrospun, (B) 1-hexagonal PtNPs/PS, fiber, (C) 1-cubic PtNPs/PS and (D) 1-Unshaped PtNPs/PS.

1, **1**-hexagonal PtNPs, **1**-cubic PtNPs or **1**-unshaped PtNPs were mixed with polystyrene and electrospun into nanofibers as was explained in the experimental section. Scanning electron microscopic (SEM) was used to assess the two geometric properties of polymers which is the fiber morphology and diameter. The diameters of the fibers were determined using Image J program. The diameter obtained for polystyrene polymer alone ranged from 1.0-2.2 µm, Fig. 5.2. It has been reported that fiber diameter depends allometrically on solution viscosity **[118]**. Thus in the presence of **1** the fiber diameter increases, ranging from 1.2 to 1.9 µm, Fig 5.3A and the diameter is even larger for the **1**-PtNPs ranging from 6 to 14 µm Fig. 5.3B (using **1**-hexagonal PtNPs as an example) as the diameter range does not differ significantly for all the **1**-PtNPs conjugates, Table 5.1
In the presence of complex **2** (for **2**/PS) the fiber diameter increases, ranging from 4 to 11 µm for **2**, Fig 5.4A and the diameters were even larger for the **2**-hexagonal PtNPs/PS ranging from 8 to 16 µm.

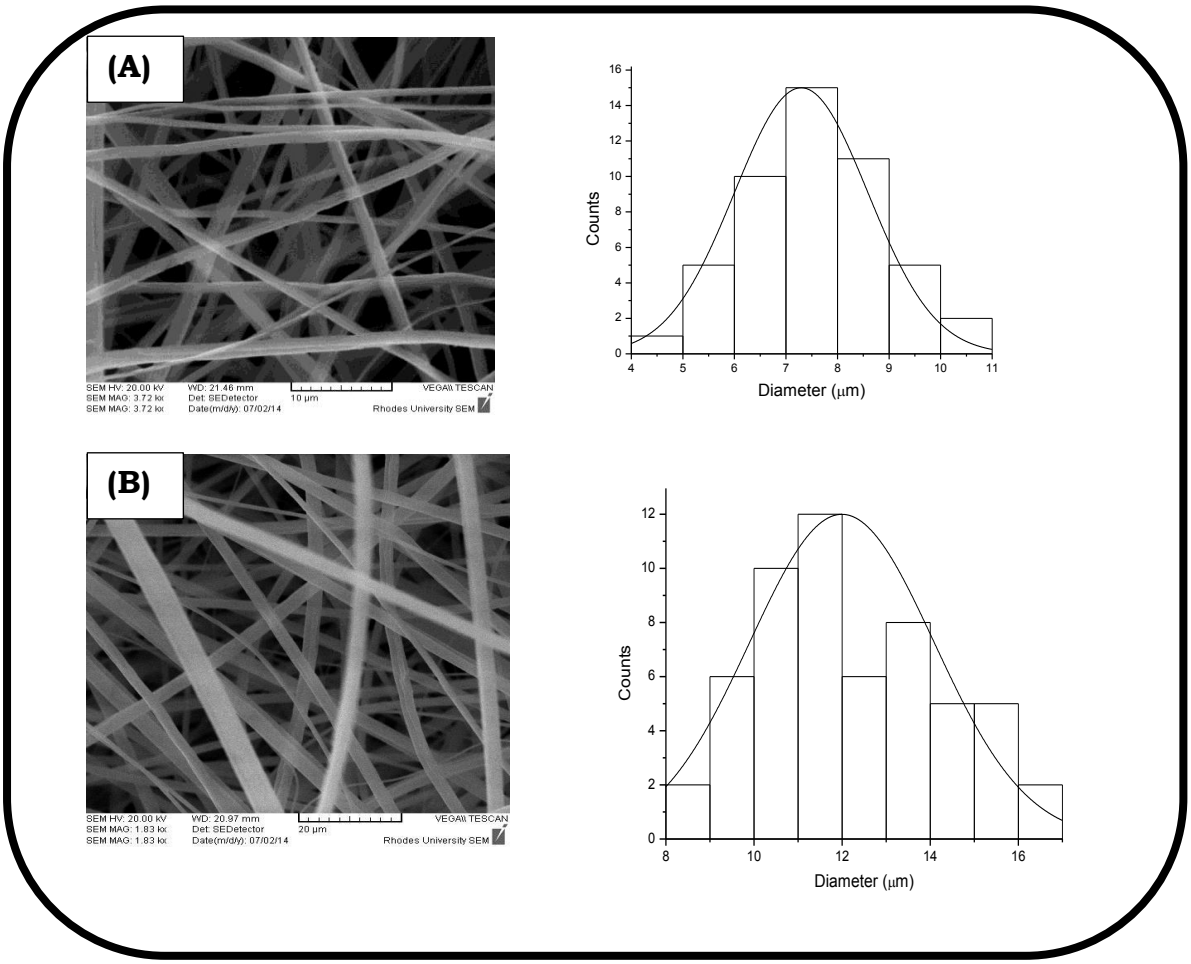

Figure 5.4: Scanning electron microscopic (SEM) images of (A) 2/PS, electrospun (B) 2-hexagonal PtNPs/PS fibers

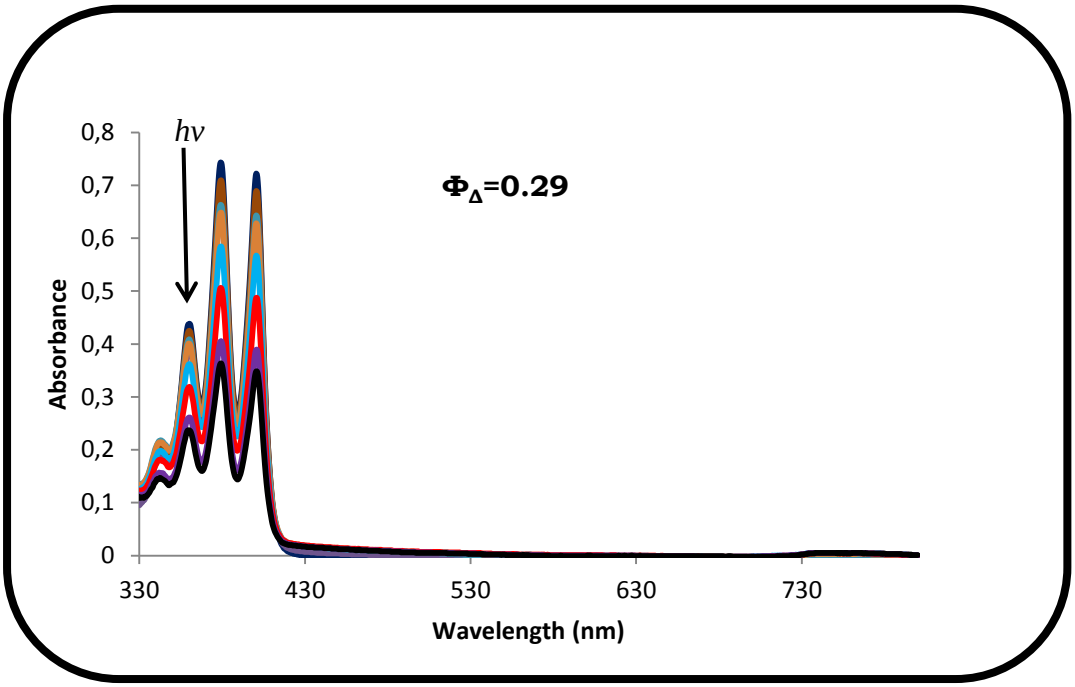

Figure 5.5: Photodegradation of ADMA in the presence of polystyrene electrospun fibers with 1-cubic PtNPs

5.2 Φ_Δ values

Φ_Δ values on the fiber were determined by suspending the modified fibers in aqueous solution and irradiating using the photolysis system described in the experimental section. Fig 5.5 shows the photodegradation of ADMA in the presence of polystyrene electrospun fibers with **1**-cubic PtNPs. The Φ_Δ was estimated to be 0.24 for **1**-hexagonal PtNPs and 0.29 for **1**-cubic PtNPs, which are improved compared to 0.21 for **1** in the fiber, Table 5.1. There was no significant improvement on **1**-unshaped PtNPs (Φ_Δ = 0.22) compared to **1** (Φ_Δ = 0.21), Table 5.1. The value is lower in the fibre (determined in aqueous media) compared to values determined in DMF (Table 5.1), due to two reasons: Φ_Δ values for the fibers are estimates and the vales in water are always lower than in organic solvents since water quenches singlet oxygen **[132]**.

The Φ_Δ values were estimated to be 0.43 for or **2**/PS and 0.47 for **2**-hexagonal PtNPs/PS, thus the value is slightly higher in the presence of PtNPs. The values for the conjugates are improved compared to porphyrin alone due to the heavy atom effect of the Pt which encourages intersystem crossing to the triplet state hence allowing for increased singlet oxygen quantum yields.

Table 5.1: Single oxygen calculations for the complexes embedded on fiber.

Complexes	**Φ_Δ[a]**	**Diameter (μm)**
1/PS	0.21 (0.32)	1.2-1.9
1-cubic PtNPs/PS	0.29 (0.48)	5-15
1-hexagonal PtNPs/PS	0.24 (0.38)	6-14
1-Unshaped PtNPs/PS	0.22 (0.34)	6-14
2/PS	0.43 (0.52)	4-11
2-hexagonal PtNPs/PS	0.47 (0.56)	8-16

[a] values in brackets are for complexes in DMF

.

CHAPTER SIX

Photodynamic antimicrobial chemotherapy (PACT) studies

As stated the introduction, the mechanism and the science behind PACT is in its infancy, but it seems to follow the same mechanistic principles as PDT, and therefore involves singlet oxygen. It is known that singlet oxygen reacts with intercellular molecules (peptides, DNA and proteins etc.) leading to oxidative damage of the cell wall and membrane, which cause cell death **[147, 148]**. Literature reports show that gram-negative bacteria are drug resistant compared to their gram positive counterparts **[149-153]**. There are two most widely used methods for quantitative determination of bacterial populations. These methods are the standard (viable, plate count) and spectrophotometric (turbidimetric) analysis **[154]**. In this study *meso*-tetra substituted porphyrin and octacarboxy substituted phthalocyanine and their conjugated were compared for PACT.

6.1 PACT using porphyrins

PACT studies that were carried out by Orenstein et al showed that it was possible to kill *Staphylococcus aureus*, a Gram positive bacteria, using deuteroporphyrin **[155]** but Gram negative bacteria such as *Escherichia coli* and *Pseudomonas aeruginosa* could not be inhibited using deuteroporphyrin alone. It was shown that to overcome this problem the bacterial cells had to be pre-treated by either ethylenediaminetetraacetic acid (EDTA) or polymyxin B nonapeptide **[1, 9]**. Table 6.1 shows **1** and its PtNPs conjugates were used only for *S. aureus* since there was no need pre-treatment as is the case with *E. coli.* The aim was to assess the effect of the shape of PtNPs. **2** and **2**-hexagonal PtNPs was tested for all *E. coli*, *S. aureus* and *C. albicans* to assess the efficiency of porphyrin against Gram (-), Gram (+) bacteria and fungi and chain length compared to complexes **1**. **3** and **4** were carried out on *E. coli* and *C. albicans* in order to compare porphyrin and Pc for PACT.

6.1.1 PACT against *E. coli*, *S. aureus* and *C. albicans* using 2 and 2-hexagonal PtNPs

In this work *E.Coli* cells were pre-treated using EDTA. The antibacterial activity of complex **2** or **2**-hexagonal PtNPs was determined using *E. coli*, *S. aureus* and *C. albicans* where CFU was plotted against illumination time Fig. 6.1. The log reduction was calculated for all the experiments done. Log reduction provides a quantitative measurement that describes the percentage of microorganism that has been killed. The log reduction of *E. coli* before pre-treatment was calculated to be 2.39 for complex **2** and 2.75 for **2**-hexagonal PtNPs and there was an improvement after the pre-treatment of *E. coli* cells as the log reduction was calculated to be 3.24 and 3.76 respectively, Table 6.1. Fig. 6.1A and C show the inactivation of *S. aureus* and *C. albican*, respectively. For *S. aureus* the log reductions are 3.82 and 4.92 (for **2** or **2**-hexagonal PtNPs, respectively). For *C. albicans* the log values are 3.30 and 3.95 (for **2** or **2**-hexagonal PtNPs, respectively). The lower log values for *C. albicans* could be due to the cell wall composition of β-glucan as it provides rigidity and structural support to the fungal cell therefore making it difficult for inactivation. **2**-hexagonal PtNPs showed better antimicrobial activity against *S. aureus* compared to *E. coli*, (before and after EDTA treatment) this could be due to the simpler cell wall structure for the former. The log values for *S. aureus* on **2** or **2**-hexagonal PtNPs are larger than for **1** or **1**-hexagonal PtNPs showing the advantage of extension of conjugation in **2** and its higher singlet oxygen quantum yields compared to **1**, Table 6.1

Table 6.1: Size, Φ_Δ and Log reduction values

Complex	**Size**	**Φ_Δ[a,b]**	**Microorganism**		
			***E. coli*[c]**	***S. aureus***	***C. Albican***
1		0.32(0.21)	-	2.26	-
1-cubic PtNPs	32	0.48(0.29)	-	4.60	-
1-hexagonal PtNPs	56	0.38(0.24)	-	3.94	-
1-unshaped PtNPs	62	0.34(0.22)	-	3.31	-
2		0.52(0.43)	2.39 (3.24)	3.82	3.30
2-hexagonal PtNPs	54	0.56(0.47)	2.75 (3.57)	4.92	3.95
3		0.26	3.24(4.12)	-	4.65
4		0.58	3.98 (5.23)	-	5.78

[a,] values for 1,2 and their conjugates in solution are in DMF. Values for 3 and 4 are in 0.1 M NaOH, [b] values in brackets are on electrospun fibers in water, [c] values in brackets are with EDTA

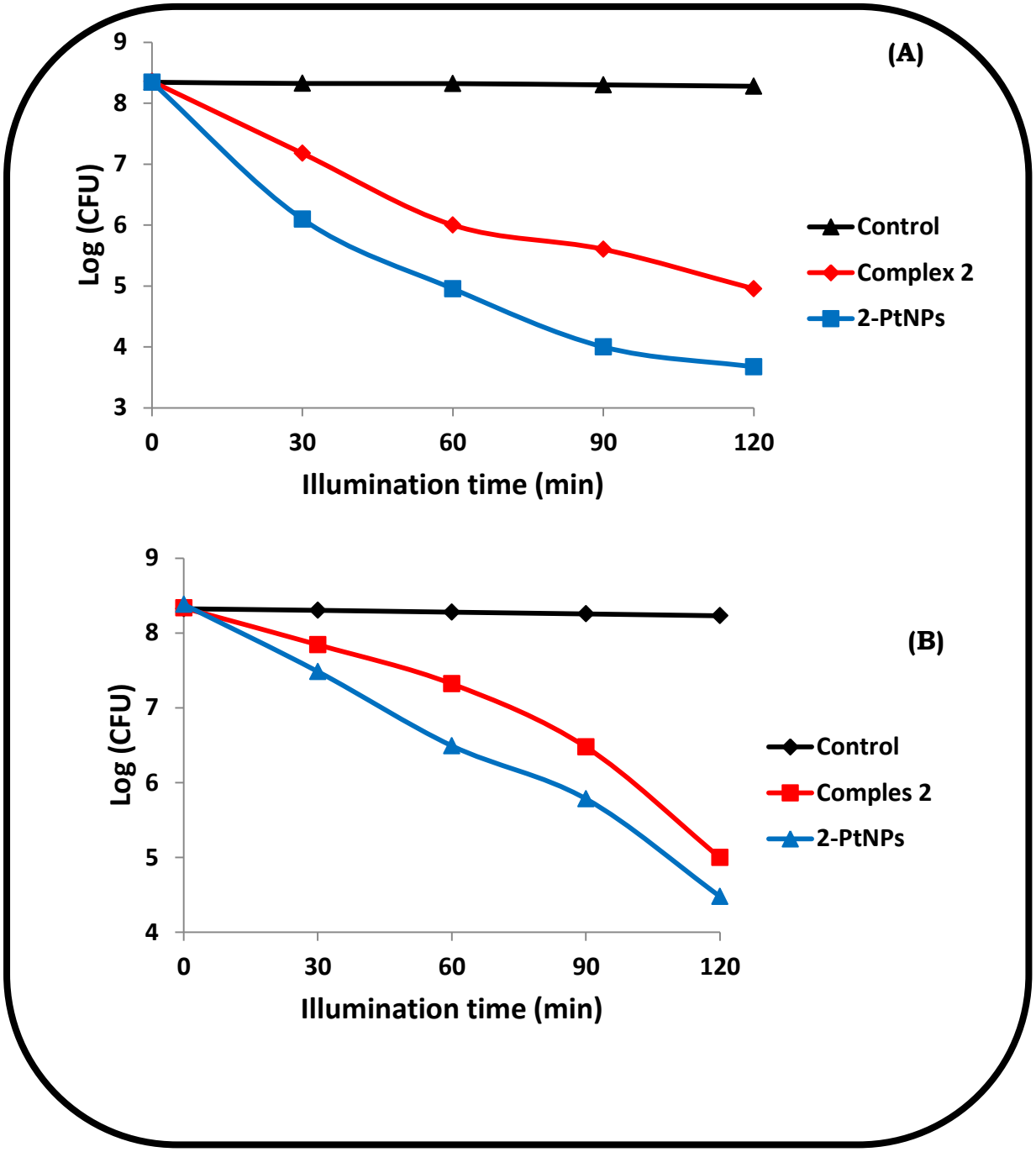
(A)
Log (CFU)
9
8
7
6
5
4
3
0
30
60
90
120
Illumination time (min)
Control
Complex 2
2-PtNPs
(B)
Log (CFU)
9
8
7
6
5
4
0
30
60
90
120
Illumination time (min)
Control
Comples 2
2-PtNPs

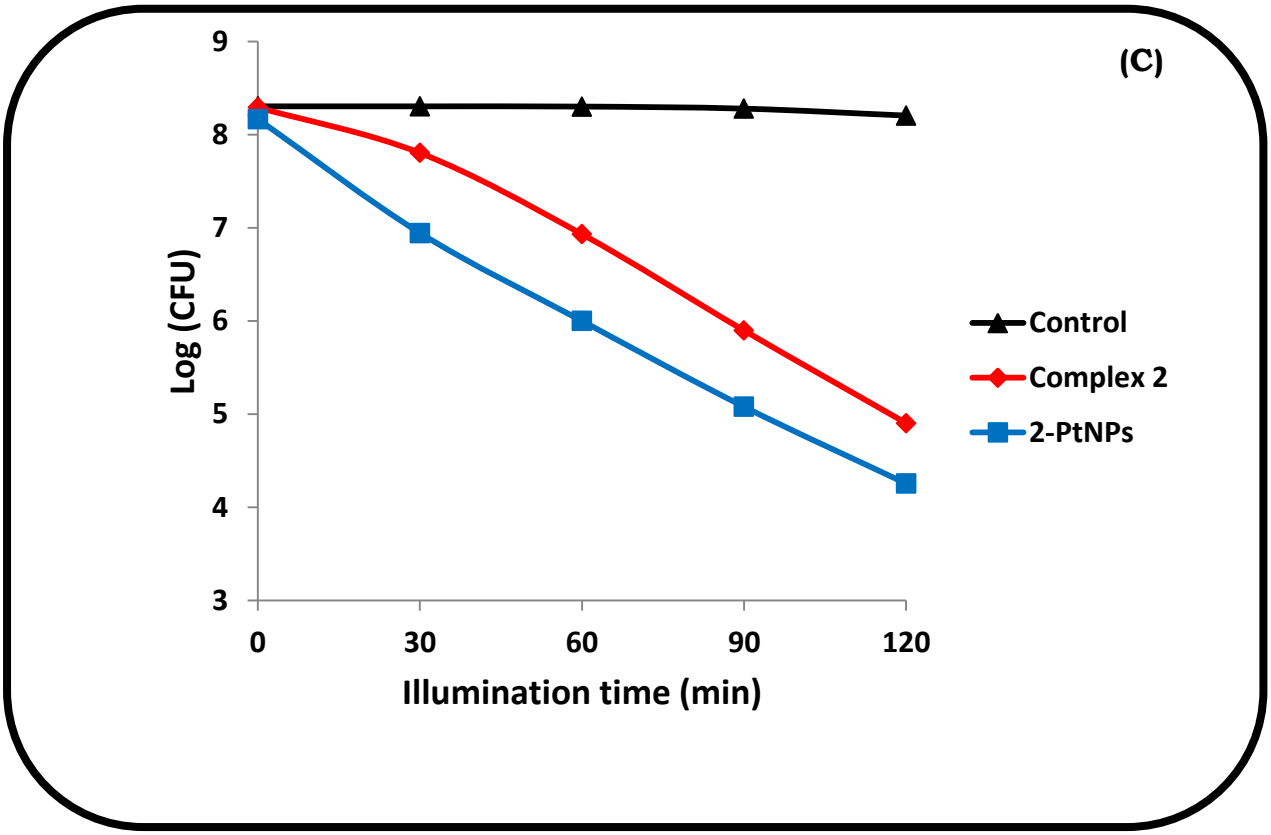

Figure 6.1: Photoinactivation of *S. aureus* (A), *E. coli* (after EDTA treatment) (B) after treating with EDTA and *C. albicans* (C) at different illumination time.

6.1.2 Complex 1 conjugated to different shaped PtNPs

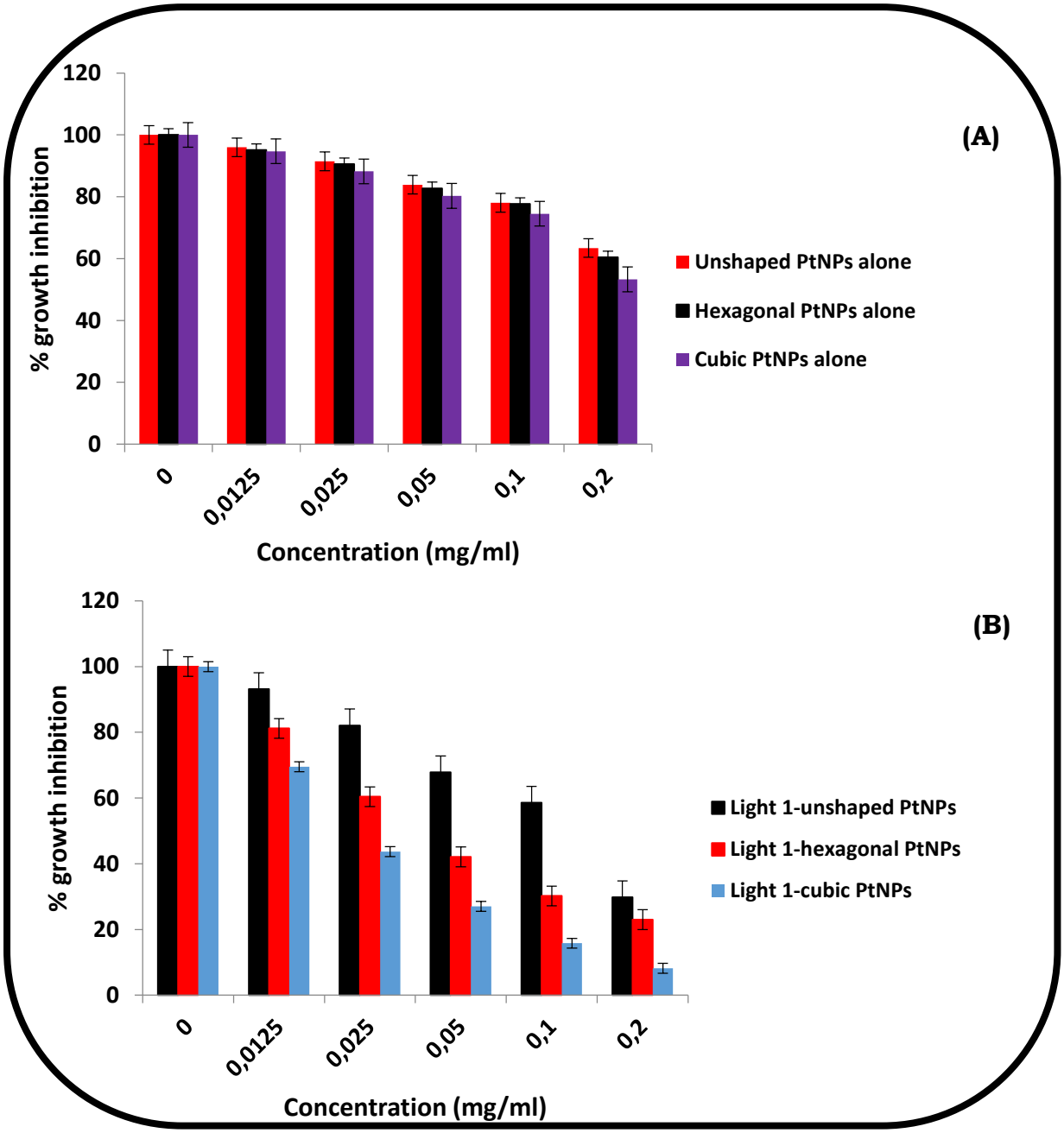

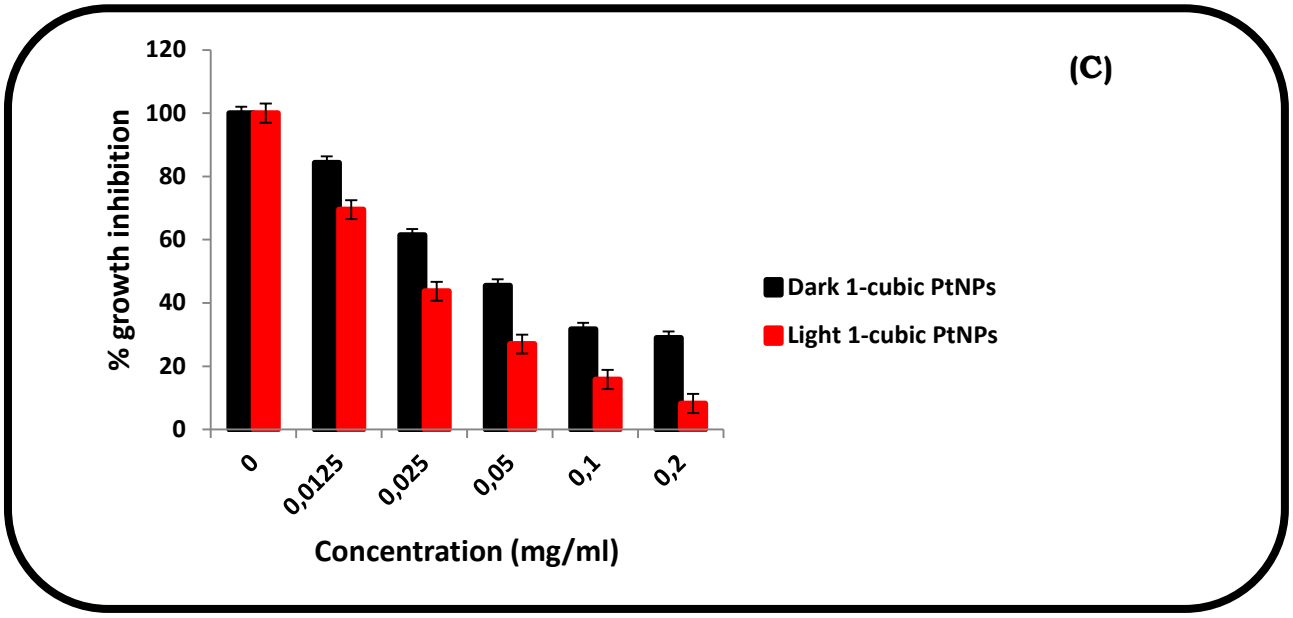

Figure 6.2: Antibacterial activity of (A) PtNPs of different shapes alone; (B) compares all conjugates (1-cubic PtNPs, 1-hexagonal PtNPs and 1-unshaped PtNPs) and (C) 1-cubic PtNPs conjugate in the dark and when illuminated in liquid broth against *S. aureus*. Illumination with visible light, irradiance = 0.05 W cm^{-2}

Fig. 6.2A shows that there was a slight increase in the inactivation of *S. aureus* (in the dark) with concentration, when PtNPs were employed alone, with cubic PtNPs showing more activity. The photoinactivation in the presence of PtNPs is due to their known antibacterial properties **[156].**

Fig. 6.2C (using **1**-cubic PtNPs as an example, P <0.05) shows that dark toxicity was observed for the conjugates. Similar plots were observed for the other **1**-PtNPs conjugates. Dark toxicity of photosensitizers has also been reported by various researchers **[157].** The dark toxicity is also due to the toxicity of PtNPs alone in Fig. 6.2A with P <0.001. Comparing all the

conjugates, Fig. 6.2B, **1**-cubic PtNPs showed the best PACT activity, with only 11 % off the bacteria surviving at 0.2 mg/ml and the P <0.001.

The corresponding log plot (with change in fluence) is shown in Fig. 6.3 with a reduction of 4.60 log units for **1**-cubic PtNPs, 3.94 log unit for **1**-hexagonal PtNPs and 3.31 log units for **1**-unshaped PtNPs therefore showing excellent PACT activity with P <0.01, when compared with the porphyrin alone with a log reduction of 2.26, Table 6.1. The high log reduction value for **1**-cubic PtNPs corresponds to its high singlet oxygen quantum yield value, Table 6.1. Comparing with the other two conjugates, **1**-unshaped PtNPs showed the least antimicrobial activity. Small particle sizes Table 6.1 have been reported **[158]** to enhance antibacterial activity due to the larger number of atoms on the surface, which will result in higher surface area, leading to improved activity. Also the uptake of nanoparticles by cells has been shown to depend on their shape **[159]**. It is thus likely that cubic PtNPs interact more favourably with cells compared to hexagonal ones. **1**-unshaped PtNPs conjugates do not have particular shape but they have a size that could influence the interaction with the bacteria cell wall therefore limiting the penetration of the cell wall, resulting in less antibacterial activity.

There is also a general greater toxicity for **1**-PtNPs (compared to due to **1** alone) due to increased singlet oxygen quantum yield of the porphyrin in the presence of PtNPs. The control in Fig. 6.3 represents the bacteria without a photosensitizer and irradiated. And it is clear there is no PACT activity without the photosensitizer.

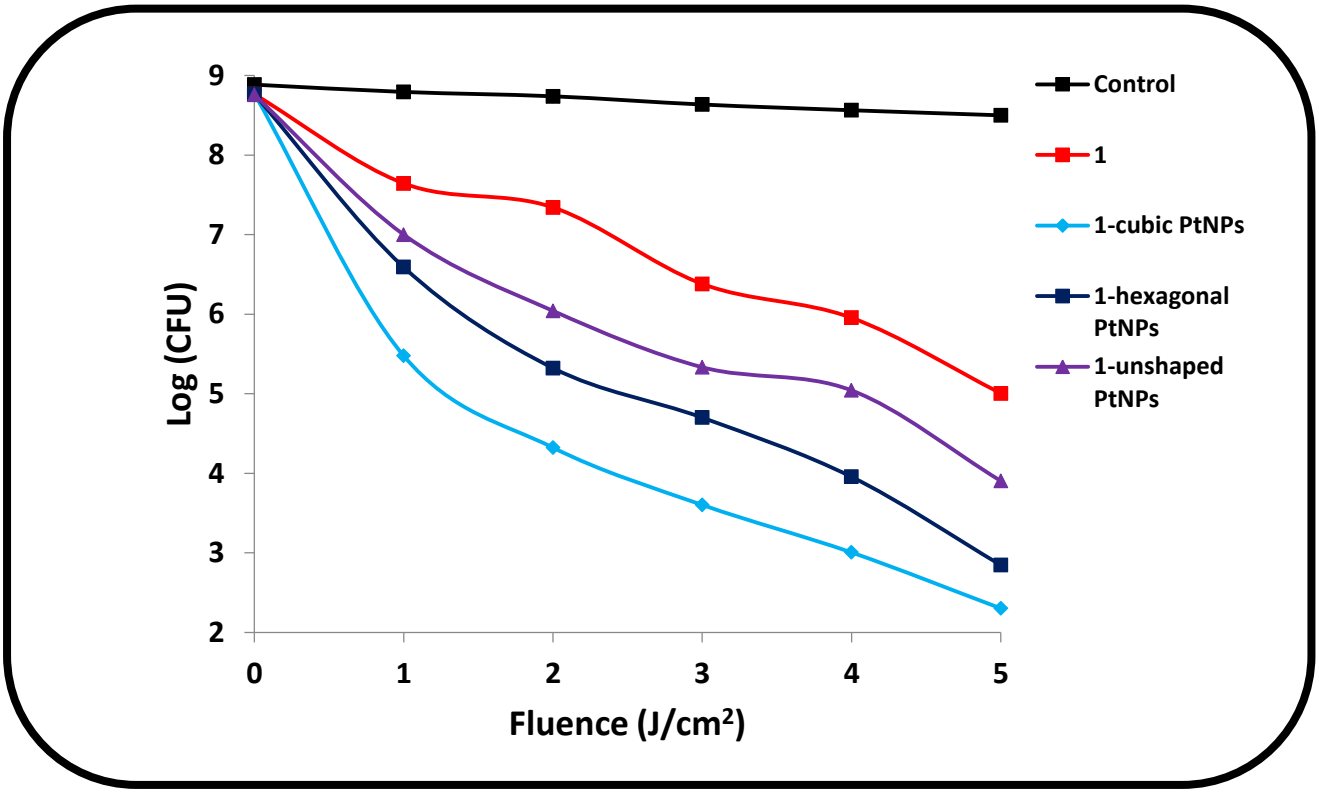

Figure 6.3: Photoinactivation of *S. aureus* at different fluences where log redution of more than 3 was obtained for 1-cubic PtNPs conjugate, 1-hexagonal PtNPs and 1-unshaped PtNPs. Concentration of the photosensitizers = 0.05 mg/mL. The values shown are of experiments which are independent of each other and the P<0.01

The log (survival %) was determined using **1** and **1**-hexagonal PtNPs (as an example) against *S. aureus*. The spectrophotometric analysis showed less survival of bacteria as light exposure time increased Fig. 6.4A and B. **1**–hexagonal PtNPs showed less bacterial survival with P<0.05, Fig. 6.4B, due to increased singlet oxygen quantum yield as compared **1** alone. The time interval used was from 0 to 90 min.

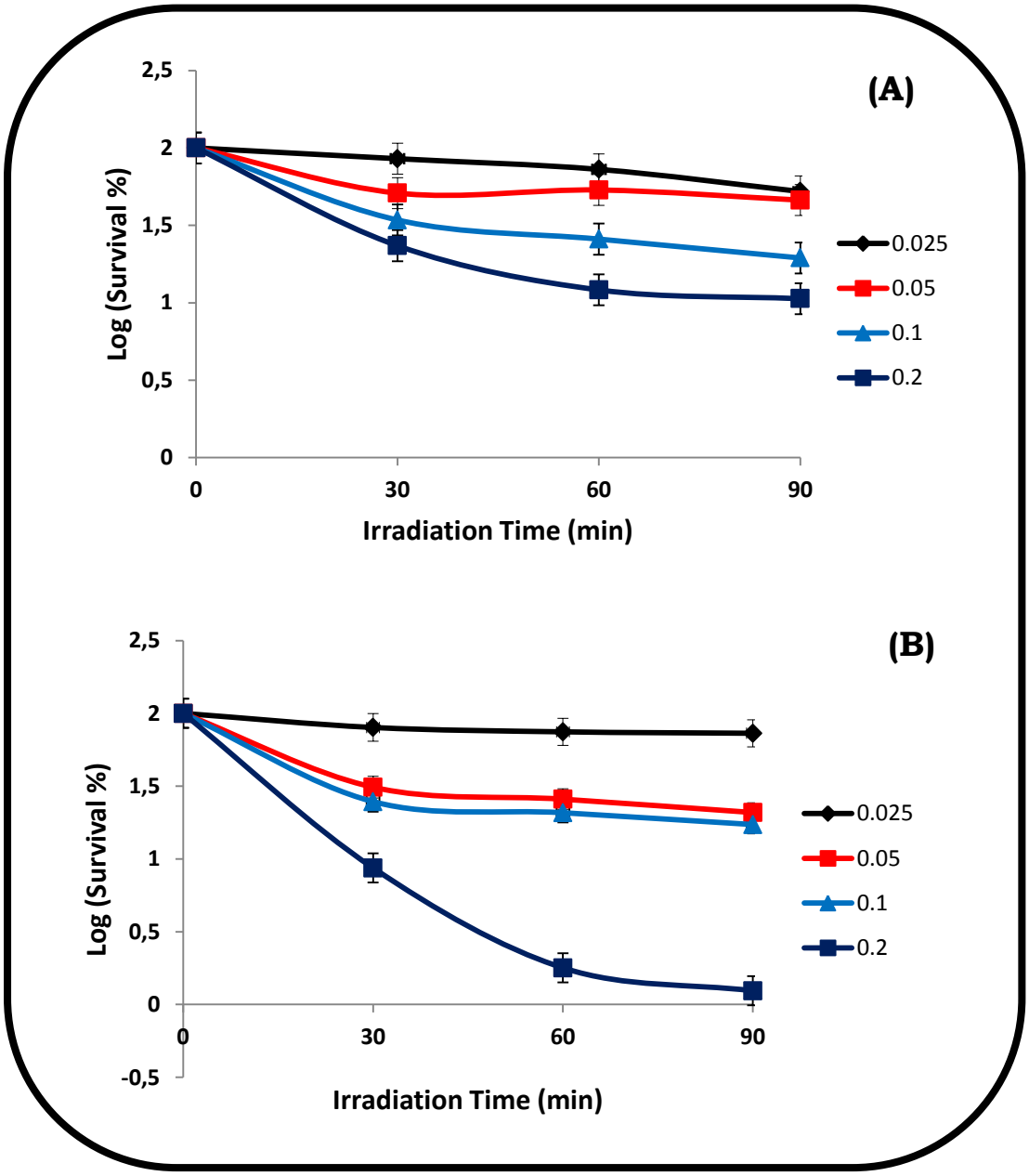

Figure 6.4: Logarithmic reduction of *S. aureus* 1(A) and (B) 1-hexagonal PtNPs conjugate, in liquid broth solution at different concentrations (0.025, 0.05, 0.1, 0.25 mg/ml) at defined irradiation time. The values shown are of experiments which are independent of each other and the P<0.05

6.1.3 PACT using electrospun fibers

The antimicrobial activities of these compounds (**1** and **2** with their conjugates) were further carried out in electrospun nano fibers where zone of clearance can be seen (Fig. 6.5 and 6.6). Fig. 6.5 shows digital images of the nutrient agar plates containing *S. aureus* in contact with electrospunfibers. When irradiated with light in the presence of bacteria, **1**-cubic PtNPs/PS, **1**-hexagonal PtNPs/PS and **1**-unshaped PtNPs/PS showed growth inhibition as this can be clearly seen by the clearing around the fibre.

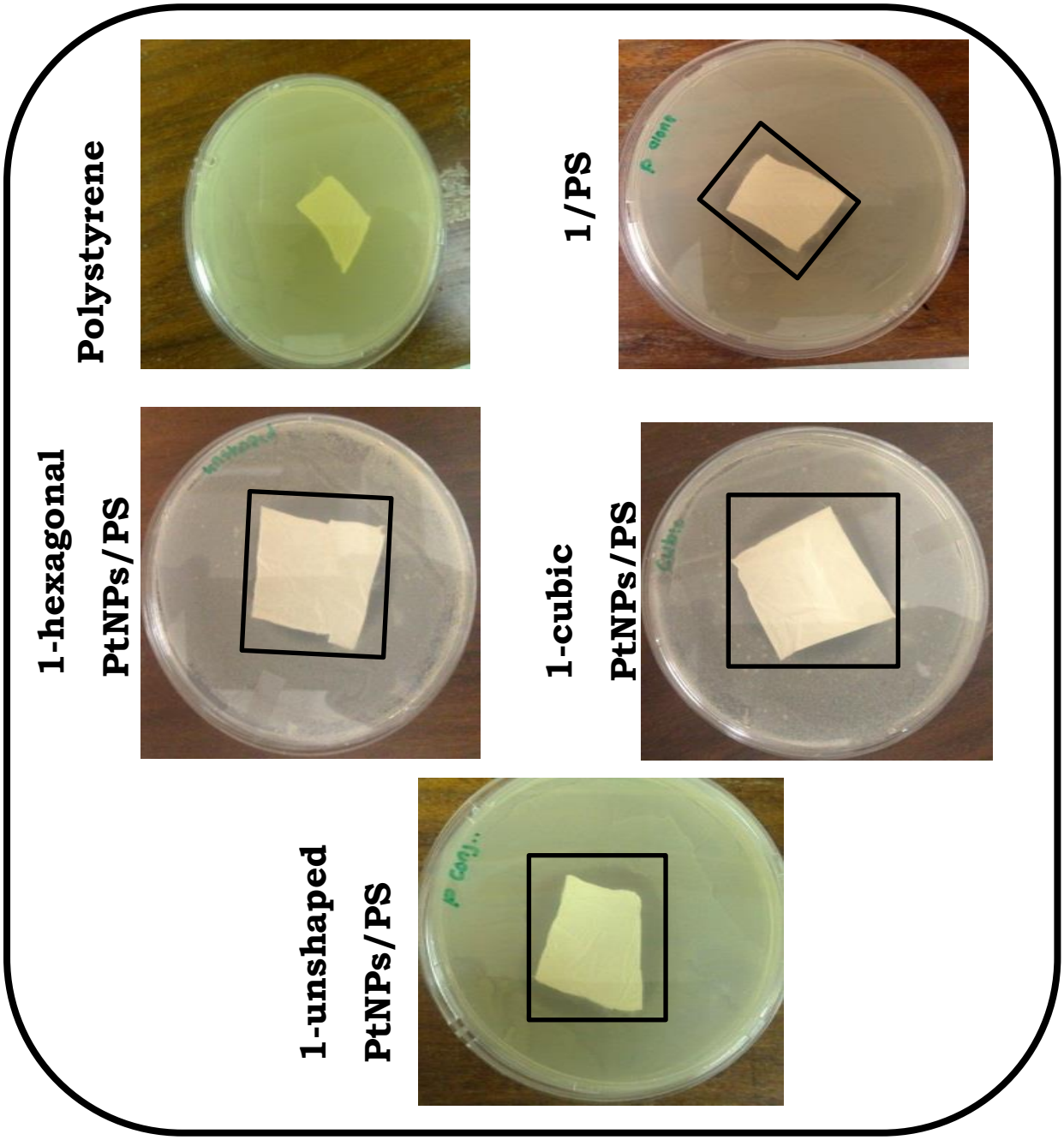

Figure 6.5: Images of the antimicrobial inhibition test using polystyrene fiber (used as a control), fibre modified with 1, fibre modified with 1-hexagonal PtNPs, fibre modified with 1-cubic PtNPs and fibre modified with 1-unshaped PtNPs under illumination.

Fig 6.6 shows digital images of electrospunfibers where zone of clearance can be seen against *E. coli* for **2**/PS and **2**-hexagonal PtNPs/PS, respectively. More of zone of clearance can be seen against *S. aureus* Fig. 6.6, compared to *E. coli*. There was no clear zone of clearance against *C. Albican* and this could be due to a different mechanism of photodynamic action **[9].** The efficiency of photo-eradication of *C. albicans* is dependent on porphyrin uptake. It has been reported that porphyrins are not taken up by yeast cells (*C. albicans*) and the phototoxic activity is largely due to the unbound photosensitiser molecules in the bulk aqueous medium **[9]**. Since for electrospun fibers, the porphyrins are not in solution, there was no PACT activity for *C. albicans*.

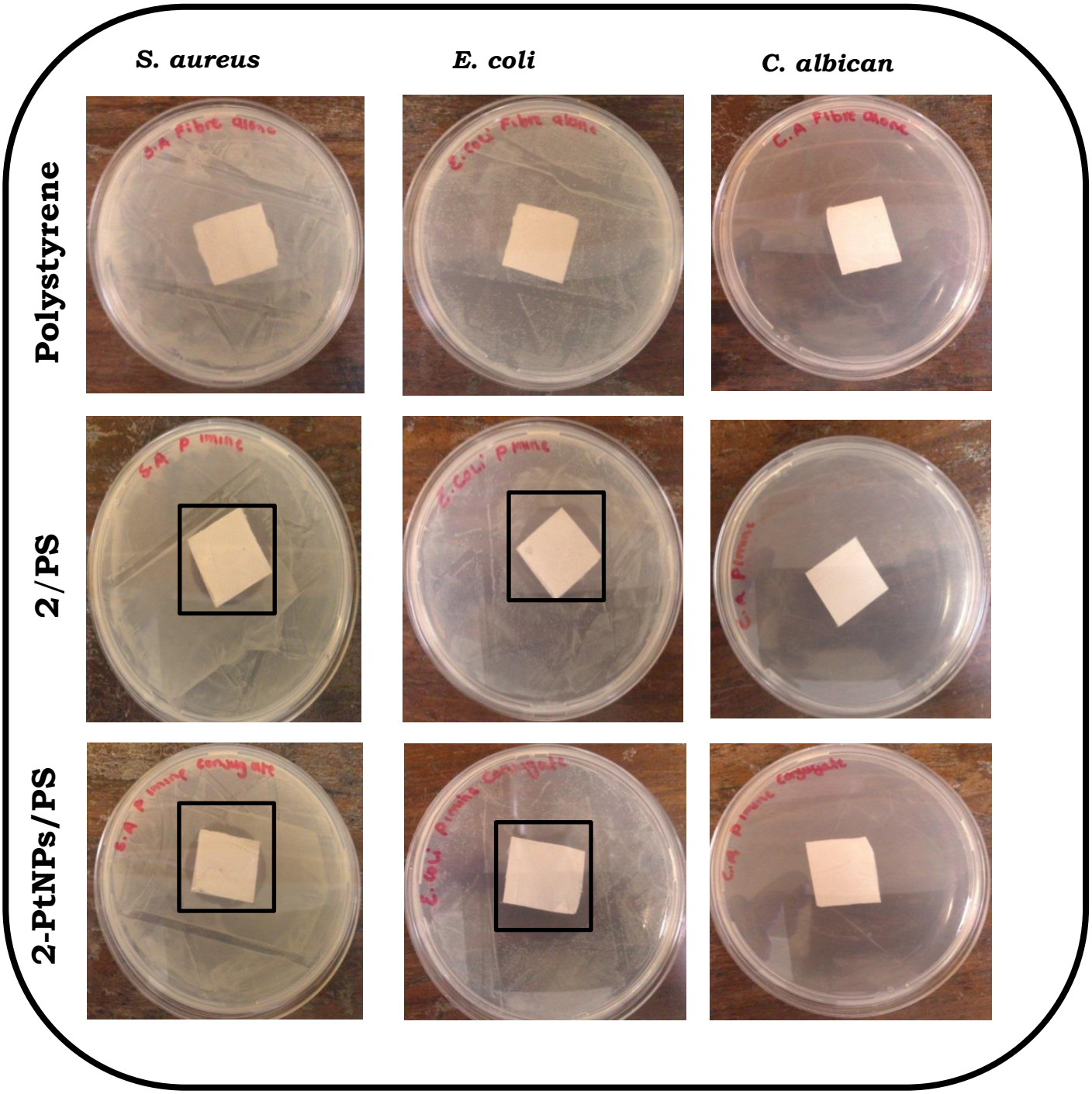

Figure 6.6: Images of the antimicrobial inhibition test using 2/PS and 2-hexagonal PtNPs/PS, under illumination with visible light. Unmodified polystyrene alone was employed as a control against *S. aureus*, *E. coli* and *C. Albican*, respectively.

TEM imaged of *S. aureus* shows how easily the photosensitizer can localize around the bacterial cells Fig. 6.7

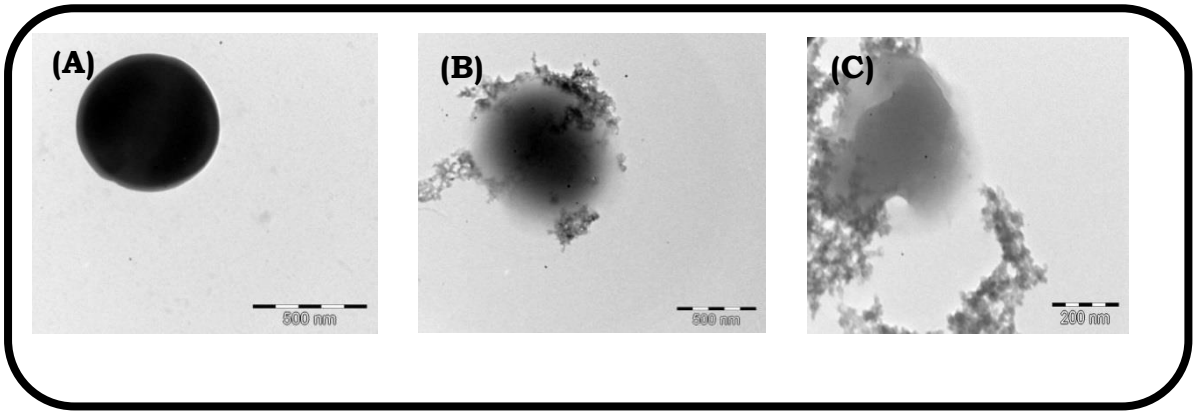

Figure 6.7: TEM imaged of *S. aureus* (A) before the introduction of a photosensitizer, (B) after the photosensitizer was introduced and then incubated and (C) is the destructed *S. aureus*.

6.2 PACT using Pcs

Antimicrobial activities were further carried out for **3** and **4**. Phthalocyanines have been shown to have antimicrobial activities and this is due to the fact that MPcs have an intense absorption in the red region of visible light, selective localization in cells and efficient generation of singlet oxygen ($^1O_2$) **[160]**. Complexes **3**, **4** were tested for the photo-inhibitory activity against *C. albicans* and *E. coli*

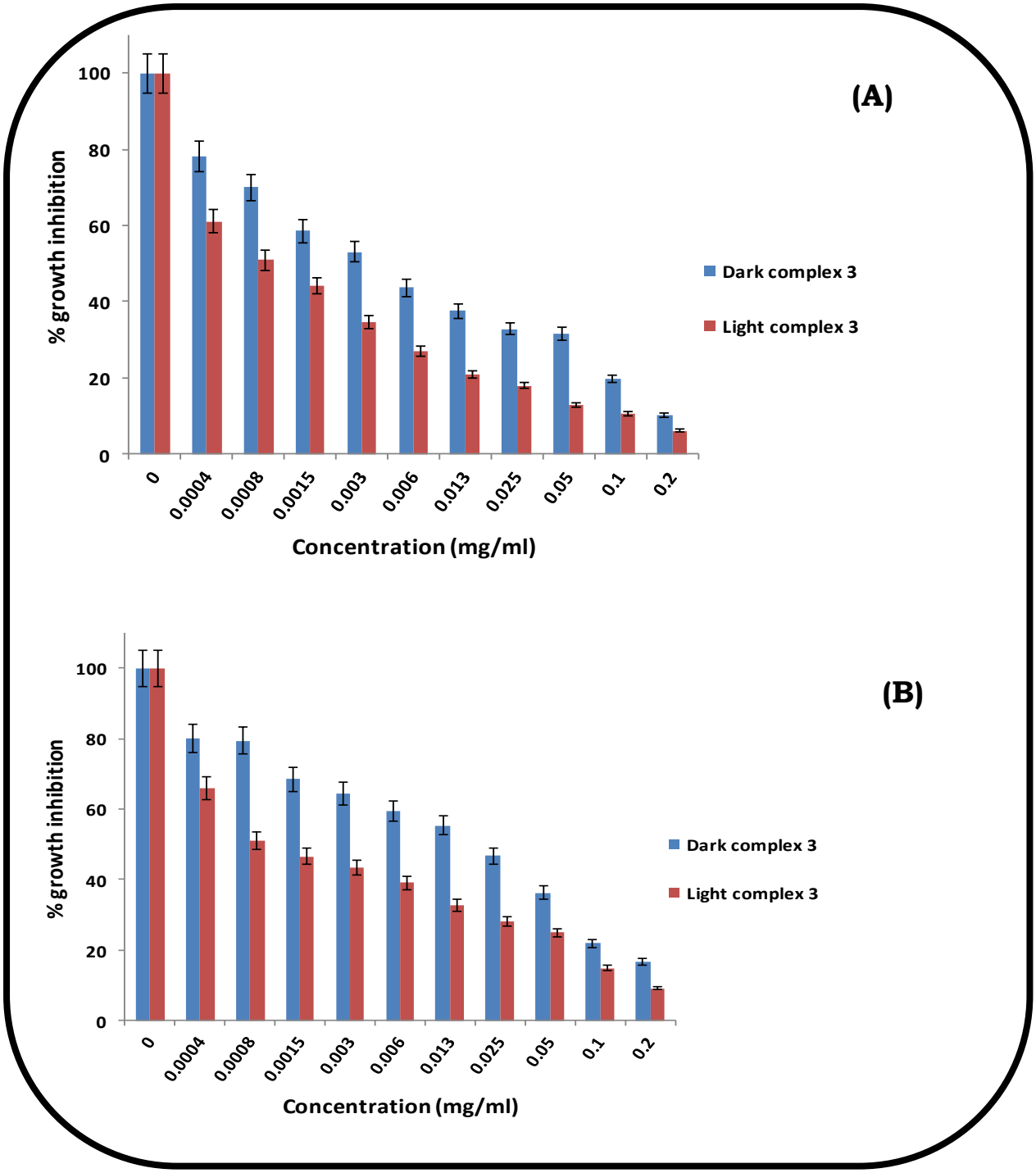

Figure 6.8: Antimicrobial activity of 3 against *C. albicans* (A) and *E. coli* (B) in the presence and absent of light. The values shown are of experiments which are independent of each other and the P<0.01

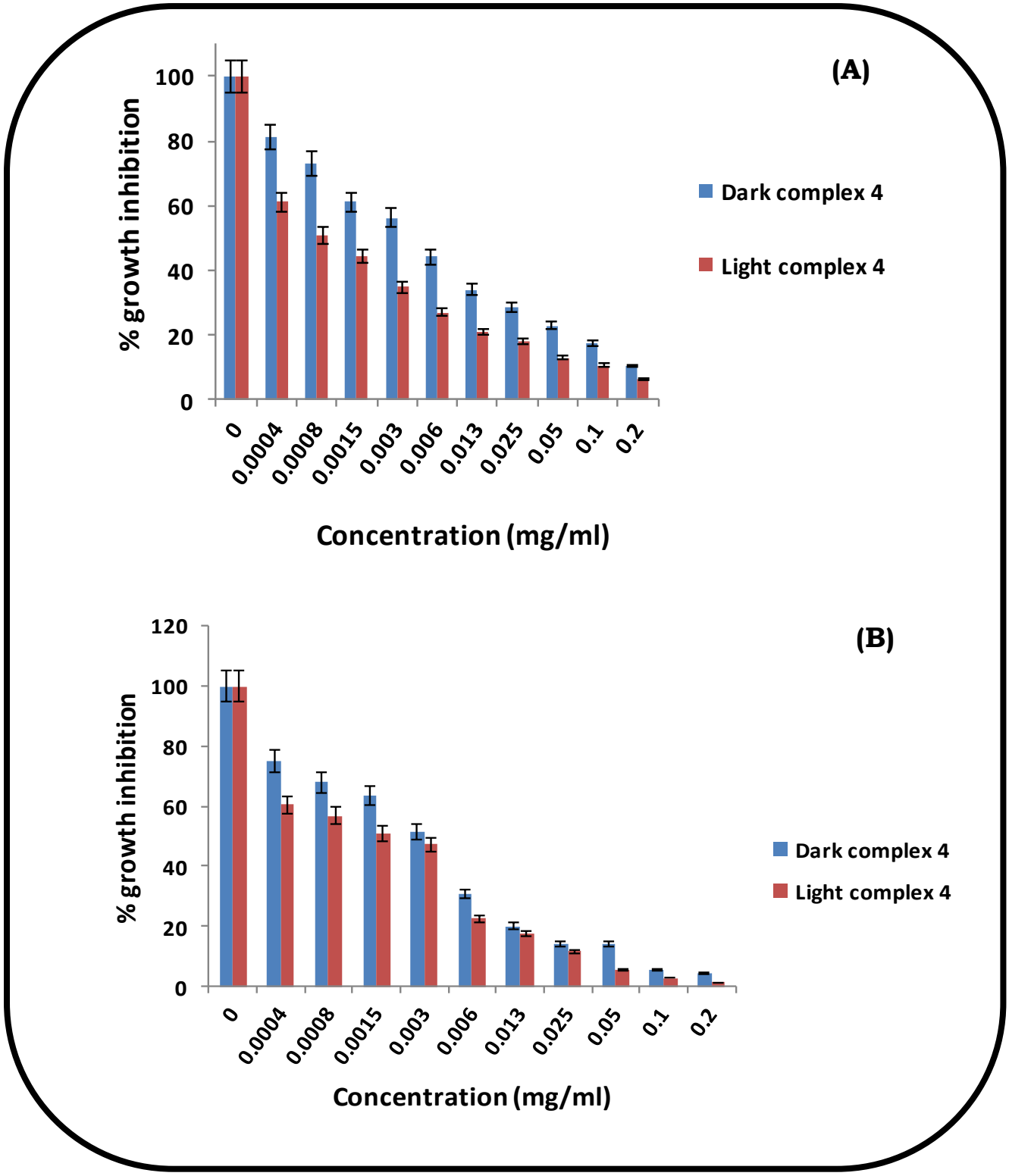

Figure 6.9: Antimicrobial activity of 4 against *C. albicans* (A) and *E. coli* (B) in the presence and absent of light. The values shown are of experiments which are independent of each other and the P<0.05

The antimicrobial photo-inhibition studies of **3** and **4** conjugates are presented in Fig. 6.8 where P< 0.01 and Fig. 6.9 with P<0.05. All the complexes showed inhibition against *C. albicans* (A) and *E. coli* (B) in the dark with an improved inhibition under illumination. Dark toxicity of the phthalocyanines is known and is observed for **3** and **4 [161]**. Platinum complexes also have shown enhancement of antiproliferative activity in the presence of visible light **[162]** hence an improved microbial inhibition is expected under illumination for **4** which is linked to Pt complex.

Higher microbial inhibitions were observed at higher concentration of complexes for both studies, in the dark and under illumination with light. Complex **4**, Fig. 6.9 gave the best inhibition. This is likely due to the additive or dual contribution of microbial growth inhibition by the Pt (through chemotherapy) and the **3** (through PDT) both present in the conjugate. Moreover, this conjugate **(4)** showed increased singlet oxygen generation, Table 6.1 hence, enhanced photochemical activity is expected showing its suitability for PACT. Higher microbial inhibition was observed against *C. albicans* compared to *E. coli* for both **3** and **4** as stated above that *E. coli* is not easily inhibited.

Approximately 0% survival was achieved for the **4** conjugate against *E. coli* at 0.2 mg/mL under illumination with light. The minimum inhibitory concentration required to inhibit the growth of 50% of organisms (MIC50) was found to be $<8 \times 10^{-4}$ mg/mL for the **4** conjugate for both *C. albicans* and *E. coli* under illumination where the P< 0.05.

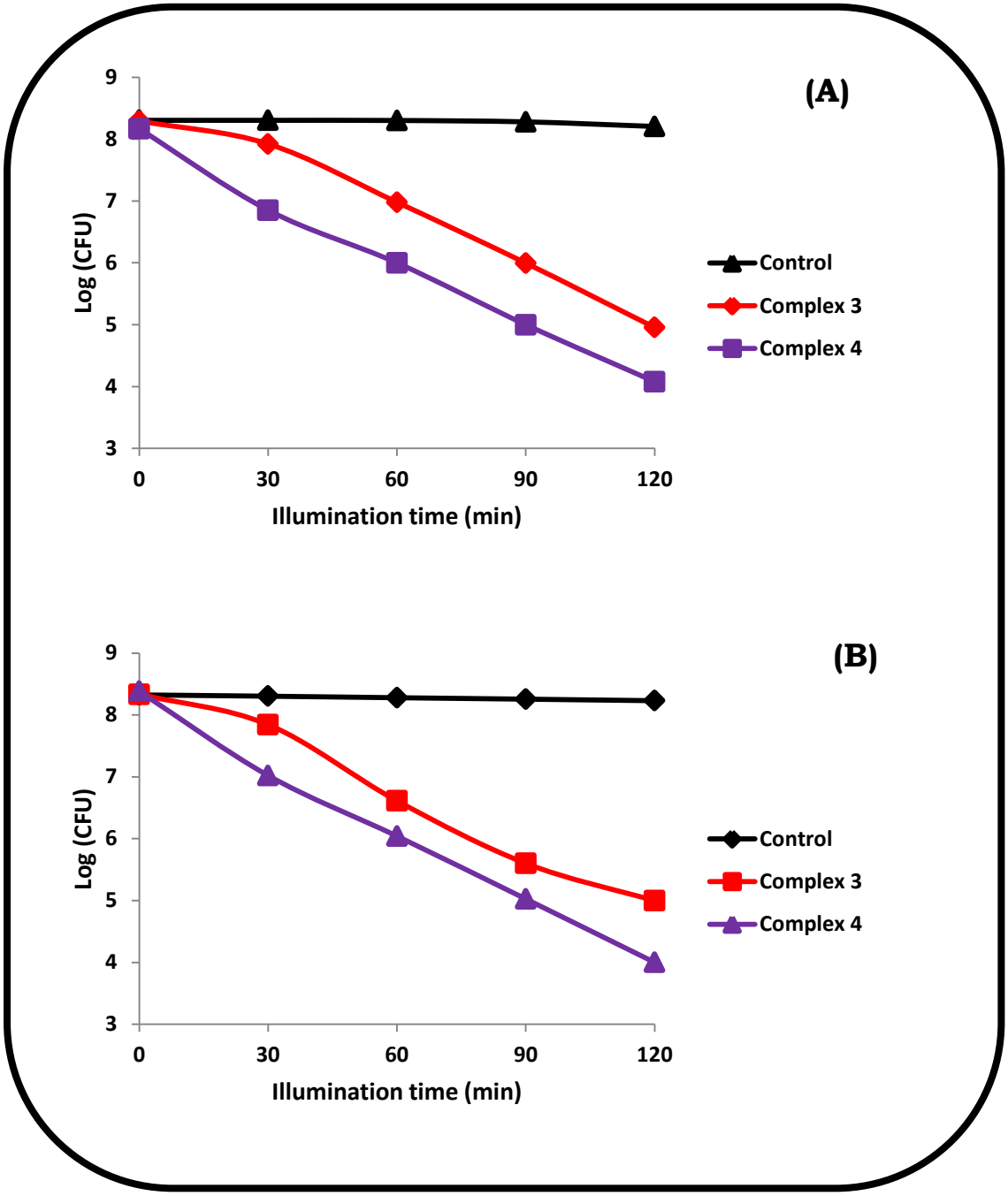

Figure 6.10: Photoinactivation of *C. albicans* (A), *E. coli* (B) after treating with EDTA at different illumination time. The values shown are of experiments which are independent of each other and the P<0.05

The *E. coli* cells were pre-treated using EDTA as mentioned previously with improved log values. The antibacterial activity of complex **3** or **4** was determined using *C. albicans* (Fig. 6.10A) and *E. coli* (Fig. 6.10B), where CFU

was plotted against illumination time. The log reduction of *C. albicans* was higher as compared to that of *E. coli* even after pre-treating the cells with EDTA. This could be that the time which was used to pretreat the cells was not long enough therefore the EDTA had not accumulated around the cells as to disrupt the cell of the bacteria. Comparing Pcs with porphyrins, Pcs (**3** and **4**) showed larger log values against *C. albicans* and *E. coli* Table 6.1, this is most likely to be due to the direct link of Pt to Pc.

CHAPTER SEVEN

CONCLUSIONS

Complex **1** was conjugated to cubic, hexagonal and unshaped PtNPs and embedded into electrospun nanofibres. The singlet oxygen quantum yields of these conjugates when in solution or embedded into electrospun nanofibres were higher for the conjugate of **1** with cubic PtNPs compared to **1**-hexagonal PtNPs and **1**-unshaped PtNPs.

The conjugates were used in PACT studies and **1**-cubic PtNPs showed more antibacterial activity against *S. aureus* as the log reduction unit obtained was 4.60 log (which indicate 99.99% of the bacteria have been killed) due to the particle size as well as the high singlet oxygen quantum yield. The log reductions for *S. aureus* were 3.94 log units for **1**-hexagonal PtNPs and 3.31 log units for **1**-unshaped PtNPs which were all above the standard log of 3, and this is an indication that 99.9% of the bacteria have been killed.

Complex **2** and its conjugate with PtNPs to form **2**-hexagonal PtNPs were successfully synthesised. **2** and **2**-hexagonal PtNPs were then successfully electrospun into polystyrene. The photodynamic antimicrobial chemotherapy (PACT) of **2** and **2**-hexagonal PtNPs activity against *S. aureus*, *E. coli* and *C. albicans* were carried when in solution as well as when embedded in electrospun nanofibres. In solution, **2**-hexagonal PtNPs gave enhanced PACT activity for all microorganisms when compared to **2** alone.

The highest log reduction was obtained for *S. aureus* with **2**-hexagonal PtNPs when comparing the porphyrin conjugates giving a value above log 4 in solution. When embedded in electrospun fibers, **2**-hexagonal PtNPs

compounds showed PACT activity against *E. coli* and *S. aureus*, but for the nanofibres showed no PACT activity against *C. albicans* at all.

Dihydroxosilicon tris(diaquaplatinum)octacarboxyphthalocyanine conjugate **4** was synthesized and its photophysicochemical behavior was evaluated comparatively to dihydroxosilicon octacarboxyphthalocyanine **3**. The conjugate was shown to generate higher amount of singlet oxygen, thus, a better photosensitizer compared to **3** alone and an indication that introduction of Pt into the MPc improves the efficiency of MPc complexes as photosensitizers. Antimicrobial studies revealed an additive effect of photodynamic activity of the MPc and cytotoxicity of platinum in the conjugate as it showed highest antimicrobial activity towards *C. albicans* and *E. coli* compared to **3** alone under illumination. The platinated Pc complexes may have potential to be used for both photodynamic applications (using Pcs) and chemotherapy (using coordinated Pt complexes). Both porphyrins and phthalocyanines showed potential and better PACT activities.

References

[1]. G. Jori, S. B. Brown, Photochem. Photobiol. Sci. 3 (2004) 403.

[2]. O. Tunger, G Dinc, B. Ozbakkaloglu, C. Atman, U. Algun, Int. J. Antimicrob. Agents. 15 (2000) 131.

[3]. M. R. Hamblin, T. Hasan, Photochem. Photobiol. Sci. 3 (2004) 436.

[4]. B. A. Cunha, in Infectious disease in critical care medicine: Methicillin-Resistance *Staphylococcus aureus*/ Vancomycime –Resistance *Enterococci* colonization and infection in the critical care unit, Infoma Healthcare USA, Inc. New York (2007).

[5]. M. Wainwright, J. Antimicrob. Chemother. 42 (1998) 13.

[6]. Z. Malik, J. Hanania, Y. Nitzan, J. Photochem. Photobiol. B: Biol. 5 (1990) 281.

[7]. P. W. Taylor, P. D. Stapleton, J. P. Luzio, Drug. Discov. Today. 7 (2002) 1086.

[8]. K. D. Winckler, J. Photochem. Photobiol. B Biol. 86 (2007) 43.

[9]. R. F. Donnelly, P. A. McCarron, M. M. Tunney, J. Microbiol. Res. 163 (2008) 12.

[10]. T. D. Felber, E. B. Smith, J. M. Knox, C. Wallis, J. L. Melnick, JAMA. 223 (1973) 292.

[11]. K. Gardlo, Z. Horska, C. D. Enk, L. Rauch, M. Megahed, T. Ruzicka, C. Fritsch, J. Am. Acad. Dermatol. 48 (2003) 896.

[12]. O. Raab, Biol. 39 (1900) 524.

[13]. T. Maisch, Laser. Med. Sci. 22 (2007) 91.

[14]. L. Ryskova, V. Buchta, R. Slezak, Cent. Eur. J. Biol 5 (2010) 406.

[15]. H. Von Tappeiner, A. Jodblauer, Dtsch. Arch. Klin. Med. 80 (1904) 487.

[16]. X. J. Fu, Y. Fang, M. Yao, BioMed. Research. Intern. 2013 (2013) 9.

[17]. A. P. Castano, T.N. Demidova, M.R. Hamblin, Photodiagn. Photodyn. Ther. 1 (2004) 279.

[18]. G. Jori, Environ. Toxicol. Oncol. 25 (2006) 505.

[19]. A. Pfitzner, B.W. Sigusch, V. Albrecht, E. Glockmann. J. Periodontol. 75 (2004) 1343.

[20]. S. Dutta, D. Ray, B.K. Kolli, K.P. Chang. Antimicrob. Agents Chemother. 49 (2005) 4474.

[21]. A. S. Garcez, M. S. Ribeiro, G. P. Tegos, S. C. Nunez, A. O. Jorge, M. R. Hamblin. Lasers Surg. Med. 39 (2007) 59.

[22]. B. Alberts, A. Johnson, J. Lewis, M. Raff, K. Roberts, P. Walters. Molecular biology of the cell. (E.d 4th) (2002).

[23]. D. Woodward, in Basic concepts and Biodiversity, Pennsylvania state university (2013.).

[24]. F. F. Sperandro, Y. Y. Haung, M. R. Hamblin, Recent patents on anti-infective drug discovery. 8 (2013) 120.

[25]. T. Maisch, R. M. Szeimies, G. Jori, C. Abelsa, J. Photochem. Photobiol. Sci. 3 (2004) 917.

[26]. C. M. B. Carvalhoa, J. P. C. Toméa, M. A. F. Faustinoa, M. G. P. M. S. Nevesa, A. C. Toméa, J. A. S. Cavaleiro, L. Costab, E. Alvesb, A. Oliveirac, Â. Cunhab, A. Almeidab J. Porphyr. Phthalocya. 13 (2009) 577.

[27]. Z. Malik, J. Hanania, Y. Nitzan, J. Photochem. Photobiol, B: Biol. 5 (1990) 293.

[28]. Z. Malik, H. Ladan, Y. J. Nitzan, Photochem. Photobiol, B: Biol. 14 (1992) 266.

[29]. P. L. Gendler, in *Meso*-substituted Phorphyrins, University of California, Berkeley, (1973).

[30]. Z.W. Küster, Physiol. Chem. 82 (1912) 463.

[31]. H. Fischer, K. Zeile, Ann. Chem. 468 (1929) 98.

[32]. P. J. Rothemund, Am. Chem. Soc. 57 (1936) 2010.

[33]. A.D. Alder, F.R. Longo, F. Kampas, J. Kin, J. Inorg. Nucl. Chem. 32 (1970) 2449.

[34]. J.S. Lindsey, I. C. Schreiman, H. C. Hsu, P.C. Kearney, A. M. Marguerettaz, J. Org. Cherm. 52 (1987) 836.

[35]. H. de Diesbach, E. von der Weid, Helv. Chim. Acta, 10 (1927) 886.

[36]. L. R. Milgrom, in The colours of life: in An introduction to the chemistry of porphyrines and related compounds, Oxford University press. (1997).

[37]. Y. Nitzan, H. Ashkenazi, Current Microbiology. 42 (2001) 414.

[38]. M. Merchat, G. Bertolini, P. Giacomini, A. Villanueva, G. Jori, J. Photochem. Photobiol B: Biol. 32 (1996) 157.

[39]. S. Banfi, E. Caruso, L. Buccafurni, V. Battini, S. Zazzaron, P. Barbieri, V. Orlandi, J. Photochem. Photobiol B: Biol. 85 (2006) 38.

[40]. W. N. Burda, K. B. Fields, J. B. Gill, R. Burt, M. Shepherd, X. P. Zhang, L. N. Shaw, Eur. J. Clin. Microbiol. Infect. Dis. 31 (2012) 335.

[41]. D. Lazzeri, M. Rovera, L. Pascua, E. N. Durantini, J. Photochem Photobiol. 80 (2004) 293.

[42]. Y. Li, T. M. Pritchett, J. Huang, M. Ke, P. Shao, W. Sun, J. Phys. Chem. A. 112 (2008) 7200.

[43]. M. O. Liu, C. H. Tai, A. T. Hu, T. H. Wei, J. Organomet. Chem. 689 (2004) 2138.

[44]. A. von Braun, J. Tscherniac, Ber. Deut. Chem. Ges. 40 (1907) 2709.

[45]. R.P. Linstead, J. Chem. Soc. (1934) 1016.

[46]. P. Gregory, J. Porphyr. Phthalocya. 3 (1999) 468.

[47]. A. G. Dandridge, H. A. E. Drescher, J. Thomas, Dyes British Patent, 322 (1929)169.

[48]. J. M. Robertson, J. Chem. Soc. (1936) 1195.

[49]. J. M. Robertson, J. Chem. Soc. (1935) 615.

[50]. D. Dini, M. Hanack, in The Porphyrin Handbook: Phthalocyanines: properties and materials, Eds. M. K. Kadish, K. M. Smith, R. Guilard, Academic Press, USA, (2003).

[51]. F. Dumoulin, M. Durmus, V. Ahsen, T. Nyokong, Coord. Chem. Rev. 254 (2010) 2792.

[52]. M. Kandaz, S. L. J. Michel, B. M. Hoffman, J Porphyr. Phthalocya. 7 (2003) 700.

[53]. C. A. Robertson, D. Hawkins, E.H. Abrahamse, J. Photochemi and Photobiol 29 (2009) 8.

[54]. N. Masilela, P. Kleyi, Z. Tshentu, G. Priniotakis, P. Westbroek, T. Nyokong, Dyes Pigments. 96 (2013) 500.

[55]. I. Scalise, E. N. Durantini, Bioorg. Med. Chem. 13 (2005) 3037.

[56]. V. Mantareva ,V. Kussovski, I. Angelov, D. Wohrlet, R. Dimitrov, E. Popova, S. Dimitrov J. Photochem. Photobiol. 10 (2011) 102.

[57]. V. Mantareva , V. Kussovski, I. Angelov, E. Borisova, L. Avramov, G. Schnurpfeild, D. Wohrle, Bioorg. Med. Chem. 15 (2007) 4829.

[58]. M. E. Vol'pin, G. N. Novodarova, N. Yu. Krainova, V. P. Lapikova, A. A. Aver'yanov, J. Inorg. Biochem. 81 (2000) 292.

[59]. S. K. Saini, A. Jena, J. Dey, A. K. Sharma and R. Singh, Mag. Res. Imag. 13 (1995) 985.

[60]. W. M. Sharman, S. V. Kudrevich and J. E. van Lier. Tet. Lett. 37 (1996) 5831.

[61]. I. J. Macdonald, T. J. Dougherty. J. Porphyr. Phthalocya. 5 (2000) 129.

[62]. N. B. McKeown, Chem. Ind. (1999) 92.

[63]. O. Dolotova, O. J. Kaliya, Porphyr. Phthalocya. 15 (2011) 632.

[64]. R. A. Bulgakov, N. A. Kuznetsova, O. V. Dolotova, E. N. Shevchenko, A. D. Plyutinskayab, O. L. Kaliyaa, T. Nyokong, Macroheterocycles. 5 (2012) 357.

[65]. N. Malinga, O. Dolotova, R. Bulgakov, E. Antunes, T. Nyokong, Dyes Pigments. 95 (2012) 579.

[66]. S. A. Mamuru, K. I. Ozoemena, T. Fukudac, N. Kobayashi, J. Mater. Chem. 20 (2010) 10715.

[67]. J. Mack, M. Stillman, Coord. Chem. Rev. 219 (2001) 993.

[68]. M. Gouterman, in The Porphyrins, (Ed. D. Dolphin), Part A. Physical Chemistry, Academic Press, New York, (1978).

[69]. A. J. McHugh, M. Gouterman, C. Weiss, Theoret. Chim. Acta. 24 (1987) 246.

[70]. A. M. Schaffer, M. Gouterman, E. R. Davidson, Theoret. Chim. Acta. 30 (1973) 9.

[71]. M. J. Stilman, T. Nyokong, in Phthalocyanines: Properties and Applications, Eds. C. C. Leznoff, A. B. P. Lever, VCH, New York, (1989).

[72]. R. Bonnett, in Chemical aspects of Photodynamic Therapy (2000).

[73]. K. M. Smith, in Porphyrins and Metalloporphyrins, Elsevier, Amsterdam, (1975).

[74]. P. J. Spellane, M. Gouterman, A. Antipas, S. Kim, Y. C. Liu, Inorg. Chem. 19 (1980) 391.

[75]. M. Gouterman, J. Mol. Spectrosc. 6 (1961) 138-163.

[76]. T. Nyokong, Z. Gasyna, M.J. Stillman, Inorg. Chem. 26 (1987) 548.

[77]. F. R. Fan, L. R. Faulkner, J. Am. Chem. Soc. 101 (1979) 4779.

[78]. J. Mack, M. J. Stillman, J. Am. Chem. Soc. 116 (1994) 1292.

[79]. M. Rai, A. Yadav, A. Gade, Biotechnol. Adv. 27 (2009) 83.

[80]. S. Pal, K. Y. Tak, J. M. Song, Appl. Environ. Microbiol. 73 (2007) 1712.

[81]. P. Fortina, L. J. Kricka, D. J Graves, J. Park, T. Hyslop, F. Tam, N. Halas, S. Surrey, S. A. Waldman, Trends. Biotechnol. 25 (2007) 146.

[82]. S. J. Park, T. A. Taton, Science (Washington, DC) 295 (2002)1503.

[83]. C. A. Mirkin, R. Letsinger, R. Mucic, J. Storhoff, Nature (London) 382 (1996) 607.

[84]. W. H. Qi, M. P. Wang, Q. H. Liu, J. Mater. Sci. Mater. 40 (2005) 2737.

[85]. R. A. Salkar, P. Jeevanandam, S. T. Aruna, Y. Koltypin, A. Gedanken, J. Mater. Chem. 9 (1999) 1333.

[86]. D. Astruc, F. Lu, J. R. Aranzaes, Ang. Wandte Chemie Int. Ed. 44 (2005) 7852.

[87]. O. Lopez-Acevedo, K. A. Kacprzak, J. Akola, Nat. Chem. 2 (2010) 329.

[88]. J. H. Fendler. Chem. Mater., 13 (2001) 3196.

[89]. E. Ozbay, Science. 311 (2006) 189.

[90]. S. A. Maier, M. L. Brongersma, P. G. Kik, Adv. Mater. 13 (2001) 1501.

[91]. P. V. Kamat, J. Phys. Chem. B. 106 (2002) 7729.

[92]. C. B. Murray, S. Sun, H. Doyle, MRS Bulletin. 26 (2001) 985.

[93]. S. Nie, S. R. Emory, Science. 275 (1997) 1102.

[94]. N. R. Panyala, E. M. Pena-Mendez, J. Have, J. Appl. Bio. Med. 7 (2009) 75.

[95]. H. T. Zhang, J. Ding, G. M. Chow, Langmuir. 24 (2008) 378.

[96]. S. R. Zarchi, WASET. 50 (2011) 614.

[97]. C. Wang, H. Daimon, T. Onodera, T. Koda, S. Sun, Angew. Chem. Int. Ed. 47 (2008) 3591.

[98]. S. Pal, Y. K. Tak, J. Song, App. Env. Microbiol. 73 (2007) 1720.

[99]. T. S. Ahmadi, Z.L. Wang, A. Henglein, M. A. El-Sayed, Chem. Mater. 8 (1996) 1163.

[100]. W. Bu, Z. Chen, F. Chen, J. Shi, J. Phys. Chem. 113 (2009) 12185.

[101]. X. Teng, H. Yang, Nano Lett. 5 (2005) 891.

[102]. S. Sapra, D. Sarma, Pramana, J. Phys. 65 (2005) 570.

[103]. J. W. Yoo, S. M. Lee, H. T. Kim, M. A. El-Sayed, Bull. Korean Chem. Soc. 25 (2004) 396.

[104]. H. Brunner, F. Maiterth, B. Treittinger, Chem. Ber. 127 (1994) 2141.

[105]. J. Zeleny, Phys. Rev. 3 (1914) 69.

[106]. D. H. Reneker, I. Chun, Nanotechnology, 7 (1996) 216.

[107]. A. Sh. Asran, V. Seydewitz, G. H. Michler, J. Appl. Polym. Sci. 125 (2012) 1673.

[108]. D. Li, Y. N. Xia, Adv. Mater. 16 (2004) 1151.

[109]. A. Frenot, I. S. Chronakis, Curr. Opin. Colloid interface Sci. 8 (2003) 64.

[110]. A. Koski, K. Yim S. Shivkumar, Mater. Lett. 58 (2004) 493.

[111] S. De Vrieze, B. De Schoenmaker, O. Ceylan, J. Depuydt, L. Van Landuyt, H. Rahier, G. Van Assche, K. De Clerck, J. Appl. Polym. Sci. 119 (2011) 2984.

[112]. B. Decostere, N. Daels, S. De Vrieze, P. Dejans, T. Van Camp, W. Audenaert, J. Hogie, P. Westbroek, K. De Clerck, S. W. H. Van Hulle, Desalination. 249 (2009) 942.

[113]. R. Neppalli, J. Eur. Polym. 46 (2010) 968.

[114]. S. Honarbakhsh, B. Pourdeyhimi, J. Mater. Sci. 46 (2011) 2874.

[115]. S. Agarwal, Polymer. 49 (2008) 5603.

[116]. Y.C. Ahn, Curr. Appl. Phys. 6 (2006) 1030.

[117]. S. Ramakrishna, K. Fujihara, W. E. Teo, T.C. Lim, Z. Ma, in introduction to electrospinning and nanofibres. World Scientific Publishing, Singapore (2005).

[118]. A. Greiner, J. H. Wendorff, Angew. Chem. Int. Ed. 46 (2007) 5703.

[119]. B. De Schoenmaker, L. Van der Schueren, O. Ceylan, K. De Clerck, J. Nanomat.,1 (2012) 1.

[120]. M. M. Demir, I. Yilgor, E. Yilgor, B. Erman, Polymer, 43 (2002) 3303.

[121]. V. N. Morozova, T. Y. Morozova, N. R. Kallenbach, Int. J. Mass Spectrom, 178 (1998) 143.

[122]. S. Jesenska, L. Plıstil, P. Kubat, K. Lang, L. Brozova, S. Popelka, L. Szatmary, J. Mosinger, J. Biomed. Mater. Res. 99 (2011) 683.

[123]. P. Henke, K. Lang, P. Kubat, J. Sykora, M. Slouf, J. Mosinger, ACS Appl. Mater. Interfaces. 5 (2013) 3783.

[124]. Y. Lhotakova, L. Plıstil1, A. Moravkova, P. Kubat, K. Lang, J. Forstova J. Mosinger, J. Fluoresc. 19 (2009) 713.

[125]. E. Y. Jeong, A. Burri, S. Y. Lee, S. E. Park, J. Mater. Chem. 20 (2010) 10869.

[126]. A. Bettelheim, B. A. White, S. A. Raybuck, R. W. Murray Inorg. Chem. 26 (1987)1017.

[127]. N.Masilela, M.Idowu and T. Nyokong, J. Photochem. Photobiol. 201(2009) 97.

[128]. M. Ambroz, A. Beeby, A.J. McRobert, M.S.C. Simpson, R.K. Svensen and D. Phillips, J. Photochem. photobiol. B: Biol. 9 (1991) 95.

[129]. W. Spiller, H. Kliesch, D. Woehrle, S. Hackbarth, B. Roeder, G. Schnurpfeil, J. Porphyr. Phthalocya. 2 (1998) 158.

[130]. S. Sun, S. Anders, T. Thomson, J. Phys. Chem. B 107 (2003) 5419.

[131]. S. Silva, P. M. R. Pereira, P. Silva, F. A. Almeida Paz, M. A. F. Faustino, J. A. S. Caveleiro, J. P. C. Tome, Chem. Comm. 48(2012) 3610.

[132] A. Ogunsipe, J. Y. Chen, T. Nyokong, New. J. Chem. 28 (2004) 822.

[133]. M. S. Patterson, S. J. Madsen, R. Wilson, J. Photochem. Photobiol B: Biology. 5 (1990) 84.

[134]. T. Nyokong, Coord. Chem. Rev. 251 (2007) 1707-1722.

[135]. R. Zugle, T. Nyokong, J. Mol. Catal. A: Chem 358 (2012) 57.

[136]. L. Leive, J. Biolo. Chem 243 (1968) 2380.

[137]. B.C. Matlock, R.W. Beringer, D.L. Ash, A.F. Page, Thermo Fisher Scientifichttp://www.thermoscientific.fr/eThermo/CMA/PDFs/Product/productPDF_58468.PDF.

[138]. R.S. Breed, W.D. Dotterrer, J. Bacteriol. 1 (1916) 321.

[139]. M. Putman, R. Burton, M.H. Nahm, J. Immunol. Methods. 302 (2005) 99.

[140]. A. C. Beveridge, B.A. Bench, S. M. Gorun, G. J. Diebold J. Phys. Chem. A 107 (2003) 5143.

[141]. A. K. Saini, C.M. Carlin, H.H. Patterson, J. Polym. Sci Part A: Polymer Chemistry 31(1993) 2758.

[142]. M. Kanehara, H. Takahashi, T. Teranishi, Angew. Chem. Int. Ed. 47(2007) 310.

[143]. M. Uttamlal, A. S. Holmes-Smith, Chem. Phys Lett. 453 (2008) 228.

[144] J.G. Guan, W. Wang, R.Z. Gong, R.Z. Yuan, L.H. Gan, K.C. Tam, Langmuir. 18 (2002) 4204.

[145]. M. Idowu, T. Nyokong, J. Lumin. 129 (2009) 362.

[146]. N. Masilela, T. Nyokong, J. Photochem. Photobiol. A: Chem. 223 (2011) 131.

[147]. T. Maisch, C. Bosl, R. M. Szeimies, N. Lehn, C. Abels, Antimicrob. Agents Chemother. 49 (2005) 1542.

[148]. P. H. Makela, M. Hovi, H. Saxén, M. Valtonen, H. Valtonen, Immunol. Lett. 19 (1988) 217.

[149]. I. Scalise, E. N. Durantini, Bioorg. Med. Chem. 13 (2005) 3037.

[150]. B. Cosimelli, G. Roncucci, D. Dei, L. Fantetti, F. Ferroni, M. Ricci, D. Spinelli, Tetrahedron 59 (2003) 10025.

[151]. J. Chen, Z. Chen, Y. Zheng, S. Zhou, J. Wang, N. Chen, J. Huang, F. Y. Huang, J. Porphyr. Phthalocya. 15 (2011) 294.

[152]. A. Minnock , D. I. Vernon , J. Schofield , J. Griffiths , J. H. Parish , S. B. Brown,J. Photochem. Photobiol. B: Biol. 32 (1996) 159.

[153]. A. Minnock, D. I. Vernon, J Schofield, J. Griffiths, J.H. Parish, S B. Brown, antimicrob. agents and chemother., (2000) 522.

[154] A. L. Koch, Anal. Biochem. 38 (1970) 252.

[155]. A. Orenstein, D. Klein, J. Kopolovic, E. Winkler, Z. Malik, N. Keller, Y. Nitzan, FEMS Med. Microbiol. Immun 19, (1997) 314.

[156]. P. Konieczny, A. G. Goralczyk, R. Szmyd, L. Skalniak, J. Koziel F. L. Filon, M. Crosera, A. Cierniak, E. K. Zuba-Surma, J. Borowczyk, E. Laczna, J. Drukala, E. Pyza, D. Semik, O. Woznicka, A. Klein, J. Jura, Intern. J. Nanomed. 8 (2013) 3975.

[157]. V. Kussovski, V. Mantareva, I. Angelov, P. Orozova, D. Wöhrle, G. Schnurpfeil , E. Borisova, L. Avramov. FEMS Microbiol Lett 294 (2009) 140.

[158]. C. Marambio-Jones, E. M. V. Hoes, J. Nanopart. Res. 12 (2010) 1551.

[159]. L. Florez, C. Herrmann, J. M. Cramer, C. P. Hauser, K. Koynov, K. Landfester, D. Crespy, V. Mailänder, Small 8 (2012) 2230.

[160]. D. Jocham, in: J.G. Moser (Ed.), Photodynamic Tumor Therapy: 2 and 3 Generation Photosensitizers, Harwood Academic, Publishers, 1998, pp. 213– 226.

[161] S. Ghammamy, M. Azimi, S. Sedaghat, Sci. Res. Essays 7 (2012) 3757.

[162] I. Kostova, Recent Pat. Anti-Cancer Drug Disc. 1 (2006) 22.